INTERNATIONAL CONFERENCE

ON SUSTAINABILITY AND SOLUTIONS

A BLUEPRINT FOR PLANETARY SUSTAINABILITY AT 2040

1st March, 2025

Editors

Dr. Supriya Deshmukh & Dr. Sajith Kumar Chandran

Organized By

IQAC, Department of Chemistry & Department of Biotechnology, Jai Hind College, 23-24, Backbay Reclamation, A-Road, Churchgate, Mumbai, India- 400020

International Journal of Multidisciplinary Research and Technology

ISSN 2582-7359 | Peer Reviewed Journal | Impact Factor 6.325

Volume 6 Issue 3 (Special Issue March 2025)

International conference on sustainability and solutions

"A Blueprint for Planetary Sustainability at 2040"

(1st march 2025)

Organized By

Department of Chemistry & Department of Biotechnology

Jai Hind College
23-24, Backbay Reclamation
A-Road, Churchgate, Mumbai, India- 400020

Editors

Dr. Supriya Deshmukh & Dr. Sajith Kumar Chandran

Taran Publication
New Delhi

International Journal of Multidisciplinary Research and Technology
Volume -6 , Issue 3 (Special Issue March 2025)

JOURNAL DETAILS

Name of Journal	**International Journal of Multidisciplinary Research and Technology**
e-ISSN	**2582-7359**
Subject	**Multidisciplinary**
Publisher	**Taran Publication**
Impact Factor	**6.325**
Website	**www.ijmrtjournal.com**
Contact Number	**8950448770, 9996906285**
Country of Publication	**India**
Editor-in-Chief	**Dr. Mandeep Kaur**

Index

International Journal of Multidisciplinary Research and Technology
ISSN 2582-7359, Peer Reviewed Journal, Impact Factor 6.325
www.ijmrtjournal.com

GREEN SYNTHESIS OF HYDROXYAPATITE NANOPARTICLE USING *MORINGA OLEIFERA* PLANT EXTRACT FOR DENTAL HYGIENE

[1]Iqra Ansari, [2]Waldon D'Mello, [3]Kruti Pandya
Department of Biotechnology
Jai Hind College Autonomous
'A' Road Church Mumbai 400020

Abstract:

Poor oral health remains a major human affliction burdening health care systems worldwide. Dental caries affect close to 3.5 billion people worldwide, according to the WHO Global Oral Health Status Report (Dental caries cause enamel demineralisation - primary mechanism involved in the etiopathogenesis of dental caries). Demineralisation is triggered at low pH values. It's a biochemical interaction at the interface of the external oral environment, biofilm colonising hard tissues and the dental hard tissues. However it's a reversible process; when the microenvironment reaches pH values 7.0 or higher and there is an availability of calcium and phosphate ions, remineralisation can occur. Such ions precipitate, covering the dental surfaces with an amorphous mineral layer. Toothpaste containing fluoride inhibits demineralisation by interfering with the metabolic pathways of microbial cells in the overlying biofilm. Accumulation of fluoride at the enamel surface leads to the precipitation of calcium fluoride-like deposits, which act as a reservoir and gradually release fluoride under conditions of decreased pH. However fluoride ingestion can cause dental fluorosis in children, concerns about fluoride's potential neurotoxicity have spurred research to find alternative active ingredients. A promising alternative active ingredient for addressing these concerns are calcium-phosphate based molecules like hydroxyapatite which exhibits excellent biocompatibility for dental application. However Hydroxyapatite nanoparticle synthesis through conventional routes are not eco-friendly and are very costly. Since research in current times is geared towards sustainability, we have synthesised HAp nanoparticle by green synthesis

Keywords: *HAp, nanoparticle, green synthesis, oral health, dental caries*

Introduction:

Nanotechnology is the scientific discipline which has opened numerous avenues for the advancement of current sciences. Exploitation of nanoparticles for the betterment of human lives has become the gold rush of the current era because of highly promising results and future prospects. Enamel is primarily made up of Hydroxyapatite (HAp) thus HAp nanoparticles (NP)

shows extreme bio-compatibility and can be used as an alternative to fluoride in commercially available toothpastes. HAp NP îs a part of the Ca-P NP family and is chemically represented as $Ca_{10}(PO_4)_6(OH)_2$. The stoichiometric ratio of HAp is calcium and phosphorus in the ratio of 1:67. HAp NP can be synthesised by various methods like sol-gel, thermal hydrolysis, hydro thermal processing, chemical vapour deposition, thermal plasma approach and microwave synthesis method. However these methods are costly and not eco-friendly, green synthesis is far cheaper while being equally eco-friendly. The leaf and flower of *Moringa oleifera* were used for the synthesis of HAp NP. *Moringa oleifera* belonging to the Moringaceae family originally native to India is often referred to as the "Miracle tree" because of its countless health benefits and nutritious value. Dental caries is an issue that annually affects billions of people around the globe, an effective way to combat the dental caries has always been using fluoride containing toothpastes which pose their own concerns. HAp NP can effectively replace fluoride in toothpaste and perform its function better while being harmless at the same time. This project aims to synthesise Hap NP by a green synthesis approach, characterise the synthesised particle by UV-Visible Spectrophotometric analysis, and determine its antimicrobial activity against *Staphylococcus aureus* - Gram positive bacteria.

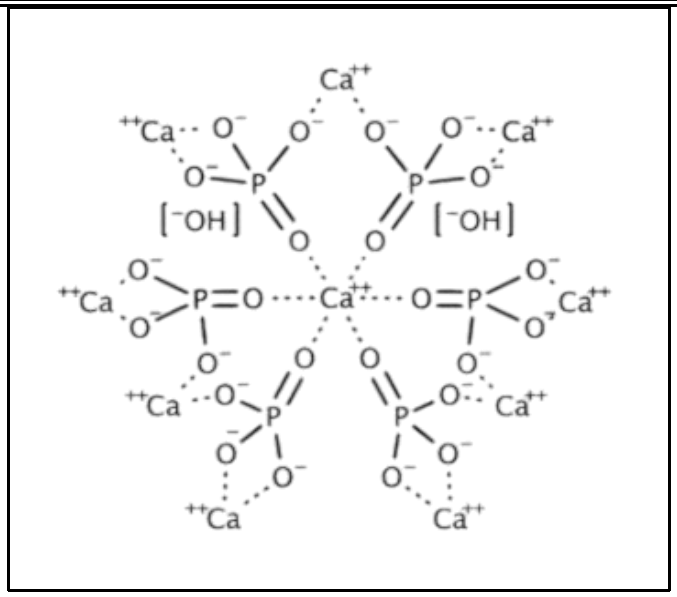

Fig 2: Hydroxyapatite nanoparticle

Materials and Methodology:

HAp nanoparticles were synthesised using a green synthesis method, where 0.01 M $Ca(OH)_2$ was dissolved in 50 ml distilled water (to super saturate the solution). The solution was stirred for 10 minutes using a magnetic stirrer. Similarly, 0.006 M H_3PO_4 solution was prepared separately in another flask. Moringa leaves and flowers were collected and surface sterilized with distilled water. 5g Moringa leaves were mixed with 50 ml distilled water and boiled for 30 minutes. The solution was cooled to room temperature, filtered and stored at 4°C. Similarly, Moringa flower extract was prepared and stored. $Ca(OH)_2$ and H_3PO_4 solutions were mixed together and 0.8 M NaOH was added slowly from a burette vertically. The pH of the solution was adjusted to 10.

30 ml of *Moringa oleifera* leaf extract was added as electron donor and 3 ml of *Moringa oleifera* flower extract was added as a capping agent. Stir continuously for 1 hour using a magnetic stirrer. Allow the solution to stand at room temperature for 24 hours.

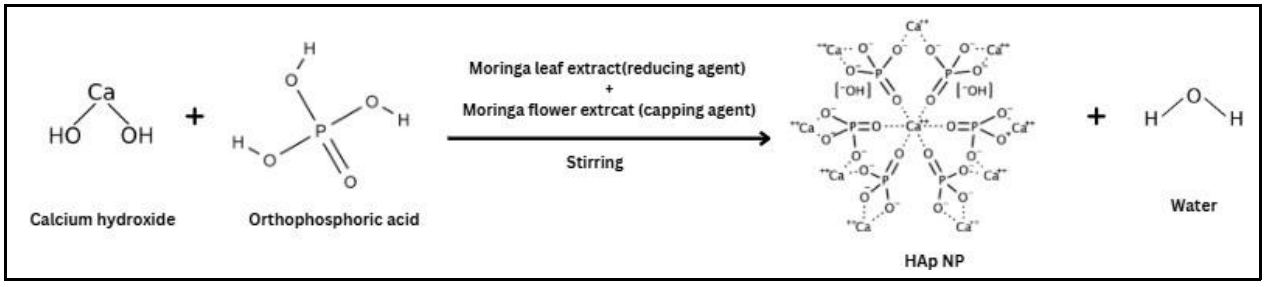

Fig 3.1: Reaction for synthesis of HAp NP

Moringa flowers Moringa leaves Flower and leaves extract

Solution of $Ca(OH)_2$ and H_3PO_4 mixed with extract

Fig 3.2: Methodology for synthesis of HAp NP

Result:

Colour change:

The Moringa extract-synthesized hydroxyapatite (HAp) nanoparticles showed a clear color change from brown to green during synthesis. This was triggered by the reducing and stabilizing effect of bioactive compounds in the Moringa extract, including polyphenols, flavonoids, and other phytochemicals. These compounds enable the green synthesis of HAp nanoparticles without the use of harmful chemicals.

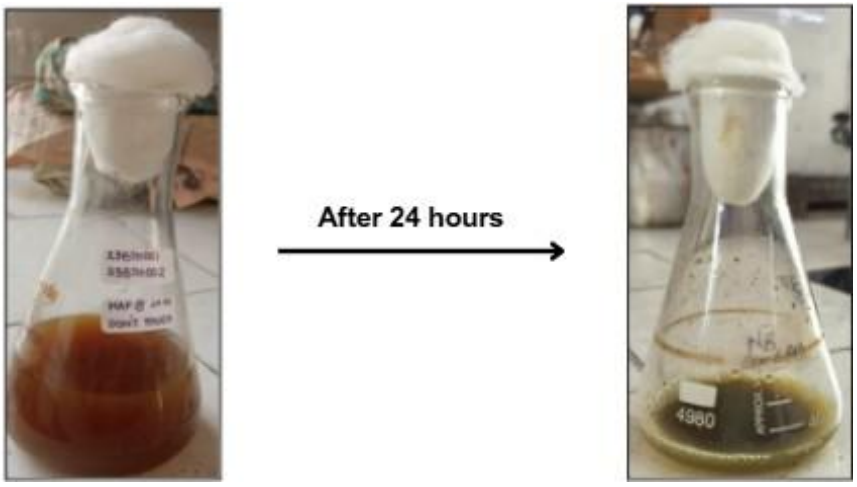

Fig 4.1: Observation of colour change

UV-Vis Spectral analysis:

The presence of HAp nanoparticles was analyzed by preliminary detection using UV-Vis Spectrophotometer (EQUIP-TRONICS Model no.827) against a blank (distilled water). The spectral range was recorded from 230 nm to 290 nm. The nanoparticle showed an absorption peak at 230nm.

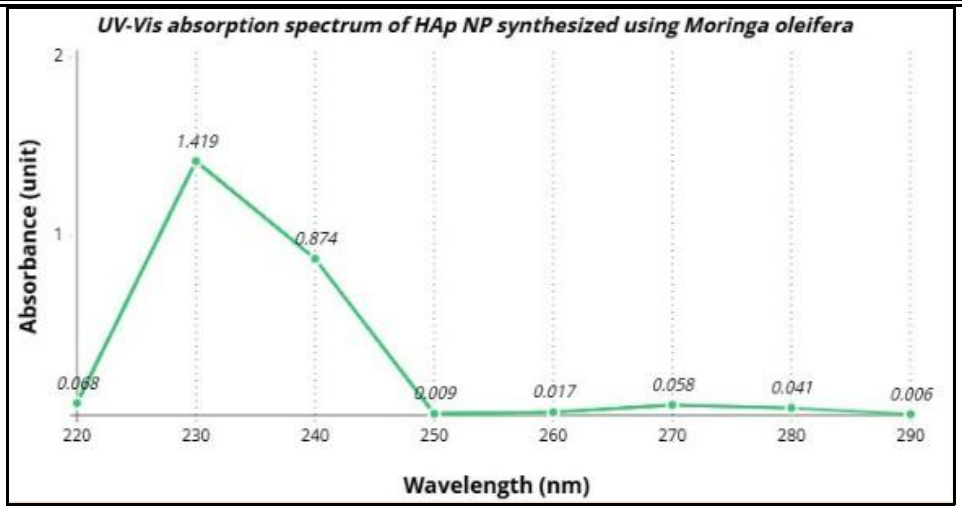

Fig 4.2:UV-Vis absorption spectrum of Hap Np synthesis

Antimicrobial activity of HAp NP:

The green synthesized HAp NP were tested for antimicrobial activity - Kirby Bauer disc diffusion method. The test organism *Staphylococcus aureus* was sub cultured and spread on nutrient agar (peptone 1g, beef extract 0.3g, NaCl 0.5g, agar 3g, distilled water 100ml, pH 7.4) using sterilized cotton swabs. The disc diffusion method was performed by placing four different types of discs including control, moringa leaf and flower extract, HAp NP and was incubated at 37 ° C for 24 hr. The zone of clearance was observed and the mean was calculated: 5 mm for moringa leaf extract, 3mm for moringa flower extract, 8.3 mm for HAp Np.

Discussion:

The bioactive compounds in the Moringa extract, such as polyphenols, flavonoids, and phytochemicals, act as reducing agents. They reduce the precursors (like calcium and phosphate ions) to form hydroxyapatite nanoparticles. It also serves as capping agents, stabilizing the nanoparticles so that they don't agglomerate and maintain uniform particle size. The observed color change (from brown to green) serves as a visual indicator of the reaction progression and successful synthesis of HAp nanoparticles.

The peak absorption at 230 nm during spectral analysis aligns nearly with the characteristic absorption range of HAp nanoparticles.

The control had not shown any zone of clearance for the treated bacterial strain whereas the HAp NP showed enhanced antimicrobial property as compared to leaf and flower extract. Hence we found that HAp NPs have the ability to suppress the growth of Gram positive bacteria commonly found in the oral cavity. Similar disc diffusion assay can be performed against specific dental caries to determine the antibacterial activity of HAp NP.

Conclusion:

Hydroxyapatite has proven to be a compound of great significance because of its numerous biomedical applications like drug delivery, bio-functional scaffolds and its resemblance to natural enamel. Dental caries cause the demineralisation of teeth because of which, it is the primary cause of tooth decay and decline in oral hygiene. This demineralisation is combated by the use of fluoride toothpaste. They inhibit demineralisation by disrupting the metabolic pathways of dental caries fluoride accumulates at the enamel surface, this leads to the precipitation of calcium fluoride-like deposits. In conditions of decreased pH these deposits gradually release fluoride to counteract the demineralisation. However the growing consumer concern on the negative effects of fluoride ingestion by use of fluoride toothpaste has led to research for developing alternatives. Research has demonstrated the possibility of HAp NP being an alternative to fluoride. For preparation of nano embedded oral hygiene products, synthesis of HAp NP was performed by a plant mediated method using *Moringa oleifera* leaf and flower extract. The leaf extract acts as a reducing agent and chelates the precursor to form the HA NP which are then capped by the flower extract. However further research is essential to understand the reaction mechanism. The synthesised HAp NP were

characterised by UV - Vis spectral analysis. Kirby Bauer disc diffusion method was performed to determine its antibacterial properties against *S. aureus* which is a Gram positive bacteria. The zones of clearance which were observed indicate the anti-bacterial nature of HAp NP. Additional research and clinical trials are required to facilitate the transition from fluoride toothpastes to HAp NP toothpastes.

Future prospects:

Scientific studies have concluded that silver possesses bactericidal, fungicidal, and antiviral properties. Its microbial action works through silver ions that deactivate important bacterial enzymes. The destruction of these enzymes results in the disturbance of the cell that stops bacterial DNA replication, which leads to cell death. In recent studies, Ag NP are known to have high antibacterial activity. Ag NP is an effective antibacterial agent due to the fact that they have a high surface-area to mass ratio which means that even small quantities can be used in toiletries, including mouthwashes. Studies also showed that dental resins are remarkably more antibacterial after having Ag NP incorporated in them. Resins that contain Ag NP inhibit the growth of bacteria, biofilm colony-forming units (CFU), and the metabolic activity of the biofilms. This causes a significant reduction in the formation of harmful biofilms and the secretion of lactic acid, which decays the tooth. The most significant aspect is that these antibacterial properties are achieved without losing the desirable physical and mechanical properties of the resins. For more effective prevention of dental caries, Ag NP can be used together with HAp.

Acknowledgement:

The authors of this project would like to acknowledge the help and support received from the Department of Biotechnology, Jaihind College..

References:

1. Mok, Z. H., Mylonas, P., Austin, R., Proctor, G., Pitts, N., & Thanou, M. (2021). Calcium phosphate nanoparticles for potential application as enamel remineralising agent tested on hydroxyapatite discs. Nanoscale, 13(47), 20002–20012. https://doi.org/10.1039/d1nr05378g
2. Alorku, K., Manoj, M., & Yuan, A. (2020). A plant-mediated synthesis of nanostructured hydroxyapatite for biomedical applications: a review. RSC Advances, 10(67), 40923–40939. https://doi.org/10.1039/d0ra08529d
3. Kumar, G. & Rajendran, Senkotuvel & Sekar, Karthi & Raji, Govindan & Girija, Easwaradas & Gopalu, Karunakaran & Kuznetsov, Denis. (2017). Green synthesis and antibacterial activity of hydroxyapatite nanorods for orthopedic applications. MRS Communications. 7. 1-6. 10.1557/mrc.2017.18. https://link.springer.com/article/10.1557/mrc.2017.18
4. Ganta, D. D., Hirpaye, B. Y., Raghavanpillai, S. K., & Menber, S. Y. (2022). Green Synthesis of Hydroxyapatite Nanoparticles Using Monoon longifolium Leaf Extract for Removal of Fluoride from Aqueous Solution. Journal of Chemistry, 2022, 1–13. https://doi.org/10.1155/2022/4917604
5. Kalaiselvi, V., Mathammal, R., Vijayakumar, S., & Vaseeharan, B. (2018). Microwave assisted green synthesis of Hydroxyapatite nanorods using Moringa oleifera flower extract and its antimicrobial applications. International Journal of Veterinary Science and Medicine, 6(2), 286–295. https://doi.org/10.1016/j.ijvsm.2018.08.003
6. Bossù, M., Saccucci, M., Salucci, A., Di Giorgio, G., Bruni, E., Uccelletti, D., Sarto, M. S., Familiari, G., Relucenti, M., & Polimeni, A. (2019). Enamel remineralization and repair results of Biomimetic Hydroxyapatite toothpaste on deciduous teeth: an effective option to fluoride toothpaste. Journal of Nanobiotechnology, 17(1). https://doi.org/10.1186/s12951-019-0454-6
7. C, N. R., L, N. K., Venkatachalam, R., & S, N. A. (2022). Green Synthesis of Hydroxyapatite Nanoparticles from Wrightia tinctoria and Its Antibacterial Activity. BioNanoScience, 12(3), 723–730. https://doi.org/10.1007/s12668-022-01012-x
8. Chen, L., Al-Bayatee, S., Khurshid, Z., Shavandi, A., Brunton, P., & Ratnayake, J. (2021b). Hydroxyapatite in Oral Care Products—A Review. Materials, 14(17), 4865. https://doi.org/10.3390/ma14174865
9. Limeback, H., Enax, J., & Meyer, F. (2023). Improving Oral Health with Fluoride-Free Calcium-Phosphate-Based Biomimetic Toothpastes: An Update of the Clinical Evidence. Biomimetics, 8(4), 331. https://doi.org/10.3390/biomimetics8040331
10. Jadhav, V., Bhagare, A., Wahab, S., Lokhande, D., Vaidya, C., Dhayagude, A., Khalid, M., Aher, J., Mezni, A., & Dutta, M. (2022).
11. Green Synthesized Calcium Oxide Nanoparticles (CaO NPs) Using Leaves Aqueous Extract of Moringa oleifera and Evaluation of Their Antibacterial Activities. Journal of Nanomaterials, 2022(1). https://doi.org/10.1155/2022/9047507
12. Cheng, L., Zhang, K., Weir, M. D., Melo, M. a. S., Zhou, X., & Xu, H. H. (2015). Nanotechnology strategies for antibacterial and remineralizing composites and adhesives to tackle dental caries. Nanomedicine, 10(4), 627–641. https://doi.org/10.2217/nnm.14.191.

International Journal of Multidisciplinary Research and Technology
ISSN 2582-7359, Peer Reviewed Journal, Impact Factor 6.325
www.ijmrtjournal.com

MICROWAVE IRRADIATION VERSUS CONVENTIONAL METHOD: SYNTHESIS AND CHARACTERIZATION OF SOME NEW SERIES OF MANNICH BASES DERIVED FROM 4-[(4-CHLORO-2 PYRIMIDINYL)AMINO]BENZONITRILE

[1]Vijay V. Dabholkar, [2]Rahul Jaiswar, [3]Dinesh Udawant
Organic Research Laboratory, Department of Chemistry
Jai Hind College, Church gate, Mumbai-400 020
K. C. College, Church gate, Maharashtra, INDIA.

Abstract:

In order to examine the viability, reaction time, and yield of the product, a number of novel Mannich base derivatives were created and synthesized using both traditional and microwave methods. Mannich bases were obtained for this by employing pTSA as a catalyst in a one-pot synthesis of 4-((4-chloropyrimidin-2-yl)amino)benzonitrile, aldehydes, and primary amine. IR, 1H NMR, 13C NMR, and elemental analysis were used to identify the structures of the newly synthesized compounds. A comparison of the conventional and microwave procedures showed that the microwave aided synthesis was easier to use, more convenient, produced better yield, and produced fewer byproducts than the old method.

Keyword: Mannichbase, Microwave irradiation, 4-((4-chloropyrimidin-2-yl)amino)benzonitrile, Aromatic aldehydes.

1. Introduction:

Improved thermal control of chemical reactions is made possible by microwave (MW) irradiation. Compared to traditional heating techniques, the quick MW heat transfer enables reactions to proceed significantly more quickly, frequently leading to higher product yields. [1–2] Moreover, it is possible to extract and selectively modify the byproducts of temperature-sensitive processes from kinetic or thermodynamic routes. An oscillating electric or magnetic field causes polar molecules or ions to be stirred, which is the basic mechanism of microwave-irradiated synthesis. Particles attempt to align themselves or be in phase with the oscillating field when it is present. Microwave synthesis only applies to materials that can absorb microwave energy.[3] For the synthesis of organic compounds, this method is therefore easy, clean, quick, effective, and economical. Therefore, microwave irradiation was used to prepare this synthesis.

Mannich reactions are more flexible than other reactions. As a result, they have long piqued the interest of chemists. A sort of nucleophilic addition reaction known as the Mannich reaction occurs when a molecule containing one or more active hydrogen atoms condenses with formaldehyde[4] and a primary or secondary amine. **Scheme 1** provides a generic schematic representation of the Mannich reaction. The Mannich bases, which make up the amino alkyl chain in it, have been discovered to be extremely significant synthetically. They function as biologically active substances and have the potential to be used as agents in the synthesis of numerous medicinally valuable chemicals. Biperiden cocaine, ethacrynic acid, atropine, ranitidine, trihexyphenidyl, fluoxe-tine procyclidine, and other amino alkyl chains containing mannich bases are clinically significant[5–7]. The reactive Mannich bases are easily transformed into other compounds, such as physiologically active amino alcohols[8].

The Mannich bases also possesses the number of potent activities such as anti-HIV[9], antimalarial[10], antifungal[11-12], anticonvulsant[13], antiviral[14], antifilarial[15], anticancer [16-17], anthelmintic[18], antibacterial[19-20], antipsychotic[21], antitubercular[22-23], analgesic[24], antiinflammatory [25-26], along with the biological activity the Mannich bases are found to their extensive use in the detergent synthesis and commonly used as a additive in it. Such as the polymers surface active reagents[27]. The Maninich bases and the derivatives of these bases are extensively used as the intermediates for the synthesis of the biologically active compounds[28-29]. Also the extensive use of this reaction is to preapare or synthesized the compound containing Nitrogens[30]. In addition to their widespread application in the field of agrochemicals as growth regulators in plants, Mannich bases are highly significant in their antibacterial activity[31].

In the current study, we used pTSA as a catalyst to synthesize the N-Mannich Bases from 4-((4-chloropyrimidin-2-yl)amino)benzonitrile, aldehydes, and primary amine. Compounds can be synthesized in a single pot using the Mannich reaction, which is classified as a multicomponent reaction (MCR) when three or more distinct reactant molecules react to generate a product. The new avenues for the advancement of organic synthesis are defined by the multicomponent reactions (MCRs). MCRs are clearly emphasized as crucial pathways and procedures in organic synthesis and medicinal chemistry[32] because of this.

The synthesis of the N-Mannich Bases from 4-((4-chloropyrimidin-2-yl)amino)benzonitrile, aldehydes and primary amine using pTSA as a catalyst was found to be the convenient method for the synthesis of the number of the Mannich bases which was characterized and found to have the extensive use in the synthetic chemistry.

2. Material and method:

Unless and otherwise noted, all Chemicals used were of commercial grade and they were used without any further purification. All reactions were monitored by thin layer chromatography using aluminium sheets precoated with silica gel 60 F254 (Merck) using either UV light or iodine vapours as visualizing agents. The products were identified fully or by comparison of melting points and spectroscopic data with the previously reported ones.

General procedure for the synthesis of novel mannich bases ***4(a-n)***

2.1 Conventional method:

A mixture of 4-((4-chloropyrimidin-2-yl)amino)benzonitrile **(1)** (3 mmol), substituted aldehyde **(2)** (3 mmol), and substituted amine **(3)** (3 mmol), in ethanol (10ml) was placed in 100 ml of R.B.F and 1.5mm pTSA were added then mixture was refluxed on a water bath for 2-3hr. The reaction was monitored by TLC. Upon completion, the reaction mass was cooled to room temperature. The solid thus obtained, further cooled to 0-5°C. Filter the solid and wash with chilled ethanol and recrystallized from 50% aq. EtoH to afford pure compound.

2.2 Microwave Irradiation Method:

A mixture of 4-((4-chloropyrimidin-2-yl)amino)benzonitrile **(1)** (3 mmol), substituted aldehyde **(2)** (3 mmol), and substituted amine **(3)** (3 mmol), in ethanol (10ml) and 1.5mm pTSA were irradiated in microwave for 5-10min. The reaction was monitored by TLC. Upon completion, the reaction mass was cooled to room temperature. The solid thus obtained, further cooled to 0-5°C. Filter the solid and wash with chilled ethanol and recrystallized from 50% aq. EtoH to afford pure compound.

3. Results:

The microwave approach and the conventional method were used to create new mannich base derivatives **(Scheme 1).** A number of chosen one-pot microwave-assisted syntheses were performed in order to demonstrate the newly established method's general effectiveness. While normal reflux conditions needed 8 hours, the reaction was observed to occur smoothly under microwave irradiation in 20 minutes. **Table 1** compared the synthesis of novel Mannich bases using the conventional method versus the microwave method. Rapid synthesis was made possible by the microwave-assisted process, which took only 20 minutes as compared to 8 hours using conventional methods. We discovered that employing the microwave approach produced new mannich base derivatives in good yields.

The majority of **compounds 4** had yields above 70%, which was higher than the yields of the derivatives of mannich bases that were produced using the traditional approach. particularly if the compounds were synthesized while being exposed to microwave radiation. The microwave process produced **Compounds 4i** in the highest yield (78.6%), whereas traditional procedures, which usually take around 8 hours, produced **Compounds 4i** in a yield of only 47.4%. Conversely, the molecule can be synthesized in just 10 minutes using the microwave method.

3.1.Scheme 1: Synthetic pathway for **compounds 4(a-n)**

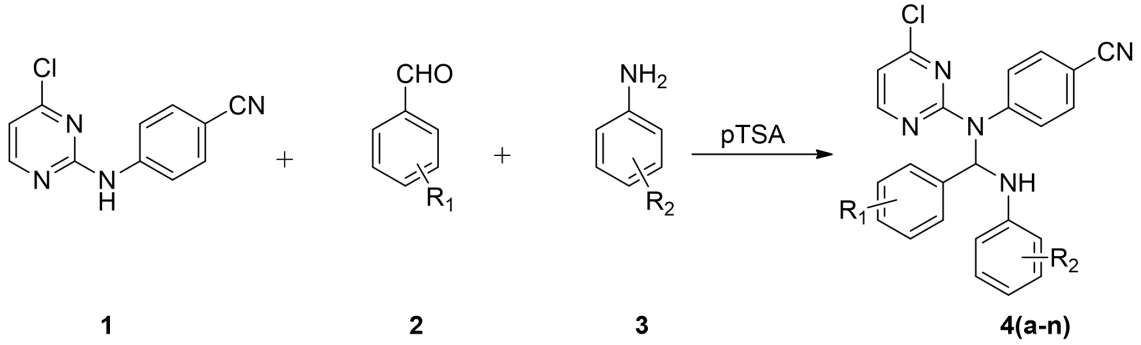

1 **2** **3** **4(a-n)**

3.2. Table 1. Comparison of traditional synthesis with microwave assistance

Code	R_1	R_2	Yield%		Reaction Time		Energy	
			Conventional	Microwave	Conventional (hr)	Microwave (min)	Conventional (Temp. C)	Microwave (PowerWatt)
4a	H	H	43.7	71.6	3	10	80-85	210
4b	4-Cl	H	42.2	70.6	6	12	80-85	210
4c	2-Cl	H	41.2	70.4	5	15	80-85	210
4d	4-Br	H	44.9	78.0	4	17	80-85	210
4e	3-OCH_3	H	43.2	77.1	7	11	80-85	210
4f	4-OCH_3	H	43.1	78.1	8	10	80-85	210
4g	3-NO_2	H	39.2	73.1	5	16	80-85	210
4h	H	CH_3	48.5	72.3	4	18	80-85	210
4i	4-Cl	CH_3	47.4	78.6	8	10	80-85	210
4j	2-Cl	CH_3	42.7	76.8	7	15	80-85	210
4k	4-Br	CH_3	41.1	76.4	6	18	80-85	210
4l	3-OCH_3	CH_3	40.9	70.1	3	20	80-85	210
4m	4-OCH_3	CH_3	46.5	71.7	4	14	80-85	210
4n	3-NO_2	CH_3	45.1	77.8	7	13	80-85	210

3.3. Table 2: The infuence of solvent on the synthesis of **(compounds 4a) 4-((4-chloropyrimidin-2-yl)(phenyl(phenylamino)methyl)amino)benzonitrile**

Entry	solvent	catalyst	Microwave		Conventional	
			Time(Min)	Yield	Time(h)	Yield(%)
1	Ethanol	pTSA	10	71.6	3	43.7
2	DMF	pTSA	11	87.2	7	55.3
3	DMSO	pTSA	10	86.1	8	52.1
4	Methanol	pTSA	14	82.6	8	51.5

Different solvents have been investigated in **Table 2** since the solvent also significantly influenced the reaction rate and isolated yield. First, we tested both the conventional and microwave methods to react 4a in ethanol **(Table 2, entry 1).** To our satisfaction, the microwave procedure produced a greater yield (71.6%) of product 4a. When we screened the solvents for this reaction, we discovered that using pTSA as a catalyst for the reaction in DMF increased the yield of the isolated product to 87.2% **(Table 2, entry 2).** The experiment showed that the polar aprotic solvent enhanced the process. **Table 2** shows that the synthesis of Mannich base was significantly enhanced in terms of reaction time and yield by using DMF and DMSO as a solvent with pTSA as a catalyst **(Table 2, entry 2-3)**. Additionally, methanol might drastically shorten reaction times and boost yield, proving that basic solvents work well **(Table 2, entry 4).** Therefore, when compared to a number of different solvents examined under microwave irradiation, **Compound 4a** was determined to be ideal in DMF.

4. Discussion:

Melting points were measured in open capillaries and are uncorrected. IR spectra was recorded on Bruker FTIR spectrophotometer. ^{1}H-NMR and ^{13}C-NMR spectra were recorded on Bruker FTNMR (500MHz) spectrophotometer with DMSO-d6 as solvent and TMS as internal standard. Solvent peaks in ^{1}H-NMR and ^{13}C-NMR spectra have been removed in tracing. The chemical shifts in parts per million (δ) are reported downfield from TMS (0 ppm). The abbreviations s, d, t, q, m and dd refer to singlet, doublet, triplet, quartet, multiplet and doublet of doublet respectively.

4-((4-chloropyrimidin-2-yl)(phenyl(phenylamino)methyl)amino)benzonitrile **(4a):**

Molecular Formula: $C_{24}H_{18}ClN_5$

Molecular Weight (gmol-1): 411.89

Melting Point (ºC): 120-125°C

IR (KBr, cm-1): 3217 (NH), 2185 (CN), 1675 (C=N)

^{1}H NMR (500 MHz, DMSO, δ ppm): 10.46 (s, 1H, NH), 7.11-8.07 (m, 9H, Ar-H), 6.47 (s, 1H, CH)

^{13}C NMR (500 MHz, DMSO, δ ppm): 160.4, 150.2, 148.9, 139.9, 139.7, 135.6, 133.4, 129.6, 128.6, 128.1, 127.3, 123.8, 123.6, 120.3, 118.6, 117.8, 111.6, 109.9.

4-((4-chloropyrimidin-2-yl)(((4-methoxyphenyl)amino)(phenyl)methyl)amino)benzonitrile **(4e):**

Molecular Formula: $C_{25}H_{20}ClN_5O$

Molecular Weight (gmol-1): 441.91

Melting Point (ºC): 130-133°C

IR (KBr, cm-1):): 3319 (NH), 2145 (CN), 1491 (C=N)

^{1}H NMR (500 MHz, DMSO, δ ppm): 10.70 (s, 1H, NH), 7.22-7.83 (m, 9H, Ar-H), 6.66 (s, 1H, CH), 3.83 (s, 3H, OCH_3).

^{13}C NMR (500 MHz, DMSO, δ ppm): 160.4, 155.0, 150.2, 148.9, 139.9, 139.7, 135.6, 133.4, 128.6, 128.1, 127.3, 123.8, 120.3, 118.6, 116.0, 114.6, 111.6, 109.9, 55.3.

4-((4-chloropyrimidin-2-yl)(phenyl(p-tolylamino)methyl)amino)benzonitrile **(4h):**

Molecular Formula: $C_{25}H_{20}ClN_5$

Molecular Weight (gmol-1): 425.91

Melting Point (ºC): 122-129°C

IR (KBr, cm-1): 3351 (NH), 2193 (CN), 1639 (C=N)

^{1}H NMR (500 MHz, DMSO, δ ppm): 10.40 (s, 1H, NH), 6.66-7.83 (m, 9H, Ar-H), 5.16 (s, 1H, CH), 2.19(3H, CH_3).

^{13}C NMR (500 MHz, DMSO, δ ppm): 160.4, 150.2, 148.9, 139.9, 139.7, 135.6, 133.4, 131.2, 130.0, 128.6, 128.1, 127.3, 123.8, 120.3, 118.6, 114.4, 111.6, 111.6, 109.9, 21.4.

4-((4-chloropyrimidin-2-yl)((4-methoxyphenyl)(p-tolylamino)methyl)amino)benzonitrile **(4l):**

Molecular Formula: $C_{26}H_{22}ClN_5O$

Molecular Weight (gmol-1): 455.94

Melting Point (ºC): 133-136°C

IR (KBr, cm-1): 3347 (NH), 2145 (CN), 1630 (C=N)

^{1}H NMR (500 MHz, DMSO, δ ppm): 10.50 (s, 1H, NH), 6.1 (s, 1H, CH), 6.92-8.02 (m, 8H, Ar-H), 4.10 (s, 3H, OCH_3), 2.5 (3H, CH_3).

^{13}C NMR (500 MHz, DMSO, δ ppm): 160.4, 159.8, 150.2, 148.9, 139.9, 139.7, 135.6, 133.4, 131.2, 130.0, 128.3, 123.8, 120.3, 118.6, 114.4, 114.2, 111.6, 109.9, 55.3, 21.4.

5. Conclusions:

1. In summary, a new series of mannich base were synthesized using pTSA catalyst which offers several advantages over the conventional heating methods such as shorter reaction times, excellent yields and simple experimental workup procedures.
2. We also studied the optimization of experimental conditions for the Mannich reaction. Compared with the conventional method, the microwave method could reduce the reaction time, improve rate and increase yields.

6. Acknowledgement:

The authors acknowledged and appreciated everyone facilitating this investigation to be achieved.

7. References:

1. Sekhon B. S., International Journal of PharmTech Research, 2010, 2, 827–833,
2. Surati M. A., Jauhari S., Desai K. R., Archives of Applied Science Research, 2012, 4, 645–661.
3. Lidström P., Tierney J., Wathey B., Westman J., Tetrahedron, 2001., 57, 9225–9283.
4. Joshi S, Khosla N and Tiwari P, Bioorganic & Medicinal Chemistry, 2004, 12, 571– 576.
5. Racane L, Kulenovic V.T, Jakic D.W, Boykin and Zamola G.K, Heterocycles, 2001, 55, 2085– 2098.
6. Kashiyama E, Hutchinso I.N and Chua M.S, Journal of Medicinal Chemistry, 1999, 42(20), 4172–4184.
7. Bhusare S.R, Pawar R.P and Vibhute Y.B, Indian Journal of Heterocyclic Chemistry, 2001, 11(1), 79–80.
8. Raman N, Esthar S and Thangaraja C, Journal of Chemical Sciences, 2004, 116(4), 209–213.
9. Sriram D, Banerjee D, and Yogeeswari P, Journal of Enzyme Inhibition and Medicinal Chemistry, 2009, 24 (1), 1–5.
10. Barlin G.B and Jiravinya C, Australian Journal of Chemistry, 1990, 43(7), 1175–1181.

11. Pandeya S.N, Sriram D, Nath G and Clerc E.De, European Journal of Medicinal Chemistry, 2007, 35 (2), 249–255.
12. Singh B.N, Shukla S.K and Singh M, Asian Journal of Chemistry, 2000, 19 (7), 5013-5018.
13. Vashishtha S.C, Zello G.A and Nienaber et al K.H, European Journal of Medicinal Chemistry, 2004, 39 (1)27–35.
14. Edwards L, Ritter H.W, Stemerick D.M and Stewart K.T, Journal of Medicinal Chemistry, 1983 ,26 (3), 431-436
15. Kalluraya B, Chimbalkar R.M, and Hegde J.C, Indian Journal of Heterocyclic Chemistry, 2005, 15(1) 15–18.
16. Ivanova Y, Momekov G, Petrov O, Karaivanova M and Kalcheva V, European Journal of Medicinal Chemistry, 2007, 42 (11-12), 1382–1387.
17. Gul H.I, Vepsalainen J, Gul M, Erciyas E and Hanninen O, Pharmaceu- tica Acta Helvetiae, 2000, 74 (4), 393-398
18. Bennet-Jenkins E and Bryant C, International Journal for Parasitology, 1996, 26 (8-9), 937-947.
19. Ashok M, Holla B.S, and Poojary B, European Journal of Medicinal Chemistry, 2007,42 (8), 1095-1101
20. Pandeya S.N, Sriram D, Nath G and De Clercq E, European Journal of Medicinal Chemistry, 2000, 35 (2), 249–255.
21. Scott M.K, Martin G.E, DiStefano et al D.L, Journal of Medicinal Chemistry, 1992, 35 (3), 552–558.
22. Sriram D, Banerjee D and Yogeeswari P, Journal of Enzyme Inhibition and Medicinal Chemistry, 2009, 24 (1), 1-5.
23. Mulla J.S, Khan A.Y, Panchamukhi S.I , Khazi M, Kalashetti A.B and Khazi I.M, Indian Journal of Novel Drug Delivery, 2011, 3 (4), 289-295.
24. Malinka W, Swiatek P, Filipek, Sapa B.J, Jezierska A, and Koll A, Farmaco, 2005, 60 (11-12), 961-968.
25. Kalluraya B, Chimbalkar R.M, and Hegde J.C, Indian Journal of Heterocyclic Chemistry, 2005, 15 (1) 15–18.
26. Koksal M , Gokhan N, Kupeli E, Yesilada E and Erdogan H, Archives of Pharmacal Research, 2007, 30 (4) , 419-424.
27. Otto F.P, US Patent, 1972, 3, 649-229.
28. Qiu J.X, Wing Yip C and Chan A.S, The Journal of Organic Chemistry, 2003, 68 (4), 1589-1590.
29. Huang P.J.J, Youssef D, Cameron T.S and Jha A, Arkivoc, 2008, 16, 165–177.
30. Holla B.S, Shivananda M.K, Shenoy M.S and Antony G, Farmaco, 1998, 53 (8-9), 531–535.
31. Shivananda M.K and Prakash Shet P, Journal of Chemical and Pharmaceutical Research, 2011, 3 (2) 303–307.
32. Domling A, Curr. Opin. Chem, 2002, 6, 306-313.

International Journal of Multidisciplinary Research and Technology
ISSN 2582-7359, Peer Reviewed Journal, Impact Factor 6.325
www.ijmrtjournal.com

SYNTHESIS AND ANTIBACTERIAL ACTIVITY OF NOVEL BENZOFURAN ESTER DERIVATIVES

[1]Vijay D. Gangana, [2]Pradnya Lokhandeb, [3]Sharad G. Shilkandec, [4]Pradip S. Shelard and [5]Om Prakash Yadava

[1,5]Department of Chemistry, Reena Mehta College of Arts,
Commerce, Science and Management Studies, Bhayandar (W), Thane – 401107.
[2]Department of Chemistry, Bhavan's College of Arts,
Commerce and Science, Munshi Nagar, Andheri (West), Mumbai – 400058.
[3]Department of Chemistry, Sheth J. N. PaliwalaCollege of Arts,
Science and Commerece, Pali-Sudhagad, Dist. Raigad – 410205.
[4]Department of Chemistry, K. J. Somaiya college of Arts,
Science and Commerce, Mohinirajnagar, Kopargaon - 423601, Dist. Ahemadnagar.

Abstract: Dehydrodiisoeugenol constitute a new group of antimitotic and potential anticancer agents that inhibit tubulin polymerization. It is a benzofuranoid type neolignan have been synthesized and diversified to its ester / hybrid derivatives (DCC / DMAP / Pyridine / DCM) using conventional methods and characterized by 1H NMR, IR, Elemental analysis and mass spectral data. These synthesized compounds were screened for their potential antibacterial activity against Gram positive and Gram negative cultures. Few of them possess promising antibacterial activity.

Keywords: Benzofuran, Dehydrodiisoeugenol, 1H NMR, TOF MS ES, IR, Gram positive and Gram negative cultures, antibacterial etc.

Introduction

Heterocyclic synthesis has emerged as powerful technique for generating new molecules useful for drug discovery1. Heterocyclic compounds provide scaffolds on which pharmacophores can arrange to yield potent and selective drugs2. Benzofuran nucleus may be combined with nitrogen heterocycles in different ways. Several benzofuran compounds are reported to possess antibacterial3, antifungal4, anti-inflammatory5, antidepressant6, analgesic7 and hypoglycemic activities8. It has been pointed out that: benzofuran nucleus is very rarely associated with a nitrogen hetrocycle. In our present work, we are synthesizing dehydrodiisoeugenol9 by subjecting isoeugenol to oxidative coupling using iodobenzene diacetate in dichloromethane. It also shows pronounced antileishmanial, antiplasmodial activities and served as a suitable starting material for the synthesis of various bioactive molecules such as fragnasol B. Since it possess various biological activities, we decided to make a library of compounds using various permutation and combinations to come up with novel hybrid derivatives of dehydrodiisoeugenol using conventional methods. The objective of this study is to condense two molecules of the same disease domain to produce more potent candidate in the same disease domain or to condense two molecules of different disease domain to produce mixed variety of those disease domain or to have drug candidate with entirely different disease domain.

Experimental

2.1 Materials and Methods :

Chemicals used were of a laboratory grade. The reactions were monitored by TLC on aluminium-backed silica plate visualized by UV-light.Melting points were determined on a Thomas Hoover capillary melting point apparatus using digital thermometer.IR spectra were recorded on a Shimadzu FTIR Prestige model as KBr pellet. 1H NMR spectra were recorded on a Varian 400 MHz spectrometer in CDCl3. Chemical shifts were recorded in parts per million down field from tetramethyl silane. Mass spectra were recorded on a TOF MS ES mass spectrometer. Elemental analysis were carried out as a percentage on a Thermo finnigan, Flash EA 1112 series, Italy.

2.2 Results and Discussion

Synthesis of Dehydrodiisoeugenol :- To a stirred solution of [A] (4.0 g, 24.35 mmol) in dichloromethane (75 ml) was added dropwise a solution of IDA (2.5 g, 7.76 mmol) in dichloromethane (100 ml) at room temperature within 4 h and stirring was continued at room temperature for 48 h. Subsequently the same amount of IDA in dichloromethane (100 ml) was added within 4 h. After stirring, the reaction mixture at room temperature for 2 h., 3 g of solid NaHCO3 was added and the stirring was continued for 5 h. Subsequently, NaHCO3 was filtered off, and the solvent was evaporated to give a yellow oil, whose purification by flash chromatography on silica gel (n-hexane : ethyl acetate, 6 : 1) resulted in [C](1.4 g, 38 %) as white needles.with m.p. 132 – 1330C. 1H NMR (400 MHz, CDCl3)∂ppm :- 1.38 (d, J = 6.8 Hz, 3H, -CH3), 1.86 (d, J = 6.6 Hz, 3H, -terminal –CH3 frpm isoeugenol moiety), 3.4 – 3.5 (m, 1H, proton 'd'), 3.87 (s, 3H, Ar x –OCH3), 3.89 (s, 3H, Ar x –OCH3), 5.10 (d, J = 9.2 Hz, 1H, -benzylic proton 'c'), 5.64 (s, 1H, -OH, D2O exchangeable), 6.0 – 6.2 (m, 1H, olefinic proton 'a'), 6.36 (d, J = 15.8 Hz, 1H, -olefinic proton 'b'), 6-7 – 7.1 (m, 5H, ArH).

Scheme 1 :

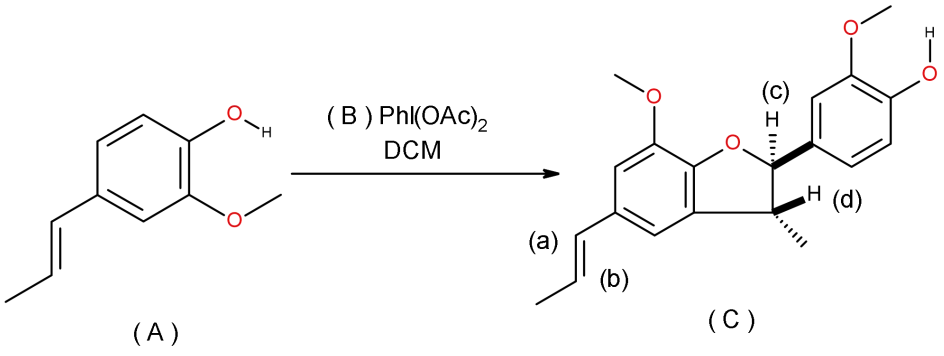

(A)

Isoeugenol

(C)

Dehydrodiisoeugenol

2.3 Diversification of Dehydrodiisoeugenol to its ester / hybrid molecules : - Compounds (1) to (4) [Table 1] were synthesized by following general method.

To a stirred solution of [A] (1 eq.) in 30 ml dichloromethane was added [C] (1.3 eq.), [D] (0.05 eq.), [E] (0.5 eq.) and stir the reaction mixture at room temperature for 5 min. To this, compound [B] (1.3 eq.) was added and stirring continued at at room temperature for next 8 h. As the reaction proceeds, urea derivative precipitates out as by product. The progress of the reaction is monitored by TLC for completion of reaction.

Work up :- The reaction mixture concentrated to minimum, preadsorbed on silica gel (100 – 200 mesh) and purified by column chromatography with increase in concentration of ethyl acetate in petroleum ether. The general yields of these reactions ranges between 50 – 60 %.

Scheme 2 :

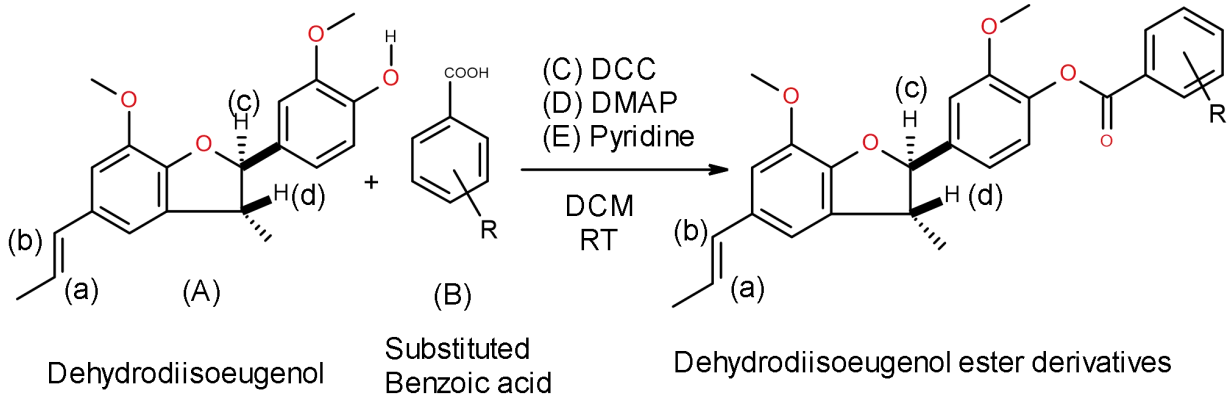

Table 1 : Dehydrodiisoeugenol ester / hybrid derivatives.

Compound No.	R
1	Benzoyl
2	4-Nitro benzoyl
3	3,4-Dimethoxy benzoyl
4	3,4,5-Trimethoxy benzoyl

Probable mechanism for fused / hybrid molecules :

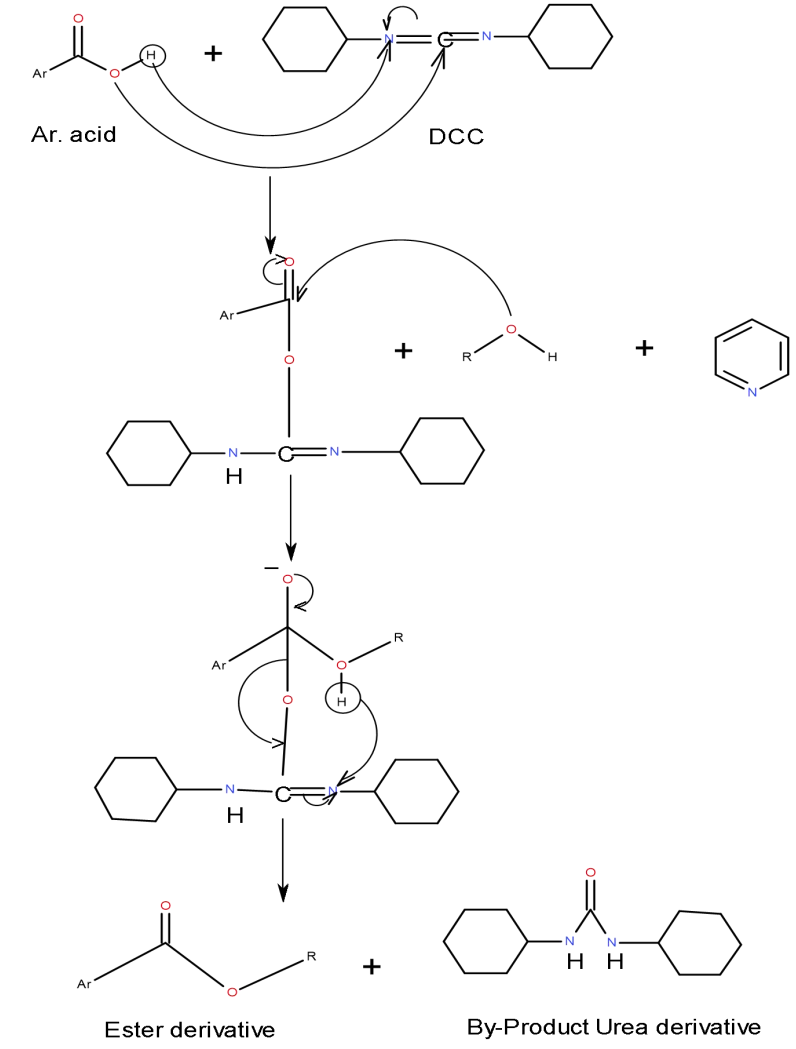

2.6 Characterization of compounds (1 - 4) :-

(1) [2-methoxy-4-[(2R,3R)-7-methoxy-3-methyl-5-[(E)-prop-1-enyl]-2,3-dihydrobenzofuran-2-yl]phenyl] benzoate :-

Off white solid; Molecular Formula C27H26O5; Melting Range 118 – 1200C; 1H NMR (400 MHz, CDCl3)∂ppm :- 1.43 (d, J = 6.8 Hz, 3H, -CH3), 1.87 (d, J = 6.5 Hz, 3H, -terminal –CH3 from isoeugenol moiety), 3.4 – 3.5 (m, 1H, proton 'd'), 3.81 (s, 3H, Ar x –OCH3), 3.91 (s, 3H, Ar x –OCH3), 3.90 (s, 3H, Ar x –OCH3), 5.19 (d, J = 9.0 Hz, 1H, -benzylic proton 'c'), 6.0 – 6.2 (m, 1H, olefinic proton 'a'), 6.36 (d, J = 15.6 Hz, 1H, -olefinic proton 'b'), 6.7 – 7.2 (m, 5H, ArH from dehydrodiisoeugenol moiety), 7.4 – 8.3 (m, 5H, ArH from benzoyl moiety). IR (KBr) cm-1: 3000 – 2800 (-CH stretching for methyl and methine group), 1730 (ester >C=O), 1610 - 1500 (aromatic); TOF MS : 431 (M + H); Elemental Analysis, Requires C 75.33 % H 6.09 % O 18.58 % Found C 75.30 % H 6.06 % O 18.61 %.

(2) [2-methoxy-4-[(2R,3R)-7-methoxy-3-methyl-5-[(E)-prop-1-enyl]-2,3-dihydrobenzofuran-2-yl]phenyl] 4-nitrobenzoate :-

Pale yellow solid; Molecular Formula C27H25NO7; Melting Range 125 – 1270C; 1H NMR (400 MHz, CDCl3)∂ppm :- 1.44 (d, J = 6.8 Hz, 3H, -CH3), 1.87 (d, J = 6.4 Hz, 3H, -terminal –CH3 from isoeugenol moiety), 3.4 – 3.6 (m, 1H, proton 'd'), 3.81 (s, 3H, Ar x –OCH3), 3.92 (s, 3H, Ar x –OCH3), 3.90 (s, 3H, Ar x –OCH3), 5.20 (d, J = 9.0 Hz, 1H, -benzylic proton 'c'), 6.0 – 6.2 (m, 1H, olefinic proton 'a'), 6.38 (d, J = 15.8 Hz, 1H, -olefinic proton 'b'), 6.7 – 7.2 (m, 5H, ArH from dehydrodiisoeugenol moiety), 8.2 – 8.6 (m, 5H, ArH from 4-nitro benzoyl moiety; IR (KBr) cm-1: 3000 – 2850 (-CH stretching for methyl and methine group), 1732 (ester >C=O), 1605 - 1500 (aromatic); TOF MS : 476 (M + H); Elemental Analysis, Requires C68.20 % H 5.30 % N 2.95 % O 23.55 % Found C 68.17 % H 5.27 % N 2.92 O 23.58 %.

(3) [2-methoxy-4-[(2R,3R)-7-methoxy-3-methyl-5-[(E)-prop-1-enyl]-2,3-dihydrobenzofuran-2-yl]phenyl] 3,4-dimethoxybenzoate :-

Off white solid; Molecular Formula C29H30O7; Melting Range 129 – 1310C; 1H NMR (400 MHz, CDCl3)∂ppm :- 1.43 (d, J = 6.7 Hz, 3H, -CH3), 1.88 (d, J = 8.2 Hz, 3H, -terminal –CH3 from isoeugenol moiety), 3.4 – 3.6 (m, 1H, proton 'd'), 3.82 (s, 3H, Ar x –OCH3), 3.91 (s, 3H, Ar x –OCH3), 3.96 (s, 3H, Ar x –OCH3), 3.97 (s, 3H, Ar x –OCH3), 5.19 (d, J = 9.0 Hz, 1H, -benzylic proton 'c'), 6.0 – 6.2 (m, 1H, olefinic proton 'a'), 6.34 (d, J = 15.8 Hz, 1H, -olefinic proton 'b'), 6.6 – 8.0 (m, 8H, ArH from dehydrodiisoeugenol and 3,4-dimethoxy benzoic acid moiety). TOF MS : 491 (M + H);IR (KBr) cm-1: 3000 – 2820 (-CH stretching for methyl and methine group), 1735 (ester >C=O), 1604 - 1500 (aromatic); Elemental Analysis, Requires C 71.00 % H 6.16 % O 22.83 % Found C 71.03 % H 6.13 % O 22.86 %.

(4) [2-methoxy-4-[(2R,3R)-7-methoxy-3-methyl-5-[(E)-prop-1-enyl]-2,3-dihydrobenzofuran-2-yl]phenyl]-3,4,5-trimethoxybenzoate :-

1H NMR (400 MHz, CDCl3)∂ppm :- 1.43 (d, J = 6.7 Hz, 3H, -CH3), 1.87 (d, J = 8.2 Hz, 3H, -terminal –CH3 from isoeugenol moiety), 3.4 – 3.6 (m, 1H, proton 'd'), 3.82 (s, 3H, Ar x –OCH3), 3.85 (s, 3H, Ar x –OCH3), 3.87 (s, 3H, Ar x –OCH3), 3.91 (s, 3H, Ar x –OCH3), 3.94 (s, 3H, Ar x –OCH3), 5.19 (d, J = 9.1 Hz, 1H, -benzylic proton 'c'), 6.0 – 6.2 (m, 1H, olefinic proton 'a'), 6.36 (d, J = 15.8 Hz, 1H, -olefinic proton 'b'), 6.7 – 7.3 (m, 5H, ArH from dehydrodiisoeugenol moiety), 8.2 – 8.6 (s, 2H, ArH from Gallic acid moiety).;IR (KBr) cm-1: 3000 – 2820 (-CH stretching for methyl and methine group), 1735 (ester >C=O), 1604 - 1500 (aromatic); TOF MS : 521 (M + H); Elemental Analysis, Requires C 69.22 % H 6.20 % O 24.59 % Found C 69.19 % H 6.17 % O 24.62 %.

Chromatographic system :

Column chromatography: For column chromatography 100 – 200 mesh Acme grade silica gel is used. The crude reaction mixture is concentrated under reduced pressure to yield crude mass which is preadsorbed on silica gel and purified by column chromatography with increase in concentration of Ethyl acetate in Petroleum ether. The fractions having similar 'rf' values were pooled together, concentrated and subjected for characterization using various spectroscopic techniques.

Thin layer chromatography : TLC plates were prepared using silica gel G (ACME, BOMBAY). Pet. ether: EtOAc (85 : 15) was used as the solvent system.

Radial chromatography : The circular glass plates of thickness 1 mm, were prepared by using silica gel (PF254, E. MERCK, 50 g) in cold distilled water (105 ml). For elution, gradually increasing concentrations of EtOAc in pet ether were employed

Biological Activity :

Antibacterial Activity using agar diffusion method10 :-

The synthesized molecules were screened for their antibacterial activity using agar diffusion method at 100 µm concentration against Gram positive (Staphylococcus aureus, Corynebacterium diphtheriae) and Gram negative (Escherichia coli, Klebsiella pneumonia, Salmonella typhi) bacterial species qualitatively. The results of the antibacterial activities are summarized in Table 3.

Table 3 : Antibacterial Activity Results

SAMPLE NO.	ACTIVE AGAINST
Dehydrodiisoeugenol	Staphylococcus aureus [Gram positive] Salmonella typhi [Gram negative] Klebsiella pneumoniae [Gram negative] Corynebacterium diphtheriae [Gram positive] Escherichia coli [Gram negative]
Std. Drug **Ampicillin**	Staphylococcus aureus [Gram positive] Salmonella typhi [Gram negative] Klebsiella pneumoniae [Gram negative] Corynebacterium diphtheriae [Gram positive] Escherichia coli [Gram negative]
2	Staphylococcus aureus [Gram positive] Klebsiella pneumoniae [Gram negative]

Conclusion :

The novel ester derivatives of dehydrodiisoeugenol were synthesized by cost effective industry viable process following the principle of green chemistry. The synthesis of ester derivatives is achieved using DCC as dehydrating agent in a reasonably good yield. The probable mechanism for the formation of ester derivative was also discussed.

The biological activity suggest that the base molecule dehydrodiisoeugenol have antimicrobial activity against both the bacterial cultures. Its derivative viz. 2 was also active against certain Gram + ve and Gram – ve cultures. Thus, ester derivative of dehydrodiisoeugenol (2) was potential antimicrobial candidate.

The structural diversity and the pronounced biological activities encountered in the benzofuran derivatives suggests that this class of compounds is worthy for further studies that may lead to derivatives by using combinatorial chemistry approach is an alternative strategy to new therapeutic discovery. In other words the generation of diverse benzofuran ester derivatives develop new therapeutic molecules that might result in candidates having better activity.

In depth analysis of these compounds through structure activity relationship studies would provide further insight and can be an interesting topic of future studies.

References :

1. Hermakens P. H., Ottenheijm H. C., Rees D. C. (1997). Solid-phase organic reactions II. A review of the literature. Tetrahedron, 53 (16), pp. 5643 - 5678. doi:10.1016/S0040-4020(97)00279-2
2. Gordon E., Barrett R. W., Dower W. J., Foder S. P. (1994). Applications of combinatorial technologies to drug discovery. Combinatorial organic synthesis, library screening strategies, and future directions.. J Med Chem, 37 (10), pp. 1385 - 1401. DOI: 10.1021/jm00036a001
3. Kirilmis C., Ahmedzade M., Süleyman S., Koca M., Kizirgil A. (2008). Synthesis and antimicrobial activity of some novel derivatives of benzofuran: Part 2. The synthesis and antimicrobial activity of some novel 1-(1-benzofuran-2-yl)-2-mesitylethanone derivatives Euro. J. Med. Chem., 43 (2), pp. 300 - 308.
4. Shazia N. A., Philip C. S., Sara J. P., Nigel C. V., David R. H. (2006). Synthesis of cicerfuran, an antifungal benzofuran, and some related analogues. Tetrahedron, 62 (17), pp. 4214 - 4226.

5. Balasaheb Y. M., Agasimundin Y. S., Shivkumar B., Devanand B. S. (2009). Microwave-assisted synthesis of benzofuran analogs of fenamates as non steroidal anti-inflammatory agents. J. Chil. Chem. Soc., 54 (1), pp. 77 - 79

6. Malik W. U., Mahesh V. K., Raishighani M. (1971). Synthesis of some benzofuranopyrazoles and benzofuranopyrimidines, two new heterocyclic systems. Indian J. Chem, 9, pp. 655 - 657.

7. Fry D. J., Ficken E. G., Burrows R. W. (1969). Brit.,1, pp. 168495.

8. Brady B. A., Kennedy J. A., Süllivan W. I. (1973). The configuration of aurones. Tetrahedron, 29 (2), pp. 359 - 362.

9. Juhász L., Kürti L., Antus S. (2000). Simple synthesis of benzofuranoid neolignans from Myristica fragrans. J. Nat. Prod. , 63 (6), pp. 866 - 870.

10. a) Finn R. K. (1959). Theory of Agar Diffusion Methods for Bioassay. Analytical Chem., 31 (6), 975 - 977. b) Al. lafi T. et. al.. (1995). The effect of the extract of the miswak (chewing sticks) used in Jordan and the Middle East on oral bacteria. International Dental Journal, 45 (3), pp. 218 - 222.

International Journal of Multidisciplinary Research and Technology
ISSN 2582-7359, Peer Reviewed Journal, Impact Factor 6.325
www.ijmrtjournal.com

IN-SILICO ANALYSIS OF NATURAL PRODUCTS DEMONSTRATING ANTI-NIPAH VIRUS ACTIVITY.

[1]Kulsoom Bano Z Sayed, [2]Deepa N Rangdal, [3]Anushka A Jadhav, [4]Shruti P Pardale, [5]Shubhangi P Patil

[1,2,4,5]Department of Chemistry, The Institute of Science, 15, Madam Cama Road, Mantralaya Fort, Mumbai, Maharashtra 400032, India
[3]Ramnarain Ruia Autonomous College, Matunga East, Mumbai, Maharashtra-400019

Abstract

Nipah virus, a paramyxovirus belonging to the genus henipavirus has the potential to cause a pandemic. Owing to its high mortality rate and less efficient medications, the development of an effective drug needs urgent attention. In this study, amongst the 6 proteins present in the viral body, the attachment glycoprotein was chosen as the target. High throughput screening of natural products was done to determine the potential inhibitor of the mentioned disease-causing protein. The screening was done based on the docking scores and ADMET profiles. Ribavirin, a broad-spectrum antiviral taken as the control, showed a -6.6 kcal/mol binding affinity. Whereas Vitedoin-B and alpha-Terpineol demonstrated binding affinities equal to -6.7 kcal/mol and -6.6 kcal/mol respectively. ADMET profiles of both the potential inhibitors are characterized by high absorption in the GI tract, good permeability through the BBB barrier, and no organ toxicity, unlike the control which is not BBB permeant, poorly absorbed by the GI tract and exhibits organ toxicity. Hence this study proposes that Vitedoin-B and alpha-Terpineol can be a potent lead component for Nipah virus.

Keywords: Nipah virus, natural products, *In-silico* analysis, high throughput screening, docking, ADMET

1. Introduction

Since its first outbreak in Malaysia in 1998, the Nipah virus (NIV), a member of the Henipavirus genus and Paramyxoviridae family, has constituted a serious threat to a number of nations, including Malaysia, Singapore, India, and the Philippines(1–4). The virus expanded to other areas after first appearing in Malaysia, frequently with significantly high death rates(1,2,5–9). The Bangladeshi and Malaysian strains of NIV are the two different strains that have been identified(9). It has been found that the latter is more virulent. India has also experienced incidences of this more hazardous strain because of its proximity to Bangladesh(2,8). Currently, there is only use of less efficient, broad-spectrum antivirals(3–5). Hence there is an urgent need for the development of drugs for this cause, for which natural products are gaining more attention these days as this is considered to be a less explored branch.

Because natural products and their derivatives typically have lower toxicity profiles than lab-manufactured drug molecules, their usage in therapeutic research is becoming more popular(10–12).

These substances have also shown encouraging outcomes in clinical studies. Numerous natural products have demonstrated efficacy against a variety of severe illnesses, such as COVID-19, HIV, cancer, drug-resistant tumours, HBV, inflammation, and malaria(13–29). Several instances of these substances, whose actions have been verified by science and documented in study articles and journals, include: *(-)-Neocaryachine*(16), *Lipojesaconitine*(16), *Taburnaemine A*(16,30), *Isochaihulactone*(16,18), *Ochrocephalamines B-D*(16), *Daphneodorins A & B*(16,20), *Kleinhospitine E*(16,21), *Beesioside*(16,21), *Myricetin*(16,18), *Chebulagic acid*(16), *Punicalagin*(16), *Ubonodin*(16), *Bifucatriol*(16,24), *Kakeromamide*(16,25), *Halymeniaol*(16,25), *8-Hydroxytytubulosine*(16), *3-α-Acetonyl-tabersonine*(16), *14,15-α-Epoxy-11-methoxytabersonine*(30), *Lochnerinine*(30), *19-I-Acetoxy-11-hydroxytabersonine*(30), *Gallinamide A*(19), *Santacruzamate A*(16,28), *Honaucin A*(16,29), *and 5,7,3',4'-Tetrahydroxy-2'-(3,3-dimethylallyl)isoflavone*(16).

This study seeks to identify novel Nipah virus therapeutics by incorporating computational approaches to natural products. In this research, we are thoroughly going to examine the *in-silico* properties of Vitedoin B and alpha-Terpineol, obtained post-completion of High Throughput Screening (HTS) of natural products from different Indian medicinal plants. This will be done in comparison with the control- Ribavirin, which is a broad-spectrum antiviral currently in use for NiV infections. PyRx, AutoDock Vina, SwissADME, ProTox-3.0, PyMOL, Biovia Discovery Studio are the software used in this study.

2. Material and Methods

2.1 Retrieval of the Structures

2vwd structure was obtained from PDB (). Before docking the, protein structure was prepared by adding charges, polar hydrogens, and deleting water molecules. This was done by using AutoDock. The prepared protein structure has been demonstrated in **Figure-1**

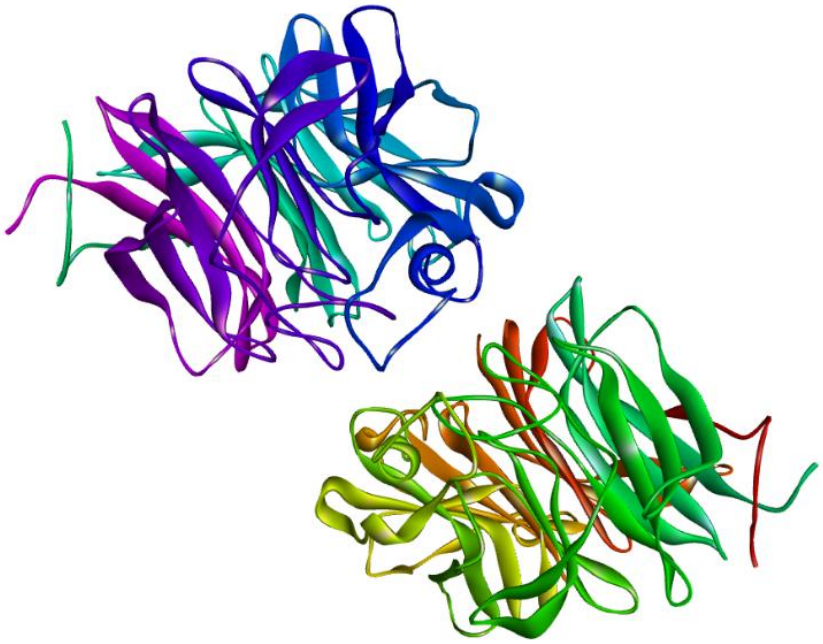

Figure-1 3D structure of the attachment glycoprotein (PDB ID: 2VWD) of NiV

Ligand structures were obtained from PubChem and IMPPAT database

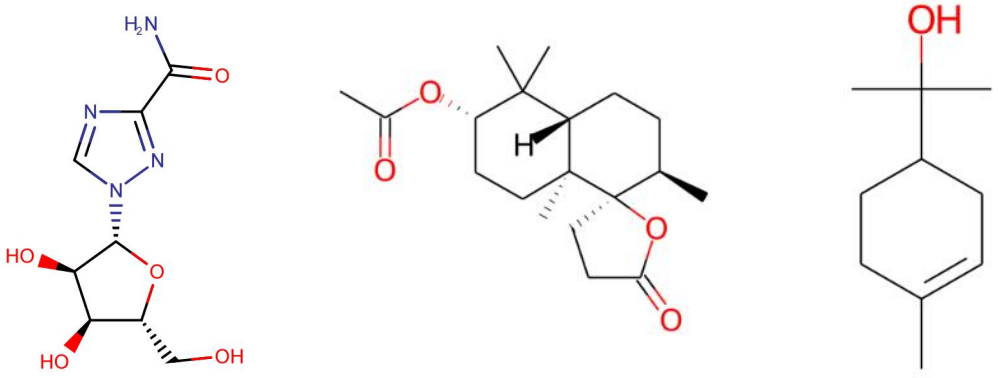

Control- Ribavirin **Vitedoin-B** **Alpha-Terpineol**

Figure-2 2D structures of the ligands- Ribavirin (control), Vitedoin B and Alpha-Terpineol

2.2 Molecular Docking

Ribavirin was first docked with 2VWD. The noted binding affinity for this complex was taken as the reference. After this the ligands- Vitedoin-B and alpha-Terpineol were docked with the protein and the binding scores were noted. Docking was done using PyRx first, followed by AutoDock to validate and confirm the docking scores. PyMOL and BIOVIA Discovery Studio were used for the visualisation of the protein-ligand complexes(31).

2.3 ADMET Profiling

The absorption, distribution, metabolism, excretion, and toxicity (ADMET) profiles of both the ligands and the control were investigated using SwissADME and ProTox-3.0. ProTox-3.0 was used to determine the toxicity class and organ toxicity whereas SwissADME provided a detailed analysis of the absorption, distribution, metabolism, and excretion properties of the control and both ligands helped generate bioavailability radar and BIOLED-Egg model.

3. Results and Discussions

3.1 Molecular Docking:

All ligands were docked with the attachment glycoprotein- 2VWD. During the course of docking, 9 poses were obtained for each ligand out of which, the pose having the highest negative binding affinity value with rmsd(ub) and rmsd(lb) having values as 0 were saved as the best post in PDB format. Binding affinity values for the control, Vitedoin B and alpha-Terpineol are -6.6 kcal/mol, -6.7 kcal/mol and -6.6 kcal/mol respectively. In Biovia Discovery studio visualization of the best pose with the prepared protein was done. Post completion of this step 2D diagrams were generated in Biovia Discovery studio to get a clear view of the types of bonds involved in protein-ligand complex formation and the amino acid residues of the protein actively participating in the bond formation with the ligands. **Figure-3** shows the protein-ligand complexes, its enlarged view showing the binding pocket, and the 2D diagram clearly stating the kinds of bonds involved in the protein-ligand complex formation.

A. Control

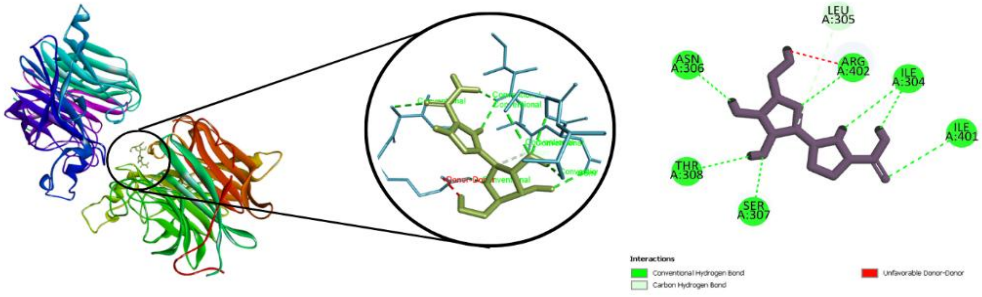

B. Vitedoin B

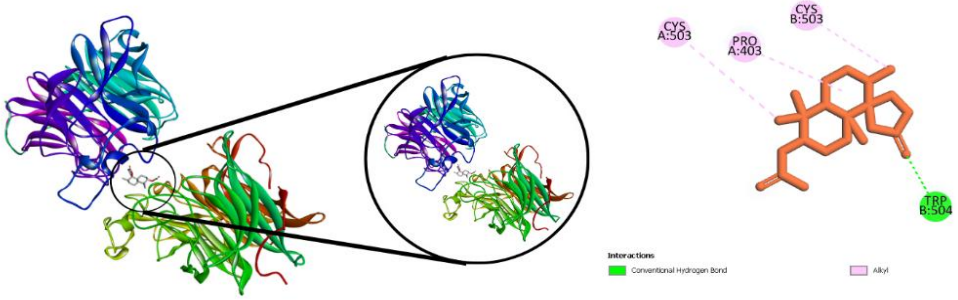

C. Alpha - Terpineol

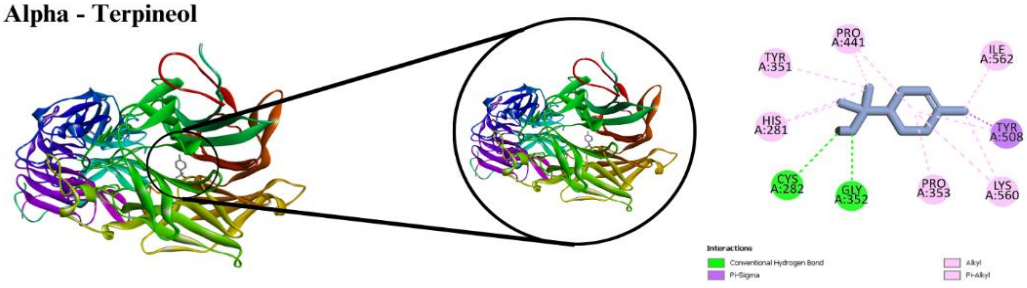

Figure- 3 Protein-Ligand complexes, enlarged view of the binding pocket and the 2D diagrams

Table 1: Docking results of control, Vitedoin B, Alpha-Terpineol

Molecules involved in binding with 2VWD	Binding affinity (kcal/mol)	Interacting active amino acid residue	Type of bond formed/ interaction observed	x, y, z co-ordinates of the binding site
Control	-6.6	ASP (A:219) HIS (A:281) CYS (A:282) LEU (A:221) PRO (A:353) ARG (A:248)	**Conventional hydrogen** **Conventional hydrogen** **Conventional hydrogen** **Pi- alkyl** **Pi- alkyl** **Unfavourable donor- donor**	x= -16.216292 y= -27.915792 z= -25.810083
Vitedoin B	-6.7	TYR (A:504)	**Conventional hydrogen**	x=-42.043783 y=-1.941174 z=-16.125174
Alpha-Terpineol	-6.6	CYS (A:282) GLY (A:352) ILE (A:562) PRO (A:441) TYR (A:508) TYR (A:508) LYS (A:560) LYS (A:560) PRO (A:353)	**Conventional hydrogen** **Conventional hydrogen** **Alkyl** **Alkyl** **Pi- sigma** **Pi- alkyl** **Alkyl** **Alkyl** **Alkyl**	x=-28.737750 y=-14.801500 z=-28.010667

Table 1 gives detailed information about the binding affinities, active amino acid residues of the protein involved in the formation of bond with the ligand and the coordinates of the binding site. The protein has 2 chains- chain A and B, the name of the chain to which the active amino acid residue belongs is given in parenthesis along with its residue number. In the table there are different kinds of bonds like- conventional hydrogen bonds, pi- alkyl, pi- sigma, alkyl and unfavorable donor-donor interactions that are formed between the protein and the ligand. The coordinates of the binding site give information about the binding pocket where the ligand is present. The control shows a non-favorable interaction whereas in Vitedoin-B and alpha-Terpineol there are all favourable interactions enhancing the stability and the docking score. The degree of enhancement varies for different kinds of bonds and can be given by the trend: **Greatly enhances** > **moderately enhances** > **reduces** based on the font colours used in the table.

3.2 ADMET Profiling:

Table 2: ADMET analysis of control, Vitedoin Band alpha-Terpineol using *in-silico* predictions

Ligands Descriptors		Control	Vitedoin B	Alpha-terpineol
	ID	37542	IMPHY001927	IMPHY012160
	Binding affinity	-6.6	-6.7	-6.6
	Toxicity class	5	5	5
Drug-likeness rules	Lipinski rule	Yes, 0 violations	Yes, 0 violations	Yes, 0 violations
	Veber rule	No	Yes	Yes
	Egan rule	No	Yes	Yes
Pharmacokinetics	BBB+/-	-	+	+
	P-gp substrate	No	No	No
	GI absorption	Low	High	High
	CYP450 inhibitors	None	None	None
Organ toxicity	Respiratory toxicity	Active	Inactive	Inactive
	Cardiotoxicity	Inactive	Inactive	Inactive
	Hepatotoxicity	Inactive	Inactive	Inactive
	Neurotoxicity	Active	Inactive	Inactive
	Nephrotoxicity	Active	Inactive	Inactive

Table 2 gives a detailed ADMET analysis of the control and the ligands (Vitedoin-B and alpha-Terpineol) usin *in-silico* predictions(32). It contains information about PubChem and IMPPAT ID, binding affinities, and toxicity class. alpha-Terpineol shows the same binding affinity as that of the control whereas Vitedoin B shows better binding affinity. The higher the negative value the better the interaction is. The control and the ligands fall in the toxicity level of class 5 within the ProTox-3.0 predicted model. Lipinski rule of 5, Veber rule, and Egan rule are drug-likeness rules. Vitedoin-B and alpha-Terpineol are seen not to violate any of the mentioned rules. On the other hand, the control only follows the Lipinski rule of 5. The absence of rule violation by the Vitedoin-B and alpha-Terpineol indicates that these compounds possess molecular properties to exhibit the desirable pharmacokinetic effect. BBB permeability, inhibitors, P-gp substrate, and GI Absorption details are also mentioned. Since the Nipah virus causes inflammation of the brain along with other symptoms, compounds with the ability to permeate through the blood-brain barrier (BBB)are considered ideal(1,5). Control doesn't demonstrate permeability through BBB but Vitedoin-B and alpha-Terpineol are BBB permeant. Additionally, out of the 3 studied compounds, none are predicted to be P-gp substrates. This is an indication that they are unlikely to be affected by P-gp efflux. This is considered a positive attribute of the molecule. P-gp efflux limits drug distribution and absorption. Control shows low absorption in the gastrointestinal tract (GI). Other Vitedoin-B and alpha-Terpineol show high absorption suggesting favourable oral bioavailability than the control. All three molecules are predicted not to inhibit major CYP450 enzymes (CYP1A2, CYP2C19, CYP2C9, CYP2D6, CYP2A4, CYP2E1). These enzymes are important to metabolize the drug. ProTox-3.0 considers hepatoxicity, neurotoxicity, respiratory toxicity, cardiotoxicity, and nephrotoxicity as organ toxicity parameters associated with the molecule(33). Control was predicted to be active in neurotoxicity, respiratory toxicity, and nephrotoxicity, while Vitedoin B and alpha-Terpineol were inactive across all tested organ toxicities. This result suggests a potentially more favorable safety profile for Vitedoin B and alpha-Terpineol than the control

Figure-4 Physicochemical radar for control, Vitedoin B, Alpha-Terpineol

The safe physicochemical region for a compound has been marked by a pink region in **Figure-4**. This region depicts the optimal ranges for different parameters like size, polarity, insolubility, unsaturation, flexibility, and lipophilicity and suggests if the compound is orally bioavailable. The colored zone represents the suitable physicochemical space for oral bioavailability(34). This space is characterized by specific ranges of values for the above-stated parameters. Lipophilicity (LIPO) is suitable when the XLOGP3 value falls between -0.7 and +5.0. Size is deemed suitable when the molecular weight is between 150 g/mol and 500 g/mol. Polarity is considered appropriate when the TPSA is between 20A² and 130A². Insolubility (INSOLU) is acceptable when the Log S (ESOL) is between -6 and 0. Instauration (INSATU) is appropriate when the Fraction Csp3 lies between 0.25 and 1. Flexibility (FLEX) is considered suitable when the number of rotatable bonds are in between 0 and 9. For the control, 1 point lies outside the safe region whereas for Vitedoin B and alpha-Terpineol, all points lie in the safe region suggesting good oral bioavailability for both.

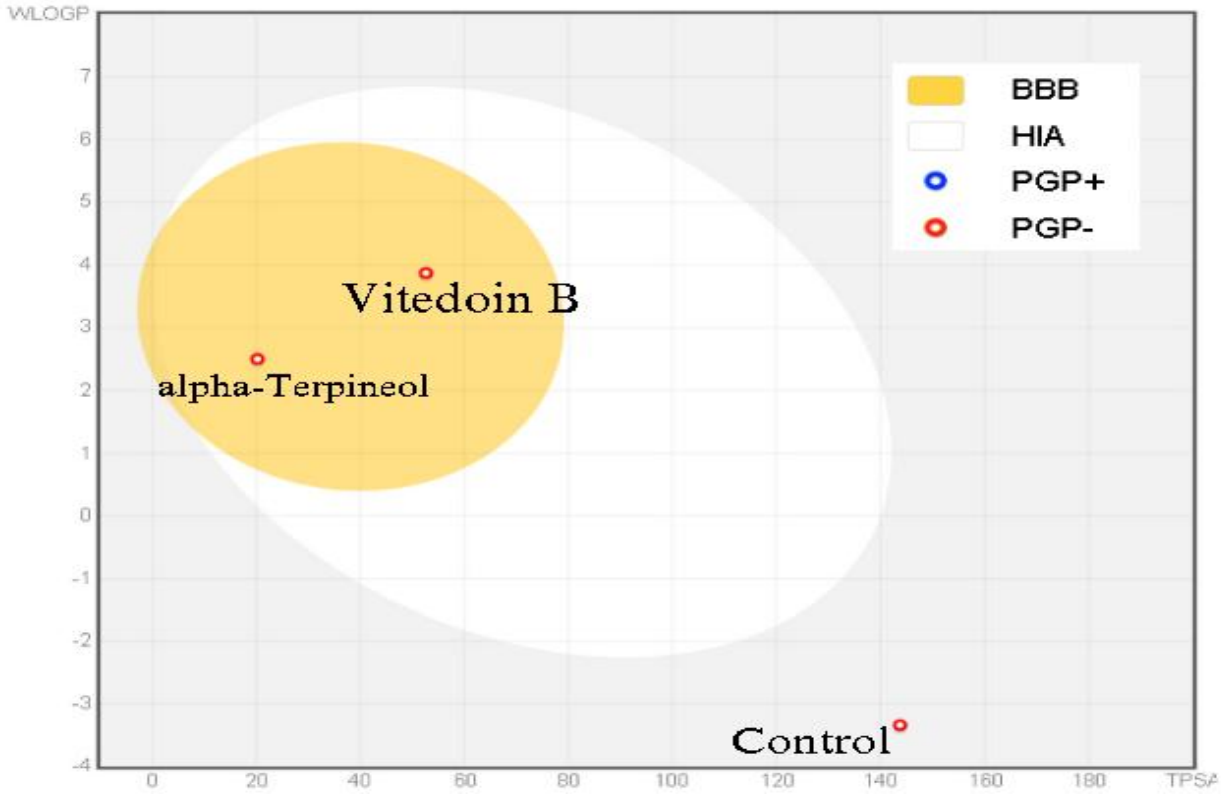

Figure-5 Boiled egg model

Figure-5 shows the BOILED-Egg model which gives information about the permeation through the blood-brain barrier

The BOILED-Egg model has 2 zones, the white and the yellow. The former predicts passive GI absorption and the latter states BBB permeability(34). As an anti-NiV medication, it is important for the molecule to permeate through the BBB hence the point should lie in the yellow zone (yolk region). Along with this, the molecule must not be a P-gp substrate as it would be effluated from the CNS by P-gp limiting its ability to fight against NiV. Thus it can be concluded that in this case, the dot should be red coloured and not blue. Both Vitedoin B and alpha-Terpineol are seen to fulfil all the important criteria.

4. Conclusion

This research suggests that Vitedoin B and alpha-Terpineol can act as potent lead components as anti-NiV medication since they demonstrate good binding affinities, favorable bonding interactions in complexation with the protein. ADMET studies characterized by BBB+, P-gp-, points lying in the safe region of the bioavailability radar as well as in the desired region of the BOILED-Egg model; also support the fact that these can turn out to be a good lead component.

Besides this, both Vitedoin B and alpha-Terpineol exhibit good ADMET profile, drug-likeness properties and low toxicity with no organ toxicity. Hence it can be concluded that these molecules should be taken ahead for research and development of novel NiV drug

Disclosure statement

No potential conflict of interest was reported by the author(s).

References

1. Dhananjay S, Kumari R, Kumar R. Recent Advancement and Novel Approaches of Nipah Virus: An Overview.
2. Nath A, Banerjee S, Poddar D, Kumar H, Mukherjee D, Parag Soni N, et al. Understanding the dynamics of nipah virus (NiV) transmission and outbreaks in India from Kerala's perspective. Future Health. 2024 Sep 26;2:158–61.
3. Saha O, Siddiquee NH, Akter R, Sarker N, Bristi UP, Sultana KF, et al. Antiviral Activity, Pharmacoinformatics, Molecular Docking, and Dynamics Studies of *Azadirachta indica* Against Nipah Virus by Targeting Envelope Glycoprotein: Emerging Strategies for Developing Antiviral Treatment. Bioinforma Biol Insights. 2024 Jan;18:11779322241264145.
4. Randhawa V, Pathania S, Kumar M. Computational Identification of Potential Multitarget Inhibitors of Nipah Virus by Molecular Docking and Molecular Dynamics. Microorganisms. 2022 Jun 9;10(6):1181.
5. Debroy B, De A, Bhattacharya S, Pal K. In silico screening of herbal phytochemicals to develop a Rasayana for immunity against Nipah virus. J Ayurveda Integr Med. 2023 Nov;14(6):100825.
6. Halpin K, Hyatt AD, Fogarty R, Middleton D, Bingham J, Epstein JH, et al. Pteropid Bats are Confirmed as the Reservoir Hosts of Henipaviruses: A Comprehensive Experimental Study of Virus Transmission. Am Soc Trop Med Hyg. 2011 Nov 1;85(5):946–51.
7. N. Jagtap M, T. Borade P, V. Bodake S, B. Darekar A. Enhancing the science in the Global transmission of Nipah virus. Asian J Pharm Res. 2024 Sep 20;295–302.
8. Paliwal S, Shinu S, Saha R. An emerging zoonotic disease to be concerned about - a review of the nipah virus. J Health Popul Nutr. 2024 Oct 28;43(1):171.
9. Tan FH, Sukri A, Idris N, Ong KC, Schee JP, Tan CT, et al. A systematic review on Nipah virus: global molecular epidemiology and medical countermeasures development. Virus Evol. 2024 Aug 7;10(1):veae048.
10. Domingo-Fernández D, Gadiya Y, Preto AJ, Krettler CA, Mubeen S, Allen A, et al. Natural Products Have Increased Rates of Clinical Trial Success throughout the Drug Development Process. J Nat Prod. 2024 Jul 26;87(7):1844–51.
11. Sharma N, Varma V, Verma S. Plant-Derived Compounds for Chemoprevention and Chemotherapy: From Molecular Mechanisms to Clinical Trials. In: George B, editor. Bioactive Compounds from Medicinal Plants for Cancer Therapy and Chemoprevention [Internet]. BENTHAM SCIENCE PUBLISHERS; 2024 [cited 2025 Jan 7]. p. 120–55. Available from: https://www.eurekaselect.com/node/233812
12. Elbadawi M, Efferth T. In Vivo and Clinical Studies of Natural Products Targeting the Hallmarks of Cancer. In Berlin, Heidelberg: Springer Berlin Heidelberg; 2024 [cited 2025 Jan 7]. (Handbook of Experimental Pharmacology). Available from: https://link.springer.com/10.1007/164_2024_716

13. Ribeiro-Filho J, Teles YCF, Igoli JO, Capasso R. Editorial: New trends in natural product research for inflammatory and infectious diseases: Volume II. Front Pharmacol. 2023 Jan 26;14:1144074.
14. Fijałkowski Ł, Skubiszewska M, Grześk G, Koech FK, Nowaczyk A. Acetylsalicylic Acid–Primus Inter Pares in Pharmacology. Molecules. 2022 Dec 1;27(23):8412.
15. Dasgeb B, Kornreich D, McGuinn K, Okon L, Brownell I, Sackett DL. Colchicine: an ancient drug with novel applications. Br J Dermatol. 2018 Feb;178(2):350–6.
16. Xu Z, Eichler B, Klausner EA, Duffy-Matzner J, Zheng W. Lead/Drug Discovery from Natural Resources. Molecules. 2022 Nov 28;27(23):8280.
17. Wu H, Ma G, Yang Q, Zhu Y, Huang L, Tian Y, et al. Discovery and synthesis of novel beesioside I derivatives with potent anti-HIV activity. Eur J Med Chem. 2019 Mar;166:159–66.
18. Su H, Yao S, Zhao W, Zhang Y, Liu J, Shao Q, et al. Identification of pyrogallol as a warhead in design of covalent inhibitors for the SARS-CoV-2 3CL protease. Nat Commun. 2021 Jun 15;12(1):3623.
19. Ashhurst AS, Tang AH, Fajtová P, Yoon MC, Aggarwal A, Bedding MJ, et al. Potent Anti-SARS-CoV-2 Activity by the Natural Product Gallinamide A and Analogues via Inhibition of Cathepsin L. J Med Chem. 2022 Feb 24;65(4):2956–70.
20. Otsuki K, Li W, Asada Y, Chen CH, Lee KH, Koike K. Daphneodorins A–C, Anti-HIV Gnidimacrin Related Macrocyclic Daphnane Orthoesters from *Daphne odora*. Org Lett. 2020 Jan 3;22(1):11–5.
21. Rahim A, Saito Y, Miyake K, Goto M, Chen CH, Alam G, et al. Kleinhospitine E and Cycloartane Triterpenoids from *Kleinhovia hospita*. J Nat Prod. 2018 Jul 27;81(7):1619–27.
22. Du R, Cooper L, Chen Z, Lee H, Rong L, Cui Q. Discovery of chebulagic acid and punicalagin as novel allosteric inhibitors of SARS-CoV-2 3CLpro. Antiviral Res. 2021 Jun;190:105075.
23. Jalil B, Rollinger JM, Atanasov AG, Singla RK, Kinghorn AD, Heinrich M. Core publications in drug discovery and natural product research. Front Nat Prod. 2024 Nov 11;3:1493720.
24. Smyrniotopoulos V, Merten C, Kaiser M, Tasdemir D. Bifurcatriol, a New Antiprotozoal Acyclic Diterpene from the Brown Alga Bifurcaria bifurcata. Mar Drugs. 2017 Aug 2;15(8):245.
25. Sweeney-Jones A, Gagaring K, Antonova-Koch J, Zhou H, Mojib N, Soapi K, et al. Antimalarial Peptide and Polyketide Natural Products from the Fijian Marine Cyanobacterium Moorea producens. Mar Drugs. 2020 Mar 18;18(3):167.
26. Meesala S, Gurung P, Karmodiya K, Subrayan P, Watve MG. Isolation and structure elucidation of halymeniaol, a new antimalarial sterol derivative from the red alga *Halymenia floresii*. J Asian Nat Prod Res. 2018 Apr 3;20(4):391–8.
27. Cheung-Lee WL, Parry ME, Zong C, Cartagena AJ, Darst SA, Connell ND, et al. Discovery of Ubonodin, an Antimicrobial Lasso Peptide Active against Members of the *Burkholderia cepacia* Complex. ChemBioChem. 2020 May 4;21(9):1335–40.
28. Pavlik CM, Wong CYB, Ononye S, Lopez DD, Engene N, McPhail KL, et al. Santacruzamate A, a Potent and Selective Histone Deacetylase Inhibitor from the Panamanian Marine Cyanobacterium cf. *Symploca* sp. J Nat Prod. 2013 Nov 22;76(11):2026–33.
29. Mascuch SJ, Boudreau PD, Carland TM, Pierce NT, Olson J, Hensler ME, et al. Marine Natural Product Honaucin A Attenuates Inflammation by Activating the Nrf2-ARE Pathway. J Nat Prod. 2018 Mar 23;81(3):506–14.
30. Zhang J, Wu Y, Li Y, Li S, Liu J, Yang X, et al. Natural products and derivatives for breast cancer treatment: From drug discovery to molecular mechanism. Phytomedicine. 2024 Jul;129:155600.
31. Kareti SR, P S. In Silico Molecular Docking Analysis of Potential Anti-Alzheimer's Compounds Present in Chloroform Extract of Carissa carandas Leaf Using Gas Chromatography MS/MS. Curr Ther Res. 2020;93:100615.
32. Paul Gleeson M, Hersey A, Hannongbua S. In-Silico ADME Models: A General Assessment of their Utility in Drug Discovery Applications. Curr Top Med Chem. 2011 Feb 1;11(4):358–81.
33. Shah A, Parmar B, Ghodawala M, Seth A. In silico drug discovery of novel small lead compounds targeting nipah virus attachment glycoprotein. J Integr Health Sci. 2018;6(2):60.
34. Daina A, Michielin O, Zoete V. SwissADME: a free web tool to evaluate pharmacokinetics, drug-likeness and medicinal chemistry friendliness of small molecules. Sci Rep. 2017 Mar 3;7(1):42717.

International Journal of Multidisciplinary Research and Technology
ISSN 2582-7359, Peer Reviewed Journal, Impact Factor 6.325
www.ijmrtjournal.com

SYNTHESIS & ANTIMICROBIAL EVALUATION OF SUBSTITUTED ARYLAZOPYRAZOLES AND ARYLHYDRAZONOPYRAZOLONES

[1]Vijay V. Dabholkar, [2]Dinesh Udawant, [3]Rahul Jaiswar
Organic Research Laboratory, Department of Chemistry
[1]Jai Hind College, Church gate, Mumbai-400 020,
[2,3] K.C. College, Church gate, Mumbai-400 020, INDIA.

Abstract:

A novel series of (3,5-dimethyl-4-(substituted phenyl diazenyl)-1H-pyrazol-1-yl)(2- (methylsulfonyl)-4-(trifluoromethyl)phenyl)methanone (5) and 3-methyl-1-(2- (methylsulfonyl)-4-(trifluoromethyl)benzoyl)-4-(2-substituted phenyl hydrazono)-1H- pyrazol-5(4H)-one (6) has been synthesized. The structural integrity of these compounds has been validated through IR, NMR, and Mass spectroscopy analyses. Selected compounds were evaluated for their antimicrobial properties against a range of bacterial and fungal strains. Notably, several of these compounds demonstrated remarkable antibacterial efficacy.

Keywords: pyrazoline-5-one, substituted aniline, hydrazine hydrate, hydrazide and antimicrobial activity.

Introduction:

Pyrazoles gained much attention as antimicrobial agents after the discovery of natural pyrazole C-glycoside pyrazofurin which showed broad spectrum antimicrobial activity[1]. The aryl-azo- pyrazoles are generally prepared by combination of aryl-azo-ethyl acetoacetate derivatives and hydrazine derivatives [2-6]. Hydrazide and their heterocyclised products display diverse biological activities including antibacterial, antifungicidal, analgesic, anti-inflammatory properties [7-14]. These heterocyclic systems find wide use in medicine, agriculture and industry. These heterocyclic systems find wide use in medicine, agriculture and industry. Incorporation of hydrazono and azo group has been reported to enhance the biological activity of heterocyclic compounds [15].

Considering the biological significance of the arylhydrazono group, arylazo group, pyrazolones, and pyrazoles, the design of arylazopyrazoles and arylhydrazonopyrazolones was undertaken. Subsequently, the target compounds were synthesized, and their antimicrobial properties were evaluated. This paper discusses the findings related to both antibacterial and antifungal activities.

Results And Discussion

3-(substituted phenyl-diazenyl)-pentane-2,4-dione **(2a-e)** was synthesized from substituted phenyl diazonium salts in conjunction with acetyl acetone. Similarly, ethyl 3-oxo-2- (substituted phenyl diazenyl)-butanoate **(3a-e)** was obtained through the reaction of substituted phenyl diazonium salts with ethyl acetoacetate. The preparation of 2-(methylsulfonyl)-4- (trifluoromethyl)-benzoic acid was conducted following established procedures [16], followed by esterification and condensation with hydrazine hydrate to yield the 2-(methylsulfonyl)-4- (trifluoromethyl)-benzohydrazide moiety **(4)**. When 2-(methylsulfonyl)-4-(trifluoromethyl)- benzohydrazide **(4)** was reacted with both 3-(substituted phenyl-diazenyl)-pentane-2,4-dione **(2a-e)** and ethyl 3-oxo-2-(substituted phenyl diazenyl)-butanoate **(3a-e)** in acetic acid, the target compounds (3,5-dimethyl-4-(substituted-phenyldiazenyl)-1H-pyrazol-1-yl)(2- (methylsulfonyl)-4-(trifluoromethyl)-phenyl)-methanone**(5a-e)** and 3-methyl-1-(2- (methylsulfonyl)-4-(trifluoromethyl)benzoyl)-4-(2-phenylhydrazono)-1H-pyrazol-5(4H)-one **(6a-e)** were produced, respectively. The structures of these compounds were verified using IR, NMR, and mass spectrometry techniques. Selected compounds underwent screening for their antimicrobial properties, revealing that several exhibited significant antibacterial activity.

Reaction Scheme

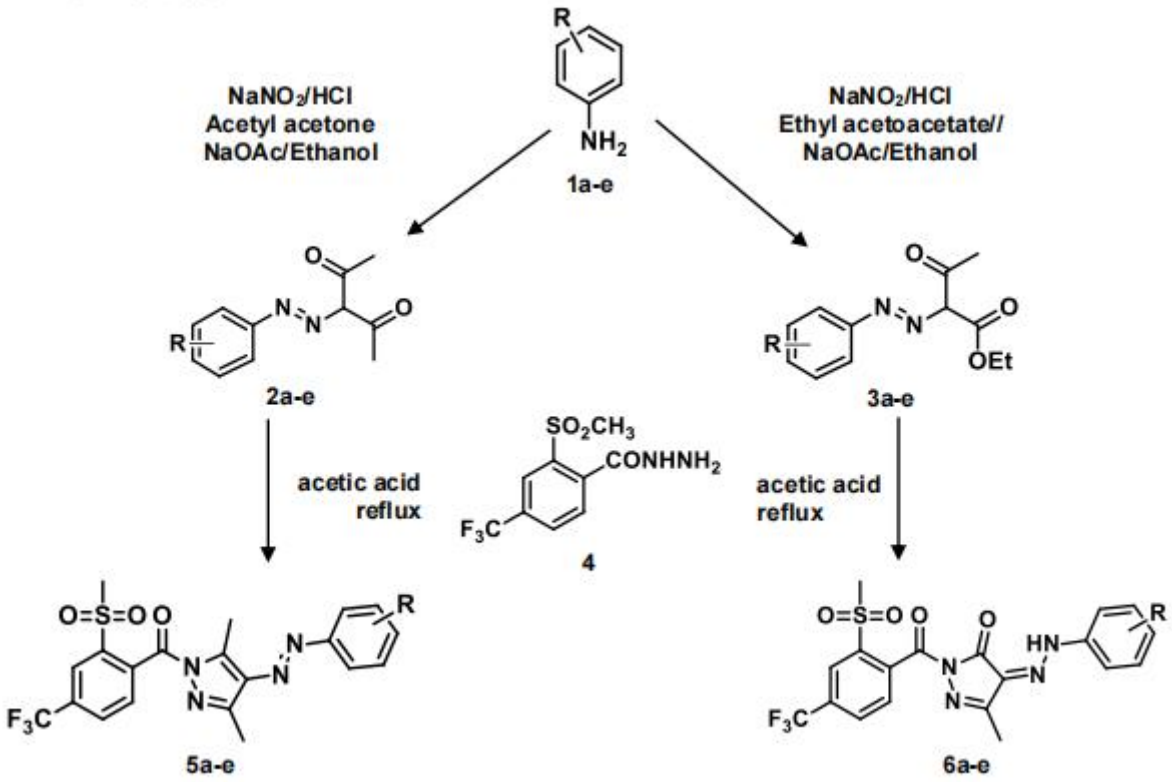

Experimental

Melting points of all synthesized compounds were determined in open capillary tubes on an electro thermal apparatus and are uncorrected. The progress of reaction was monitored by thin layer chromatography on silica gel coated aluminium plates (Merck) as adsorbent and UV light as visualizing agent. ^{1}H NMR and ^{13}C NMR spectra were recorded on Varian 500 MHz NMR spectrophotometer using CDCl3/DMSO-d6 as solvent and TMS as an internal standard (chemical shifts in δ ppm). C, H, N estimation was recorded on Carlo Erba 1108 (CHN) Elemental Analyzer.

Synthesis of 3-(substituted phenyl-diazenyl)-pentane-2,4-dione (2a-e) : General Procedure.

Substituted aniline (1a-e) (0.01 mole) was dissolved in a mixture of hydrochloric acid (8 mL) and water (6 mL) and subsequently cooled to 0 ˚C using an ice bath. A cold aqueous solution of sodium nitrate (0.03 mole) was then introduced. The resulting diazonium salt solution was filtered into a cooled mixture of acetyl acetone (0.01 mole) and sodium acetate (0.05 mole) in ethanol (50 mL) and stirred for a duration of 2-3 hours. The resultant solid was washed with water and recrystallized from ethanol, yielding 3-(substituted phenyl-diazenyl)-pentane-2,4- dione **(2a-e)**. The yields, melting points, and additional characterization data for these compounds are presented in Table I.

Synthesis of ethyl 3-oxo-2-(substituted phenyl diazenyl)-butanoate (3a-e):

Substituted aniline (1a-e) (0.01 mole) was dissolved in a mixture of hydrochloric acid (8 mL) and water (6 mL) and subsequently cooled to 0 ˚C using an ice bath. A cold aqueous solution of sodium nitrate (0.03 mole) was then introduced. The resulting diazonium salt solution was filtered into a cooled mixture of ethyl acetoacetate (0.01 mole) and sodium acetate (0.05 mole) in ethanol (50 mL) and stirred for a duration of 2-3 hours. The resultant solid was washed with water and recrystallized from ethanol, yielding ethyl 3-oxo-2-(substituted phenyl diazenyl)- butanoate (3a-e). The yields, melting points, and additional characterization data for these compounds are presented in Table I.

The physical characterization of synthesized compound **(2a-e)** and **(3a-e)** was given in **Table I**.

Table-I Physical data of compounds (2a-e) and **(3a-e)**

Compounds	R	M.P. (°C)	Yield (%)
2a	H	78-81	63
2b	4-Cl	79-82	69
2c	4-CH_3	81-84	58
2d	2-OCH_3	71-74	71
2e	2-Cl	86-89	78
3a	H	58-61	70
3b	4-Cl	74-77	74
3c	4-CH_3	76-79	68
3d	2-OCH_3	93-97	64
3e	2-Cl	78-81	66

Synthesis of (3,5-dimethyl-4-(substituted-phenyldiazenyl)-1H-pyrazol-1-yl)-(2-(methyl sulfonyl)-4-(trifluoromethyl)-phenyl)-methanone (5a-e)

General Procedure.

To a solution of 3-(substituted phenyl-diazenyl)-pentane-2,4-dione (2a-e) (0.002 mole) in 20 mL of glacial acetic acid, a 25 mL solution of 2-(methylsulfonyl)-4-(trifluoromethyl)- benzohydrazide (4) (0.002 mole) was introduced. The resulting mixture was subjected to reflux for a duration of 10 to 12 hours. Following this, the mixture was allowed to cool and stand overnight. The resultant product was then filtered, rinsed with cold water, and purified through recrystallization from ethanol, yielding the desired product (5a-e).

Synthesis of 3-methyl-1-(2-(methylsulfonyl)-4-(trifluoromethyl)-benzoyl)-4-(2- phenylhydrazono)-1H-pyrazol-5(4H)-one (6a-e)

General Procedure.

To a solution of ethyl 3-oxo-2-(substituted phenyl diazenyl)-butanoate **(3a-e)** (0.002 mole) in 20 mL of glacial acetic acid, a 25 mL solution of 2-(methylsulfonyl)-4-(trifluoromethyl)- benzohydrazide (4) (0.002 mole) was introduced. The resulting mixture was subjected to reflux for a duration of 10 to 12 hours. Following this, the mixture was allowed to cool and stand overnight. The resultant product was then filtered, rinsed with cold water, and purified through recrystallization from ethanol, yielding the desired product (6a-e).

The spectral analysis of representative compounds will be as follows:

(3,5-dimethyl-4-(phenyldiazenyl)-1H-pyrazol-1-yl)(2-(methylsulfonyl)-4-(trifluoromethyl)- phenyl)-methanone (5a):

Brownish yellow solid, yield 73%; **m.p.** (°C): 183-187; **IR** (KBr, cm-1): 3037-3085 (Ar. C- H), 1545-1565 (C=N), 1725 (C=O), **^{1}H NMR** (500 MHz, DMSO, δ ppm): 2.53 (s, 3H, CH_3), 2.93 (s, 3H, CH_3), 3.81 (s, 3H, CH_3), 7.13-8.21 (m, 8H, Ar-H) ppm,**^{13}C NMR** (500 MHz, DMSO, δ ppm): 14.1 (CH_3), 20.1 (CH_3), 49.46 (CH_3), 101.3-150.2 (C=C, Ar-C), 155.3 (C=N), 162.3 (C=O), **Mass:** EI MS m/z: 451.41 $[M+1]^+$

(3,5-dimethyl-4-(p-tolyldiazenyl)-1H-pyrazol-1-yl)(2-(methylsulfonyl)-4-(trifluoromethyl)- phenyl)-methanone (**5c**):

Dark pale yellow solid, yield 69%; **m.p.** (°C): 191-194; **IR** (KBr, cm-1): 3069-3100 (Ar. C- H), 1565-1595 (C=N), 1695 (C=O), **^{1}H NMR** (500 MHz, DMSO, δ ppm): 2.43 (s, 6H, 2-CH_3), 2.83 (s, 3H, CH_3), 3.61 (s, 3H, CH_3), 7.29-8.37 (m, 7H, Ar-H) ppm,**^{13}C NMR** (500 MHz, DMSO, δ ppm): 12.1 (CH_3), 18.3 (CH_3), 24.2 (CH_3), 48.96

(CH3), 104.1-152.3 (C=C, Ar-C), 149.1 (C=N), 161.5 (C=O), **Mass:** EI MS m/z: 465.12 $[M+1]^+$

(Z)-3-methyl-1-(2-(methylsulfonyl)-4-(trifluoromethyl)-benzoyl)-4-(2-phenylhydrazono)-1H- pyrazol-5(4H)-one (6a):

Dark yellow solid, yield 71%; **m.p.** (°C): 179-184; **IR** (KBr, cm-1): 3177 (NH), 3059 (Ar. C- H), 1625-1649 (C=N), 1729 (C=O), **^{1}H NMR** (500 MHz, DMSO, δ ppm): 2.43 (s, 3H, CH3), 3.73 (s, 3H, CH3), 6.9 (s,1H, NH), 7.13-8.21 (m, 8H, Ar-H) ppm, **^{13}C NMR** (500 MHz, DMSO, δ ppm): 16.1 (CH3), 21.1 (CH3), 50.46 (CH3), 111.3-154.2 (Ar-C), 152.3 (C=N), 161.2 & 165.5 (2XC=O), **Mass:** EI MS m/z: 453.41 $[M+1]^+$

(Z)-3-methyl-1-(2-(methylsulfonyl)-4-(trifluoromethyl)-benzoyl)-4-(2-(p-tolyl)-hydrazono)-1H-pyrazol-5(4H)-one (**6c)**:

Dark brownish yellow solid, yield 74%; **m.p.** (°C): 182-185; **IR** (KBr, cm-1): 3157 (NH), 3039-3088 (Ar. C-H), 1610-1639 (C=N), 1719 (C=O), **^{1}H NMR** (500 MHz, DMSO, δ ppm): 2.49 (s, 6H, 2-CH3), 3.51 (s, 3H, CH3), 6.79 (s,1H, NH), 7.09-8.47 (m, 7H, Ar-H) ppm,**^{13}C NMR** (500 MHz, DMSO, δ ppm): 15.1 (CH3), 23.1 (CH3), 54.21 (CH3), 115.3-157.4 (Ar-C), 151.5 (C=N), 160.4 & 164.1 (2XC=O), **Mass:** EI MS m/z: 467.10 $[M+1]^+$

Antimicrobial Evaluation

Antibacterial activities

The antibacterial properties of all compounds were evaluated against gram-positive bacteria (Bacillus subtilis and Staphylococcus aureus) as well as gram-negative bacteria (E. coli, Salmonella typhi, and Klebsiella pneumoniae) at a concentration of 50 µg/mL utilizing the agar cup plate method [17]. A methanol system served as the control in this experiment. Additionally, a control experiment was conducted under the same conditions, employing tetracycline as a standard for comparison. The area of inhibition of measured in millimetres Table II.

TABLE II: Antibacterial Activity of compound 5 and 6

Antibacterial Activity of compound 5 and 6					
Comp.	**Zone of inhibition (in mm)**				
	Gram Positive		**Gram negative**		
	Bacillus subtilis	**hylococcus aureus**	**Klebsiella promioe**	**monella typhl**	**E.coli**
5a	49	42	48	46	65
5b	51	47	54	51	59
5c	69	43	71	62	61
5d	65	46	72	63	58
5e	41	40	62	41	52
6a	59	43	49	52	53
6b	61	41	53	51	55
6c	57	44	47	56	51
6d	55	43	51	59	57
6e	58	47	56	54	59
Tetracycline	79	55	84	73	72

Antifungal activity

The fungicidal efficacy of all compounds was evaluated at a concentration of 1000 ppm against the in vitro plant pathogenic organisms detailed in Table III. The antifungal properties of each sample were assessed on these specific plant pathogenic strains using potato dextrose agar (PDA) medium. This PDA medium was prepared with 200 grams of potato, 20 grams of dextrose, 20 grams of agar, and 1 litre of water, utilizing five-day-old cultures. The

compounds intended for testing were suspended at 1000 ppm in the PDA medium and subsequently autoclaved at 120 °C for 15 minutes under 15 atm pressure. Following autoclaving, the medium was transferred into sterile Petri dishes, and the organisms were inoculated after the plates had cooled. The percentage inhibition of fungal growth was calculated after a period of five days using the formula provided below.

Percentage of inhibition = 100(X-Y)/X Where, X: Area of colony in control plate,

Y: Area of colony in test plate

TABLE III: Antifungal Activity of compound 5 and 6

Antifungal Activity of compound 5 and 6				
Comp.	**Zone of inhibition at 1000ppm**			
	C. albicans	**Penicillium Ex.**	**A. niger**	**Trichothesium Sp.**
5a	61	57	66	55
5b	68	61	62	63
5c	62	57	56	65
5d	71	59	68	67
5e	63	55	66	59
6a	59	63	61	58
6b	51	69	53	64
6c	61	53	58	53
6d	55	62	59	61
6e	67	66	61	65

Conclusion

In summary, we have synthesized a novel series of (3,5-dimethyl-4-(substituted phenyl diazenyl)-1H-pyrazol-1-yl)(2-(methylsulfonyl)-4-(trifluoromethyl)phenyl)methanone (5) and 3-methyl-1-(2-(methylsulfonyl)-4 (trifluoromethyl)benzoyl)-4-(2-substituted phenyl hydrazono)-1H-pyrazol-5(4H)-one (6) compounds. It is evident that the synthesized compounds are biologically active.

Acknowledgements.

The authors express their gratitude to the Management of K. C. College and Jai Hind College in Mumbai, India, for their unwavering support and for providing the essential facilities. Additionally, the authors extend their thanks to The Director of TIFR Mumbai for the provision of the spectral data.

References:

1. A. Bekhit et.al., Eur. J. Med. Chem. 43 (2008) 456–463.
2. P.J. Shah, B.P. Patel and H.S. Patel, Journal of the University of Chemical Technology and Metallurgy, 2012, 47(3), 257.
3. P. J. Shah, H. S. Patel and B. P. Patel, Elixir Org. Chem.,2011,37,3623.
4. P.Patel, H.S.Patel and P.J.Shah, Bulgarian Chemical Communications, 2010, 42(4), 274.
5. M.Amir, S. M. Hasan and A.Wadood, Orient J Chem., 2002, 18(2), 351.
6. V. Dabholkar & Rahul Gavande, J.Serb.Chem.Soc. 68(10)723–727(2003)
7. N. Terzioglu, A.Gursoy, Eur. J. Med. Chem., 2003, 38,781.
8. Y.Janin, Bioorg. Med. Chem., 2007, 15, 2479.
9. S. G. Kucukguzel, E. E. Oruc, S.Rollas, F.Sahin, A.Ozbek, Eur. J. Med. Chem., 2002, 37,197.
10. R Kalsi, M Shrimali, T. N.Bhalla, J. P.Barthwal, Indian J. Pharm. Sci., 2006, 41, 353.
11. M. R.Rao, K.Hart, N.Devanna, and K. B. Chandrasekhar, Asian J. Chem., 2008, 20, 1402.

12. Nayyar, R.Jain, Curr. Med. Chem., 2005,12,1873.
13. Kaymakcioglu, K. B.; Eur. J. Med. Chem, 2006, 41, 1253.
14. E.Gursoy, N.Guzeldemirci-Ulusoy, Eur. J. Med. Chem., 2007, 42,320.
15. P.V. Ramana, L.K. Ravindranath, J. Ind Chem. Soc. 76 (1999) 112–113.
16. Rhone Poulenc agriculture Ltd., EP0527036 A, 1992
17. Barry, A. L. The Antimicrobial Susceptibility Test: Principal and Practices, 4th ed., Philadelphia: Illuslea and Feger, 1976, 180.

International Journal of Multidisciplinary Research and Technology
ISSN 2582-7359, Peer Reviewed Journal, Impact Factor 6.325
www.ijmrtjournal.com

"HARNESSING MICROBIAL FUEL CELLS FOR SUSTAINABLE BIOELECTRICITY GENERATION"

[1]Aditi Rajesh Iyer, [2]Isha Vishwakarma, [3]Shreyas Surve, [4]Mrunalini Sambhare, [5]Pooja Mehta

[1]Student, Shri Vile Parle Kelavani Mandal's Mithibai College of Arts, Chauhan Institute of Science & Amrutben Jivanlal College of Commerce and Economics (Empowered Autonomous), Mumbai

[2]Student, Shri Vile Parle Kelavani Mandal's Mithibai College of Arts, Chauhan Institute of Science & Amrutben Jivanlal College of Commerce and Economics (Empowered Autonomous), Mumbai(Maharashtra), India

[3]Student, Shri Vile Parle Kelavani Mandal's Mithibai College of Arts, Chauhan Institute of Science & Amrutben Jivanlal College of Commerce and Economics (Empowered Autonomous), Mumbai(Maharashtra), India

[4]Faculty, Shri Vile Parle Kelavani Mandal's Mithibai College of Arts, Chauhan Institute of Science & Amrutben Jivanlal College of Commerce and Economics (Empowered Autonomous), Mumbai

Abstract:

Microbial Fuel Cells (MFC) are bio-electrochemical devices seeking to utilize the Extracellular Electron Transfer (EET) mechanisms seen in Exo-Electrogenic Microbes commonly found in wastewater and can be considered an alternative electricity generation source. In this study, we aimed to devise a small-scale and cost-effective MFC using readily available materials to generate an electrical current and to evaluate the efficiency of substrates capable of generating the highest amount of electrical current. Sewage Water, organic fertilizer, and enhancers were tested for obtaining voltage and current recorded by a multimeter, over 5 days. The sewage water generated the highest voltage, peaking at 0.029V and 0.072 mA, after 48 hours. Isolation from the sewage water setup was carried out on a Thioglycolate agar and Methylene blue agar to check for dye reduction and exo-electrogenic activity. The isolates showing halo on the agar were purified on slants and reinoculated in a synthetic wastewater MFC and showed current and voltage outputs of 0.003 V and 0.008 mA, confirming their exo-electrogenic activity. The isolate showing more promising results in terms of producing voltage and current output, was found to be Gram-positive Bacillus spp. It was further identified by 16srRNA sequencing. Further studies using electrogenic isolates will be required to determine the true potential of MFCs to provide a sustainable sewage treatment facility.

Keywords: Microbial Fuel Cells (MFC), Extracellular Electron Transfer (EET), Exo- Electrogenic Microbes.

Introduction:

The advent of bio-electrochemical systems (BES), most notably, the Microbial Fuel Cell (MFC) and Microbial Electrolysis Cell (MEC) has opened up a wide array of research opportunities in utilising microorganisms as catalysts in varying industrial functions such as bioelectricity generation, microbial electrosynthesis (MES), microbial desalination cells (MDC) etc (Logan et al., 2019; Semenec & E Franks, 2015). Resource scarcity and lack of sustainable waste remediation technologies, along with the countdown of fossil fuel depletion to climate change demand an urgent requirement for sustainable technologies to produce energy and bioremediate wastes (Liu et al., 2017; Logan et al., 2019; Yee et al., 2020).

The biofilms occurring on electrically active substrates comprise a complex matrix of extracellular polymeric substances made up of polysaccharides, lipids, and nucleic acids. Studies of these biofilms have revealed natural processes of Extracellular Electron Transfer (EET) generally attributed to interactions between bacteria and/or other electrically active substrates (Dolch et al., 2014; Semenec & E Franks, 2015). Electroactive microorganisms possessing capabilities of EET to and from solid-state electron acceptors and donors, provide opportunities for simultaneous bioelectricity generation with waste bioremediation technologies (Liu et al., 2017; Lovley & Holmes, 2022; Obi & Asogwa, 2015).

A MFC exploits this ability of bacteria to donate catabolic electrons to an anaerobic anode to generate a reduction potential in the anode half-cell, that allows the electrical energy to multiply as the bacteria grow in the anodic chamber. These electrons are transported outside the cell using c-type cytochromes, as a result of metabolic breakdown of nutrients (Dolch et al., 2014; Rabaey et al., 2004). Electricity generation from MFCs is a widely researched topic, and yet, few have found current densities large enough for household grids (Dolch et al., 2014; Pant et al., 2010). Defined substrates such as Glucose, Acetate, Lactate, Glycerol and Synthetic Wastewater tend to show higher current and voltage output (Sonawane et al., 2022). However, complex substrates such as Domestic,

Municipal and Industrial Wastewater show a comparatively lower outage (Sonawane et al., 2022). The choice of specific electrodes, either metal oxides or composite-based materials also affects the performance of an MFC. (Yaqoob et al., 2020).

This research aims to contribute to this existing path of research by devising a small-scale MFC to isolate and identify potential exo-electrogens from domestic wastewater samples and to assess their electrogenic capacity.

Material and methods:

Constructing a dual-chambered microbial fuel cell

A dual-chambered H-cell was constructed to be operated under batch conditions for 5 days. (Fig 1.) Three substrates were utilized for preliminary runs of the MFC: domestic sewage water sample (acquired from BMC Sewage Treatment Plant, Malad West), domestic sewage water + Fluid Thioglycollate Medium, and domestic Sewage water with organic fertilizer (1g). The total volume of the substrates used was 300 ml and was kept in the anodic chamber of the H- cell. The cathodic chamber comprised 300 ml of 10 mM, pH 7 phosphate buffer for good conductivity and provision of oxygen as an electron acceptor. The two chambers were constructed using 500ml polyethylene terephthalate (PET) bottles. The salt bridge consisted of a 12 cm poly vinyl chloride (PVC) pipe (diameter 1.5 cm) which was filled with the salt bridge solution composed of agar (100 g/L) and KCL, NaCl and KNO_3 salts (0.5g each). Graphite rods were used as the electrodes, with 50% of its length dipped in the substrate and buffer solutions respectively. The junctions of the salt bridge and the inserted graphite electrodes were sealed with epoxy resin to maintain microaerophilic conditions in the anodic chamber and prevent leakage of the solutions. The electrodes were connected in a series mode with a 100- ohm resistor and insulated copper wires. Measurements of current and voltage were recorded using a digital multimeter at an interval of one day. Each MFC set-up was run for approximately five days until a significant reduction of current is recorded due to depletion of nutrients. All apparatus were disinfected thoroughly with absolute alcohol. Salt bridge, media and phosphate buffer were autoclaved at 121^{o}C/15psi for 20 min.

Isolation of Exo-electrogens:

After running the setup and obtaining a steady current and voltage output, an aliquot of the substrate was taken from the cell and used for isolation of exo-electrogenic bacteria on a novel media by (Nazeer & Fernando, 2022) (g/L) (Glucose-2, NH_4Cl-0.46, yeast extract-0.1, peptone-0.5, K_2HPO_4-5.05, KH_2PO_4- 2.84, MnO_2-1.5, cysteine-0.025 and agar–15), Thioglycollate media supplemented with MnO_2 (1.5g of agar in 100 ml and 0.15g of MnO_2), and a Methylene Blue Media (nutrient agar made in 100 ml with the addition of a few crystals of methylene blue dye till sky blue). Colonies exhibiting halo on novel media indicated the presence of exo-electrogens. The principle follows the ability of exo-electrogens to transport electrons out of their cell walls. This is indicated by clearance around the colony due to a reduction of Manganese dioxide (Mn^{4+}) added to the molten agar to a reduced form (Mn^{2+}) incorporated in the medium. Cysteine was added to scavenge residual oxygen.

Evaluation of power generation in MFC using isolated exo-electrogens

The colonies showing clearance were isolated into pure culture and preserved on slants. The pure culture was used as an inoculum in the anode containing synthetic wastewater comprising Fructose (161.0 mg/L), Glucose (161.0 mg/L), $NaHCO_3$ (111.0 mg/L), KH_2PO_4 (44.5 mg/L), $(NH_4)SO_4$ (74.2 mg/L), $MgCl_2$ (37.1 mg/L), $CaCl_2$ (30.7 mg/L) and $(NH_4)_2Fe(SO_4)_2$ (3.1 mg/L) (Potrykus *et al.*, 2021). The current and voltage output produced confirmed the pure culture as a definite exo-electrogen.

16S rRNA Sequencing of pure culture exo-electrogen

The pure culture that demonstrated positive results for exo-electrogenic activity was analysed using 16S rRNA sequencing, for identification purposes.

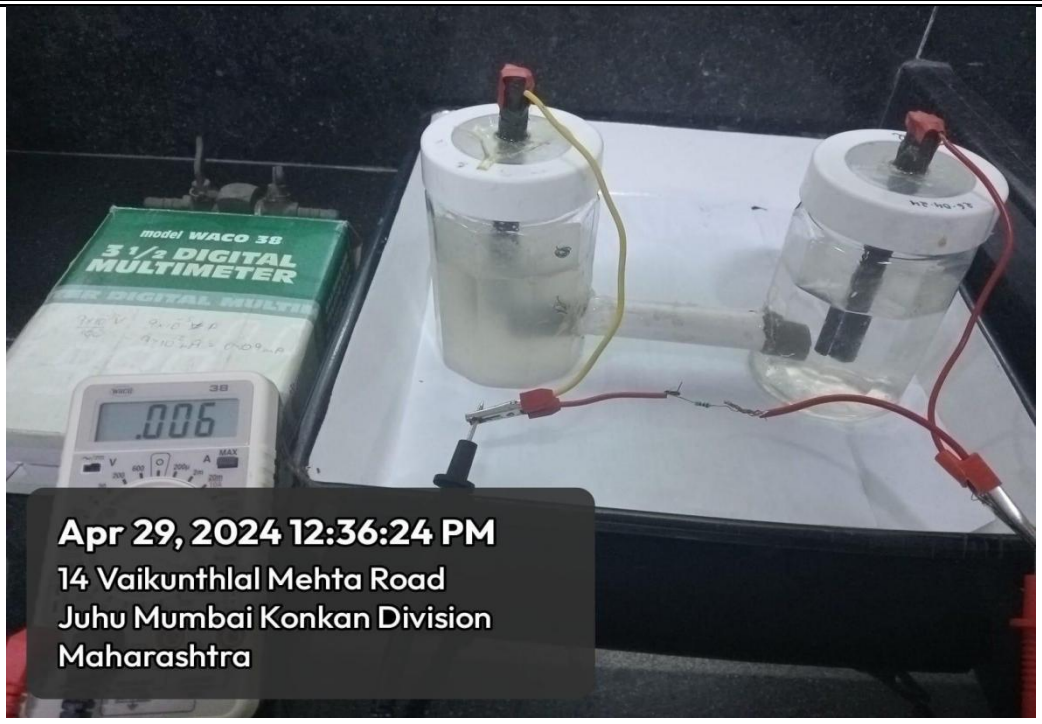

Figure 1 MFC Cell Set up with wires attached to a Multimeter

Results:

Time Set-up	48 hrs		72 hrs		120 hrs	
	Voltage (V)	Current (mA)	Voltage (V)	Current (mA)	Voltage (V)	Current (mA)
Sewage Water	0.029	0.072	0.004	0.006	0.0	0.0
Sewage+ Fluid Thioglycollate Broth	0.011	0.034	0.000	0.000	0.0	0.0
Sewage+ organic fertiliser)	0.000	0.000	0.000	0.000	0.0	0.0

Table 3.1: Results obtained from initial run of the MFC with the three different substrates used over a period of 5 days

Colony Characteristics	***C1***	***C2***
Shape	Circular	Circular
Size	Medium Sized	Small
Colour	Colourless	Blue Precipitate in the centre
Opacity	Opaque	Opaque
Appearance	Dull	Bright
Elevation	Flat	Raised
Gram Character	Positive	Positive
Morphology	Rods in chains	Cocci in clusters

Table 3.2: colony characteristics obtained from the two purified colonies C1 and C2

No discolouration was observed around any colonies on Novel medium and thioglycolate medium containing MnO_2. However, two colonies labelled as C1 and C2 gave a larger discolouration around the colony. These colonies were further purified and preserved. The colony characteristics obtained were as follows:

The power generated by two separate synthetic wastewater-fed MFC that were inoculated with

C1 and **C2** independently is given in Table 3.3.

Time Set-up	24 hrs		72 hrs		120 hrs	
	Voltage (V)	Current (mA)	Voltage (V)	Current (mA)	Voltage (V)	Current (mA)
C1	0.002	0.000	0.003	0.008	0.002	0.008
C2	0.005	0.000	0.002	0.000	0.000	0.000

Table 3.3: Results obtained after running the MFC over 5 days with C1 and C2 respectively

Figure 2 C1 showing 0.003 V reading on the multimeter

Figure 3 C1 showing 0.008 mA reading on the multimeter

More power generation was exhibited by C1 and was selected for identification using 16S rRNA technique. Based on 16S rRNA sequencing C1 exo-electrogen was identified as *Bacillus rugosus.*

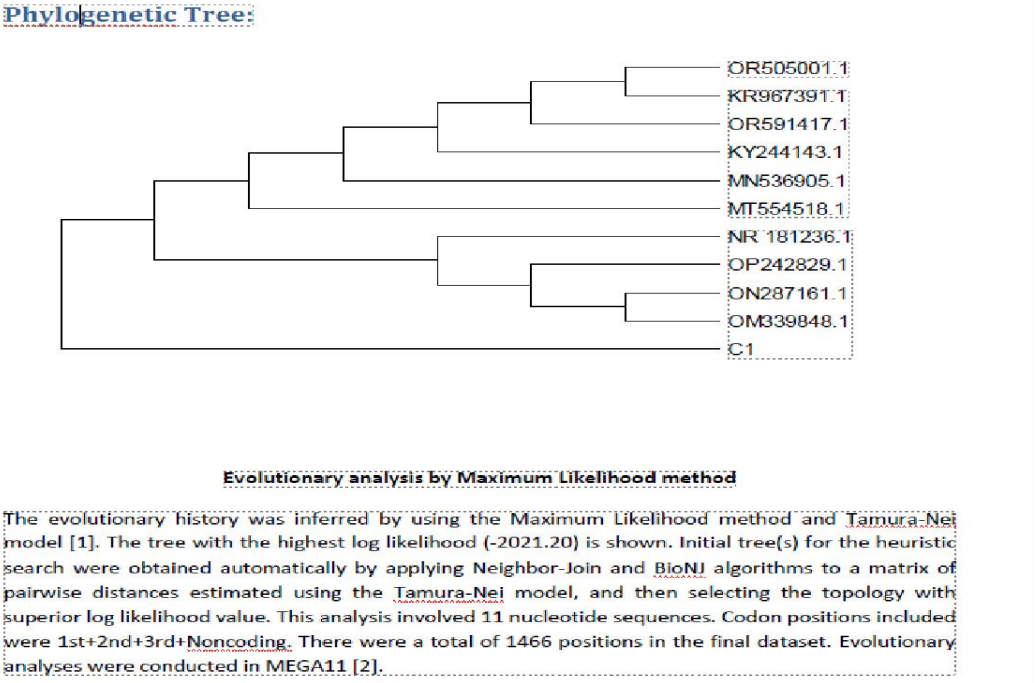

Discussion:

According to our study, MFCs was supported by domestic sewage water, which promoted exo- electrogenic microbial activity leading to power generation. After 48 hours, the sewage water sample's production peaked at 0.029 V and 0.072 mA, but by 120 hours, it had drastically decreased which may be because of nutrient depletion. The findings of Sonawane et al. (2022), who stressed the significance of constant nutrient replenishment and ideal microbial growth circumstances, are in keeping with this pattern of early high performance followed by a sharp fall.

The exo-electrogenic isolate was identified as *Bacillus rugosus. Bacillus species* have been reported (Hu et al., 2022; and You et al., 2018) to have the innate capacity to promote EET via biofilm formation and directing electron transfer processes. Long-term, sustainable energy recovery from wastewater requires further optimization in areas such as substrate management, electrode material selection, and microbial community enhancement.

Conclusion:

The need for sustainable and renewable sources of energy, as well as the accumulation of waste, have necessitated the innovation of technologies that are clean and can address the growing environmental concerns. MFCs have hence emerged as promising alternatives that could potentially address this problem by contributing to bioremediation as well as bioelectricity generation. Our study demonstrated the presence of exo-electrogens in domestic waste water sample which was isolated and identified as *Bacillus rugosus*. However, dip in the power generation over 5 days highlights the need for further research to optimise the MFC in order to produce a sustained current which can be run for longer periods of time.

Acknowledgements:

The authors of this research work acknowledge SVKM's Mithibai College Mithibai College of Arts, Chauhan Institute of Science and Amrutben Jivanlal College of Commerce and Economics (Empowered Autonomous) for providing seed grant and the necessary facilities.

References:

1. Bai, L., Zhou, M., & Gu, C. (2016). Advanced Nanomaterials for the Design and Construction of Anode for Microbial Fuel Cells. Advanced Electrode Materials, 457–483. https://doi.org/10.1002/9781119242659.CH12
2. Boas, J.V., Oliveira, V.B., Simões, M. and Pinto, A.M.F.R. (2022). Review on microbial fuel cells applications, developments and costs. Journal of Environmental Management, 307, p.114525. doi:https://doi.org/10.1016/j.jenvman.2022.114525.
3. Chabert, N., Amin Ali, O. and Achouak, W. (2015) 'All ecosystems potentially host electrogenic bacteria', Bioelectrochemistry (Amsterdam, Netherlands), 106. Available at: https://doi.org/10.1016/j.bioelechem.2015.07.004.
4. Dolch, K., Danzer, J., Kabbeck, T., Bierer, B., Erben, J., Förster, A. H., Maisch, J., Nick, P., Kerzenmacher, S., & Gescher, J. (2014). Characterization of microbial current production as a function of microbe-electrode-interaction. Bioresource Technology, 157, 284–292. https://doi.org/10.1016/j.biortech.2014.01.112
5. Hu, Y. et al. (2022) 'Microbiologically influenced corrosion of stainless steels by Bacillus subtilis via bidirectional extracellular electron transfer', Corrosion Science, 207, p. 110608. Available at: https://doi.org/10.1016/j.corsci.2022.110608.
6. Jiansheng, H. et al. (2014) 'Performance evaluation and bacteria analysis of AFB-MFC enriched with high-strength synthetic wastewater', Water science and technology : a journal of the International Association on Water Pollution Research, 69, pp. 9–14. Available at: https://doi.org/10.2166/wst.2013.390.
7. Kamaraj, S.-K. et al. (2015) 'Use of Novel Reinforced Cation Exchange Membranes for Microbial Fuel Cells', Electrochemical Acta, 176, pp. 555–566. Available at: https://doi.org/10.1016/j.electacta.2015.07.042.
8. Li, M. et al. (2018) 'Microbial fuel cell (MFC) power performance improvement through enhanced microbial electrogenicity', Biotechnology Advances, 36(4), pp. 1316–1327. Available at: https://doi.org/10.1016/j.biotechadv.2018.04.010.
9. Logan, B.E. et al. (2019) 'Electroactive microorganisms in bioelectrochemical systems', Nature Reviews Microbiology, 17(5), pp. 307–319. Available at: https://doi.org/10.1038/s41579-019-0173-x.
10. Martin, E. et al. (2010) 'The influence of operational conditions on the performance of a microbial fuel cell seeded with mesophilic anaerobic sludge', Biochemical Engineering Journal, 51(3), pp. 132–139. Available at: https://doi.org/10.1016/j.bej.2010.06.006.
11. Naik, S. and Jujjavarapu, S. (2020) 'Simultaneous bioelectricity generation from cost- effective MFC and water treatment using various wastewater samples', Environmental Science and Pollution Research, 27. Available at: https://doi.org/10.1007/s11356-019- 06221-8.
12. Nawaz, A. et al. (2022) 'Microbial fuel cells: Insight into simultaneous wastewater treatment and bioelectricity generation', Process Safety and Environmental Protection, 161,
13. pp. 357–373. Available at: https://doi.org/10.1016/j.psep.2022.03.039.
14. Nazeer, Z. and Fernando, E.Y. (2022) 'A novel growth and isolation medium for exoelectrogenic bacteria', Enzyme and Microbial Technology, 155, p. 109995. Available at: https://doi.org/10.1016/j.enzmictec.2022.109995.
15. Obi, C. N., & Asogwa, G. C. (2015). Electromicrobiology: An Emerging Reality—A Review. OALib, 02(11), 1–10. https://doi.org/10.4236/oalib.1102088

16. Obileke, K. et al. (2021) 'Microbial fuel cells, a renewable energy technology for bio- electricity generation: A mini-review', Electrochemistry Communications, 125, p. 107003. Available at: https://doi.org/10.1016/j.elecom.2021.107003.
17. Pant, D. et al. (2010) 'A review of the substrates used in microbial fuel cells (MFCs) for sustainable energy production', Bioresource Technology, 101(6), pp. 1533–1543. Available at: https://doi.org/10.1016/j.biortech.2009.10.017.
18. Potrykus, S. et al. (2021) 'The Influence of External Load on the Performance of Microbial Fuel Cells', Energies, 14, p. 612. Available at: https://doi.org/10.3390/en14030612.
19. Rabaey, K., Boon, N., Siciliano, S. D., Verhaege, M., & Verstraete, W. (2004). Biofuel cells select for microbial consortia that self-mediate electron transfer. Applied and Environmental Microbiology, 70(9), 5373–5382. https://doi.org/10.1128/AEM.70.9.5373-
20. 5382.2004
21. Rousseau, R. et al. (2020) 'Microbial electrolysis cell (MEC): Strengths, weaknesses and research needs from electrochemical engineering standpoint', Applied Energy, 257, p. 113938. Available at: https://doi.org/10.1016/j.apenergy.2019.113938.
22. Sangeetha, T., & Muthukumar, M. (2011). Catholyte performance as an influencing factor on electricity production in a dual-chambered microbial fuel cell employing food processing wastewater. Energy Sources, Part A: Recovery, Utilization and Environmental Effects, 33(16), 1514–1522. https://doi.org/10.1080/15567030903397966
23. Semenec, L., & E Franks, A. (2015). Delving through electrogenic biofilms: from anodes to cathodes to microbes. AIMS Bioengineering, 2(3), 222–248. https://doi.org/10.3934/bioeng.2015.3.222
24. Sonawane, J.M., Mahadevan, R., Pandey, A. and Greener, J. (2022). Recent progress in microbial fuel cells using substrates from diverse sources. Heliyon, 8(12), p.e12353. doi:https://doi.org/10.1016/j.heliyon.2022.e12353.
25. Torres, C.I. et al. (2010) 'A kinetic perspective on extracellular electron transfer by anode- respiring bacteria', FEMS Microbiology Reviews, 34(1), pp. 3–17. Available at: https://doi.org/10.1111/j.1574-6976.2009.00191.x.
26. Ueoka, N., Kouzuma, A. and Watanabe, K. (2018) 'Electrode plate-culture methods for colony isolation of exoelectrogens from anode microbiomes', Bioelectrochemistry, 124,
27. pp. 1–6. Available at: https://doi.org/10.1016/j.bioelechem.2018.06.008.
28. Yaqoob, A.A., Mohamad Ibrahim, M.N., Rafatullah, M., Chua, Y.S., Ahmad, A. and Umar,
29. K. (2020). Recent Advances in Anodes for Microbial Fuel Cells: An Overview. Materials, 13(9), p.2078. doi:https://doi.org/10.3390/ma13092078.
30. You, L.-X. et al. (2018) 'Flavins mediate extracellular electron transfer in Gram-positive Bacillus megaterium strain LLD-1', Bioelectrochemistry, 119, pp. 196–202. Available at: https://doi.org/10.1016/j.bioelechem.2017.10.005.
31. Yee, M. O., Deutzmann, J., Spormann, A., & Rotaru, A. E. (2020). Cultivating electroactive microbes- from field to bench. Nanotechnology, 31(17). https://doi.org/10.1088/1361- 6528/ab6ab5
32. Zaybak, Z., Logan, B. E., & Pisciotta, J. M. (2018a). Electrotrophic activity and electrosynthetic acetate production by Desulfobacterium autotrophicum HRM2. Bioelectrochemistry, 123, 150–155. https://doi.org/10.1016/j.bioelechem.2018.04.019

International Journal of Multidisciplinary Research and Technology
ISSN 2582-7359, Peer Reviewed Journal, Impact Factor 6.325
www.ijmrtjournal.com

IN SILICO EXPLORATION OF MARINE NATURAL PRODUCTS AS NOVEL THERAPEUTICS FOR ACUTE MYELOID LEUKEMIA

[1]Ranikumari S Sharma, [2]Esha Deepak Tare, [3]Deepa N Rangdal, [4]Manasi A Shinde, [5]Shruti P Pardale, [6]Shubhangi P Patil

Department of Chemistry, The Institute of Science, 15, Madam Cama Road,
Mantralaya, Fort, Mumbai, Maharashtra 400032, India

Abstract

Acute myeloid leukemia (AML) is one of the leading blood cancer worldwide and in approximately 30-35% of the cases it is observed due to mutation in FMS-like tyrosine kinase3 (FLT3) protein, making a significant challenge in clinical management. In this study, we aimed to screen novel natural products (NPs) obtained from marine resource which can be act as a lead component against FLT3 via silico approach. Here we thoroughly discussed molecular docking, Dynamic simulation, ADMET (absorption–distribution–metabolism–excretion–toxicity) and network pharmacology. We screened over 100 phytochemicals isolated from marine microorganism, algae, sponges and invertebrates. Isodehydroluffariellolide and 3-Acetyl sesterstatin1 are promising natural products have been identified from marine resource which shows -8.6 kcal/mol and -8.0 kcal/mol binding affinity with our targeted protein. Further, these NPs undergo evaluation via Lipinski and other toxicity criteria to ensure drug like properties and compared with 2 FDA approved drugs. Our findings disclose two drug candidates, demonstrating stable binding affinity and favors ADMET criteria. These compounds can be acts as potential drug candidate against Acute myeloid leukemia.

Keywords: Acute myeloid leukemia, marine natural products, molecular docking, dynamic simulation, ADMET

1. Introduction

Treatment of Acute myeloid leukemia (AML) remains a challenge due to its complexity, heterogeneity and subtypes(1).Further, Conventional treatments like targeted therapies, chemotherapy and bone marrow transplantation remains backbone still this is not sufficient the way cases are increasing innumerably(2). More than 40 percent patient suffering from AML are below the age of 60 years(3). Hence, treatment of AML using natural products which involve the exploration of bioactive phytochemicals primarily derived from marine species proven to be an effective therapeutic agents compared to synthetic drugs(4). Computational method plays a significant role in drug design which includes docking and molecular dynamic simulation, offer a powerful tool for identification and screening of potential inhibitor(5,6).

AML progress as a result of genetic mutation in genes such as FMS-like tyrosine kinase3 (FLT3) including NPM1 and RUNX1(7–9). Out of these some are spontaneous mutations while other maybe inherited. Hence AML is considered as severe blood cancer which accounts for approximately 1.2% of all cancer death globally(10). To treat AML, the FDA has approved several medications, including Dexamethasone, Olutasidenib, and Pemigatinib(11). The Isodehydroluffariellolide and 3-Acetyl sesterstatin1 NPs and their derivatives are highly potential to inhibit such mutations in genes. In recent years, natural products (NPs) have emerged as a valuable and most effective source of lead component for drug discovery(12). In this study we have screened hundreds of phytochemicals obtained from marine source by performing extensive screening, which remains less explored hence, there is scope to explore(13). By performing various ligand-based modelling such as docking and simulation, we search to illuminate the molecular interactions between the potential inhibitor and protein residues(14). We attempt to identify the lead component having high binding affinity and selectivity for the FLT3 protein through rigorous computational screening and analysis(15).

2. Materials and methods

2.1 Preparation of protein

The 3D structure of FLT3 protein was downloaded from Protein Data Bank (PDB ID:6IL3) of Research Collaborators for Structural Bioinformatics (RCSB) database as shown in **Figure 1.** This protein is pre-processed by deleting all the non-standard residues in UCSF Chimera. Further, all the additional chains are separated except

A chain and water molecules are removed from the protein, this protein structure was saved in PDBQT format. Finally, using AutoDockTools version 1.5.7, polar hydrogens were get added along with kollman charges. Grid box of FLT3 protein is generated having the dimension of the receptor X = 81.804, Y = 61.550 and Z = 23.220 Å.

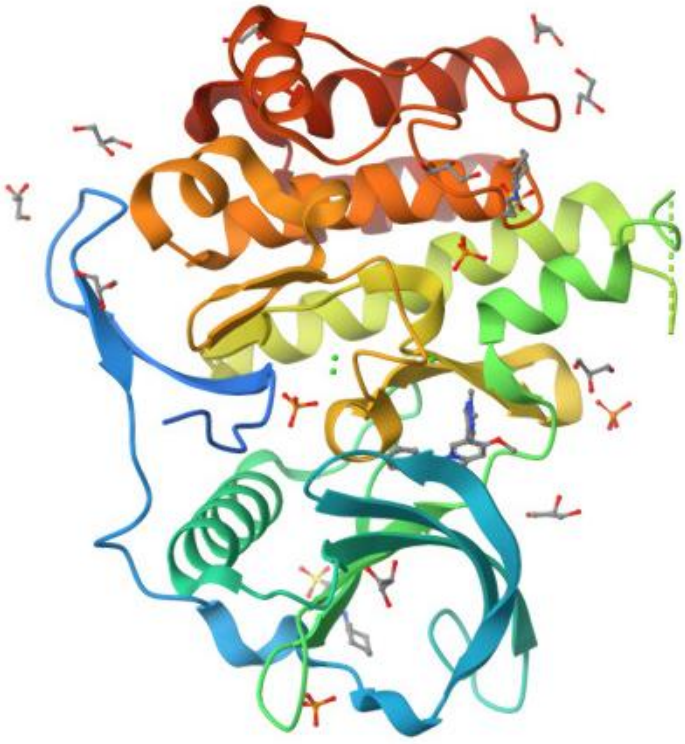

Figure 1 The three-dimensional structure of FLT3 (PDB ID: 6IL3) protein.

2.2. Preparation of ligands

The natural products are extracted from *Hyrtios erectus*- a species of marine sponge which is terpenoids in nature(16). The ligand preparation is carried out by using SMILES from PubChem database (PubChem CID of Isodehydroluffariellolide- 6450975; 3-Acetyl sesterstatin1-21629516) as depicted in **Figure 2**. Initially the 3D structures were downloaded in SDF format from PubChem database and by using UCSF Chimera it is saved in PDB format. Geometry optimization of ligands was performed in Avogadro software. Later, by the addition of gasteiger charges in AutoDockTools all the ligand structures were saved in PDBQT format.

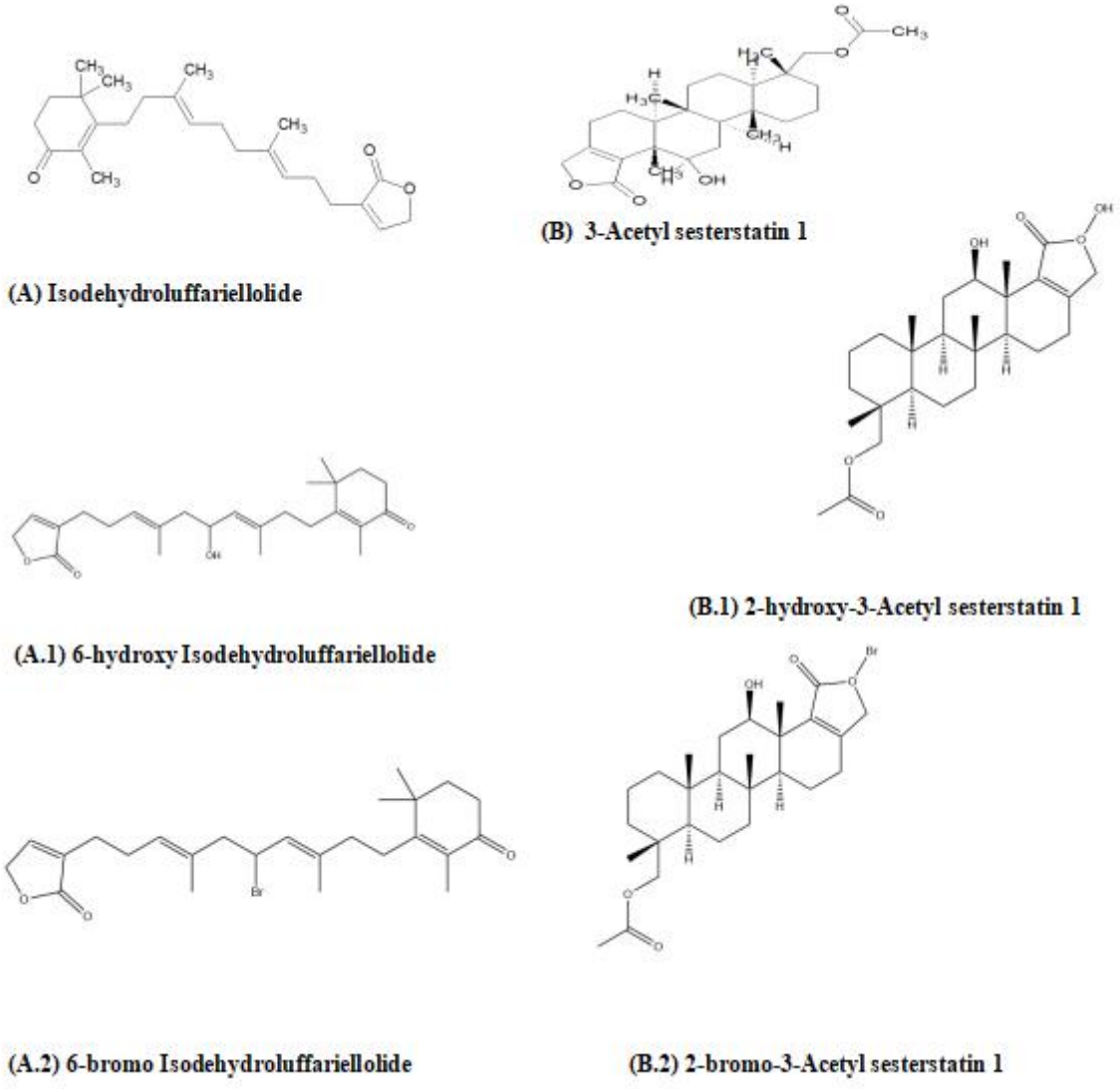

Figure 2 The molecular structure of terpenoid marine sponge (*Hyrtios erectus)* phytoconstituents(A) and (B), and their derivatives (A1) (A2) (B1) (B2).

2.3. Molecular docking

Molecular docking is a computational method by which a protein can bind to ligand molecule. This binding process helps to investigate the binding relationship that occurs between a protein to a variable possible site on the ligand(17). For this study we used AutoDock Vina software to analyze the interaction between phytochemicals of marine sponge (*Hyrtios erectus)* and receptor FLT3 (PDB ID: 6IL3). These interactions reveals the information of binding energy with their best poses. This is later compared with standard Dexamethasone(11). The protein-ligand complex having the lowest binding energy and best dock pose was taken into consideration for further visualized in Discovery studio software.

2.4. ADMET study and toxicity prediction

The potential lead component is thoroughly studied by *in silico* absorption–distribution–metabolism–excretion–toxicity and toxicity analysis(18). This ADMET study is performed with the help of SwissADME online web server (http://www.swissadme.ch/). Further, toxicity of lead component is done by using ProTox3.0 web server in which prediction of numerous parameters such as hepatotoxicity, carcinogenicity, cytotoxicity, immunotoxicity, mutagenicity, toxicity level and LD_{50} were carried out(19).

3. Results and Discussion

3.1 Molecular docking

The protein-ligand complex interactions were determined by screening selected potential component as phytochemicals from marine sponge (*Hyrtios erectus)* against FLT3 in order to obtain best dock pose with lowest binding energy and types of interactions(20). **Table 1** shows the molecular docking score of selected phytoconstituents extracts from marine sponge and their derivatives on FLT3 (PDB ID: 6IL3) protein. Also, these interactions were compared with the docking score of FDA approved standard Dexamethasone. As shown in **Table 1,** the standard Dexamethasone has low docking score which is -6.7 kcal/mol as compared with our lead components and their derivatives (6-hydroxy Isodehydroluffariellolide, 6-bromo Isodehydroluffariellolide, 2-hydroxy-3-Acetyl sesterstatin1, 2-bromo-3-Acetyl sesterstatin1)

Out of all the selected natural products and their derivatives, Isodehydroluffariellolide, 6-bromo Isodehydroluffariellolide and 2-hydroxy-3-Acetyl sesterstatin1 shows lowest binding energy which are -8.6 kcal/mol, -8.9 kcal/mol and -8.7 kcal/mol respectively.

The protein receptor FLT3 binding sites were predicted with target ligand marine terpenoids for best docking pose as shown in **figure 3. (A), (B) and (C)** The ligands bind firmly with the active sites of FMS-like tyrosine kinase3 protein through one alkyl interaction, conventional hydrogen bond interaction and rest of with van der waals interactions. These binding interactions of protein-ligand complex were observed through Discovery studio visualizer software.

Table 1

Molecular docking score of selected compounds of Marine sponge (*Hyrtios erectus)* and their derivatives against FLT3 (PDB ID: 6IL3) using AutoDockVina.

Natural products	Binding energy (kcal/mol)
Dexamethasone (standard)	-6.7
Isodehydroluffariellolide	-8.6
3-Acetyl sesterstatin 1	-8.0
6-hydroxy Isodehydroluffariellolide	-6.0
6-bromo Isodehydroluffariellolide	-8.9
2-hydroxy-3-Acetyl sesterstatin1	-8.7
2-bromo-3-Acetyl sesterstatin1	-8.0

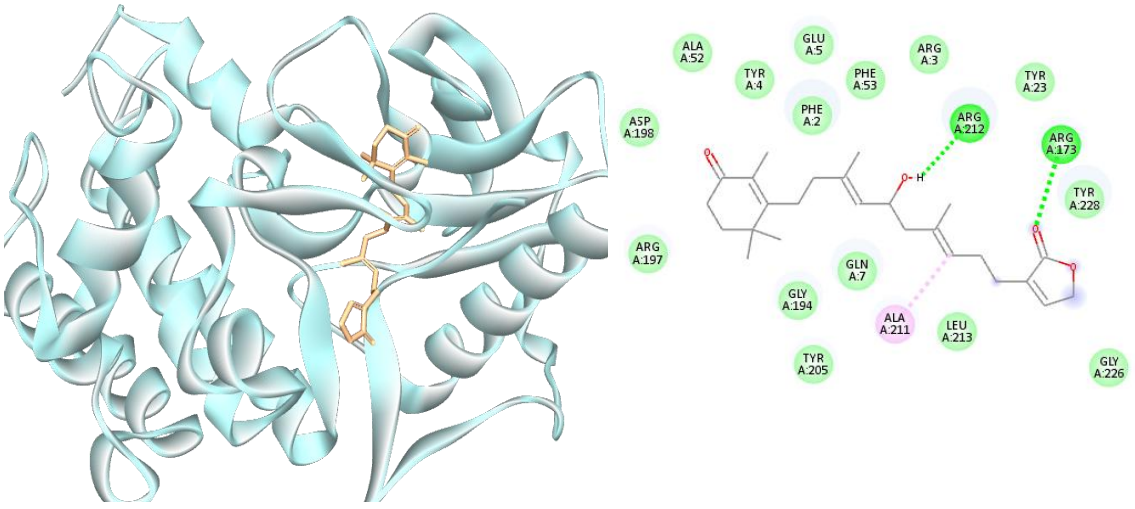

Figure 3. (A) 3D and 2D Interactions of compound 6-hydroxy Isodehydroluffariellolide with active binding sites of receptor FLT3 (PDB ID: 6IL3)

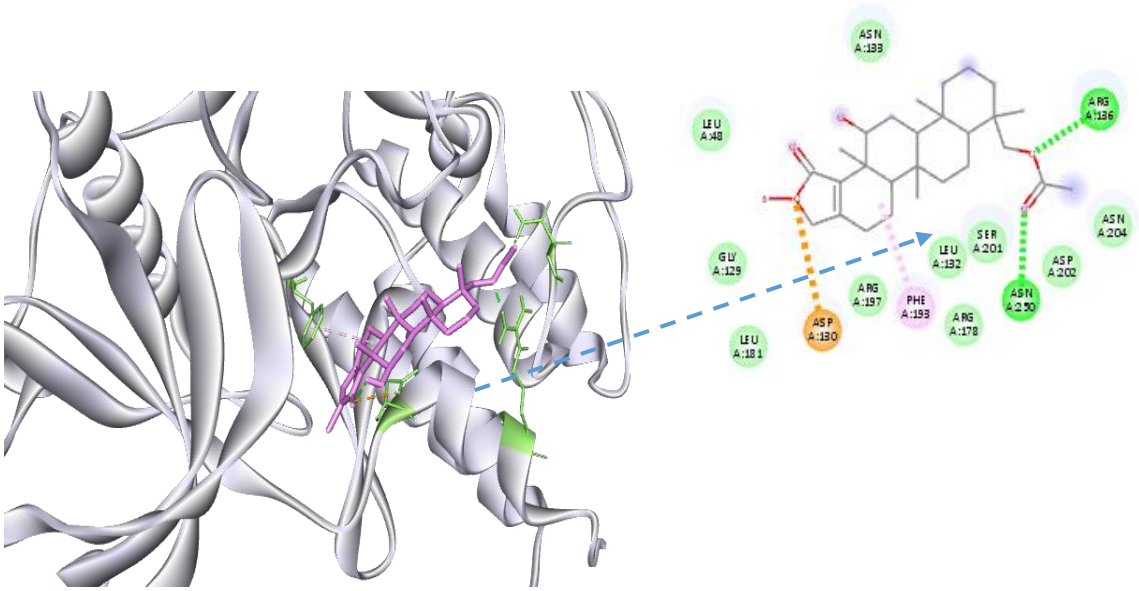

(B) 3D and 2D Interactions of compound 2-hydroxy-3-Acetyl sesterstatin1 with active binding sites of receptor FLT3 (PDB ID: 6IL3)

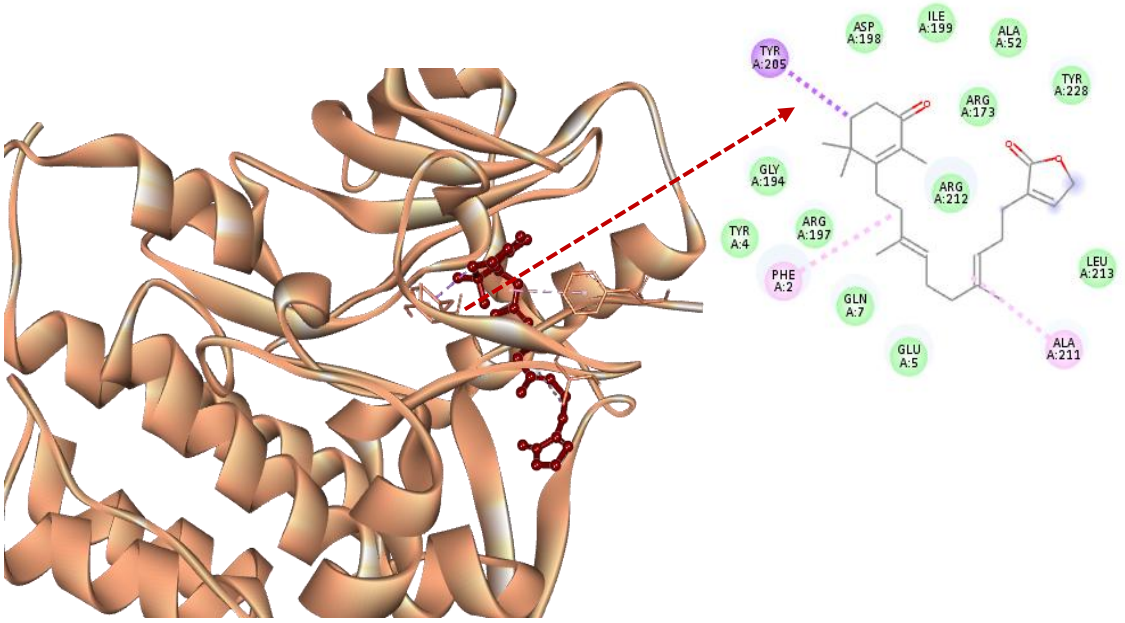

(C) 3D and 2D Interactions of compound Isodehydroluffariellolide with active binding sites of receptor FLT3 (PDB ID: 6IL3)

3.2. In Silico ADME-tox prediction

The most common and important parameters for the NPs being a good drug candidate are absorption, distribution, metabolism, excretion and toxicity (ADMET) prediction. This prediction is conducted in ProTox 3.0. Parameters like hepatotoxicity, carcinogenicity, immunotoxicity, mutagenicity, cytotoxicity, LD_{50} and toxicity level are represented in **Table 2**. According to results, both Isodehydroluffariellolide, 6-hydroxy Isodehydroluffariellolide and 6-bromo Isodehydroluffariellolide shows the toxicity level of 4 which signifies these phytoconstituents are less toxic. Similarly, these phytoconstituents of marine sponge (*Hyrtios erectus)* were further studied through SwissADME databas. The parameters which are important to consider for a drug to be an effective are molecular weight should be <500Da, Hydrogen bond donors <5, Hydrogen bond acceptor <10, LD_{50} dose between 3000-5000 mg/kg (slightly toxic) and the drug should possess minimum bioavailability score of 0.55. Further, according to FDA drug requirement the drug should not cross the Blood Brain Barrier (BBB) and exhibit high gastrointestinal absorption. From **Table 3**, since 2-hydroxy-3-Acetyl sesterstatin1, 2-bromo-3-Acetyl sesterstatin1 and 3-Acetyl sesterstatin1 have LD_{50} less than 3000 hence it results into moderately toxic and could be eliminated.

Table 2 Toxicity predictions of selected compounds from Marine sponge (*Hyrtios erectus)*

Natural Product	Hepatoxicity	Carcinogenicity	Immunotoxicity	Mutagenicity	Cytotoxicity	LD_{50} (mg/kg)	Toxicity level
Dexamethasone(standard)	Inactive	Inactive	Moderately active	Inactive	Inactive	3000	5
Isodehydroluffariellolide	Inactive	Inactive	Inactive	Inactive	Inactive	3300	4
3-Acetyl sesterstatin 1	Inactive	Slightly Active	Active	Inactive	Inactive	1400	**4**

6-hydroxy Isodehydroluffariellolide	Inactive	Inactive	Active	Inactive	Inactive	3300	4
6-bromo Isodehydroluffariellolide	Inactive	Inactive	Active	Inactive	Inactive	3300	4
2-hydroxy-3-Acetyl sesterstatin 1	Inactive	Inactive	Inactive	Inactive	Inactive	1400	**4**
2-bromo-3-Acetyl sesterstatin **1**	Inactive	Inactive	Active	Inactive	Inactive	1400	**4**

Table 3 (A). ADME results of Marine natural products

Natural product	Molecular weight (g/mol)	Bioavailability score	H-bond donors	H-bond acceptors	GI absorption	Lipinski rule of five	BBB
Dexamethasone (standard)	392.46	0.55	3	5	High	Yes	No
Isodehydroluffariellolide	384.55	0.55	0	3	High	Yes	No
3-Acetyl sesterstatin 1	444.6	0.55	1	5	High	yes	No

Table 3 (B). ADME results of derivatives

Derivatives	Molecular weight	H-bond donors	H-bond acceptor	BBB
Dexamethasone(standard)	392.46	3	5	No
6-hydroxy Isodehydroluffariellolide	400.55	1	4	No
6-bromo Isodehydroluffariellolide	463.45	0	3	No
2-hydroxy-3-Acetyl sesterstatin 1	461.61	2	6	No
2-bromo-3-Acetyl sesterstatin 1	524.51	1	5	No

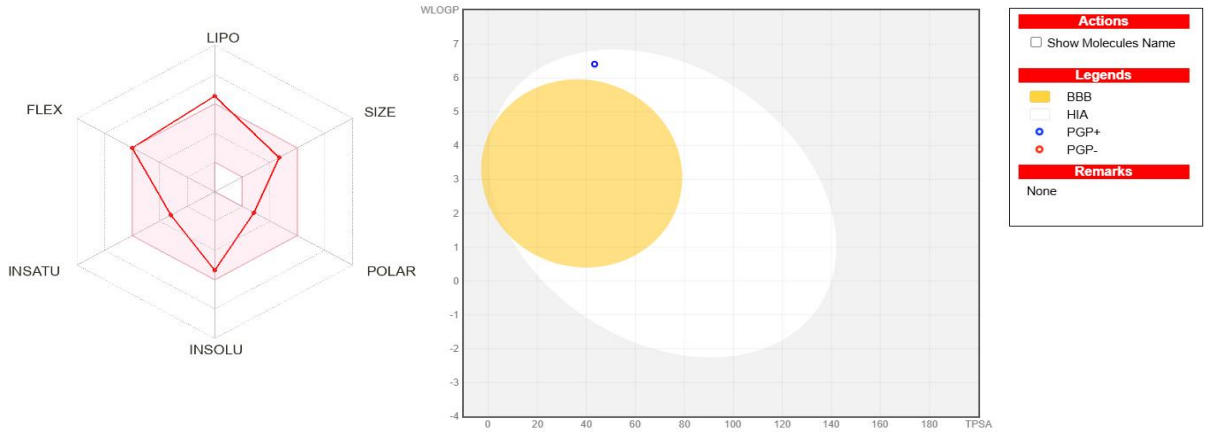

Figure 4 The bioavailability radar and BOILED-Egg model of Isodehydroluffariellolide (*Hyrtios erectus)*

Figure 4 shows the bioavailability radar of the compound Isodehydroluffariellolide. The pink area signifies the optimal physicochemical space for oral bioavailability. In this Isodehydroluffariellolide compound is orally bioavailable as it fits in the colored zone. The white region in the BOILED-Egg model signifies the gastrointestinal absorption while the yellow region indicates the brain permeability(21).The BOILED-egg model of Isodehydroluffariellolide predicts that the compound permeates passively through gastro-intestinal tract and does not show blood brain barrier (BBB) permeability as displayed in **figure 4**

Conclusion

This study concludes FLT3 inhibitory activity of selected phytoconstituents extracted from marine sponge (*Hyrtios erectus)* in the treatment of AML. Among the selected phytoconstituents, Isodehydroluffariellolide compound exhibited promising FLT3 inhibitory activity. The docking study suggests that Isodehydroluffariellolide compound would be the lead component as anti-AML drug showing strong interactions with the active sites of FLT3 receptor with best dock score of -8.6 kcal/mol. Furthermore, the ADMET analysis indicates that the Isodehydroluffariellolide compound has best drug likeness and pharmacokinetic profile with low toxicity and risk. As a result, overall data suggest Isodehydroluffariellolide compound as a potential candidate for the development of novel AML medications.

Acknowledgment

We acknowledge and are grateful to the Director of the Institute of Science, Mumbai, for the support and recognition. No financial support was received for the authorship or publication of this article.

References

1. Forsberg M, Konopleva M. AML treatment: conventional chemotherapy and emerging novel agents. Trends Pharmacol Sci. 2024 May;45(5):430–48.
2. Sabakhtarishvili G, Ansari A, Tabbara IA. Maintenance Therapy in Acute Myeloid Leukemia. Am J Clin Oncol. 2025 Jan;48(1):38–43.
3. Luz Arana-Luna L, Antonio De La Peña Celaya J, Hernández-Ruiz E, Luis Alvarez Vera J, Eugenia Espitia Ríos M, Manuel Pérez Zúñiga J, et al. Management of Acute Myeloid Leukemia in Patients under 60 Years of Age. In: Paolo Piccaluga P, Paolini S, editors. Advances in Hematological Malignancies [Internet]. IntechOpen; 2024 [cited 2025 Jan 22]. Available from: https://www.intechopen.com/chapters/89686
4. Saikia M, Retnakumari AP, Anwar S, Anto NP, Mittal R, Shah S, et al. Heteronemin, a marine natural product, sensitizes acute myeloid leukemia cells towards cytarabine chemotherapy by regulating farnesylation of Ras. Oncotarget. 2018 Apr 6;9(26):18115–27.
5. Mohamed LM, Eltigani MM, Abdallah MH, Ghaboosh H, Bin Jardan YA, Yusuf O, et al. Discovery of novel natural products as dual MNK/PIM inhibitors for acute myeloid leukemia treatment: Pharmacophore modeling, molecular docking, and molecular dynamics studies. Front Chem. 2022 Jul 22;10:975191.

6. El-Shemy HA, Aboul-Enein KM, Lightfoot DA. Predicting *In Silico* Which Mixtures of the Natural Products of Plants Might Most Effectively Kill Human Leukemia Cells? Evid Based Complement Alternat Med. 2013;2013:1–10.
7. Ibrahim OM, Rettig MP, Chendamarai E, Jayasinghe RG, Ding L, DiPersio J. Identifying Surface Protein Markers for AML Immunotherapy. Blood. 2023 Nov 2;142(Supplement 1):6809–6809.
8. Shimosato Y, Yamamoto K, Jia Y, Zhang W, Shiba N, Hayashi Y, et al. NPM1-fusion proteins promote myeloid leukemogenesis through XPO1-dependent HOX activation. Leukemia. 2025 Jan;39(1):75–86.
9. Yamagata T, Maki K, Mitani K. Runx1/AML1 in Normal and Abnormal Hematopoiesis. Int J Hematol. 2005 Jul 1;82(1):1–8.
10. Jani CT, Ahmed A, Singh H, Mouchati C, Al Omari O, Bhatt PS, et al. Burden of AML, 1990-2019: Estimates From the Global Burden of Disease Study. JCO Glob Oncol. 2023 Sep;(9):e2300229.
11. Freyer CW, Hughes ME, Carulli A, Bagg A, Hexner E. Pemigatinib for the treatment of myeloid/lymphoid neoplasms with *FGFR1* rearrangement. Expert Rev Anticancer Ther. 2023 Apr 3;23(4):351–9.
12. Asfa SS, Arshinchi Bonab R, Önder O, Uça Apaydın M, Döşeme H, Küçük C, et al. Computer-Aided Identification and Design of Ligands for Multi-Targeting Inhibition of a Molecular Acute Myeloid Leukemia Network. Cancers. 2024 Oct 25;16(21):3607.
13. Cragg GM, Newman DJ, Yang SS. Natural Product Extracts of Plant and Marine Origin Having Antileukemia Potential. The NCI Experience. J Nat Prod. 2006 Mar 1;69(3):488–98.
14. Carranza-Aranda A, Jave-Suárez L, Flores-Hernández F, Huizar-López MDR, Herrera-Rodríguez S, Santerre A. *In silico* and *in vitro* study of FLT3 inhibitors and their application in acute myeloid leukemia. Mol Med Rep. 2024 Oct 4;30(6):229.
15. Abaza Y, McMahon C, Garcia JS. Advancements and Challenges in the Treatment of AML. Am Soc Clin Oncol Educ Book. 2024 Jun;44(3):e438662.
16. Chakraborty K, Francis P. Hyrtioscalaranes A and B, two new scalarane-type sesterterpenes from *Hyrtios erectus* with anti-inflammatory and antioxidant effects. Nat Prod Res. 2021 Dec 17;35(24):5559–70.
17. Carranza-Aranda A, Jave-Suárez L, Flores-Hernández F, Huizar-López MDR, Herrera-Rodríguez S, Santerre A. *In silico* and *in vitro* study of FLT3 inhibitors and their application in acute myeloid leukemia. Mol Med Rep. 2024 Oct 4;30(6):229.
18. Bultum LE, Tolossa GB, Lee D. Combining empirical knowledge, in silico molecular docking and ADMET profiling to identify therapeutic phytochemicals from Brucea antidysentrica for acute myeloid leukemia. Endale M, editor. PLOS ONE. 2022 Jul 27;17(7):e0270050.
19. Min GJ, Cho BS, Park SS, Park S, Jeon YW, Shin SH, et al. Geriatric assessment predicts nonfatal toxicities and survival for intensively treated older adults with AML. Blood. 2022 Mar 17;139(11):1646–58.
20. In silico Research Laboratory, Eminent Biosciences, Mahalakshmi Nagar, Indore – 452010, Madhya Pradesh, India, Gokhale P, Chauhan APS, Arora A, Khandekar N, Nayarisseri A, et al. FLT3 inhibitor design using molecular docking based virtual screening for acute myeloid leukemia. Bioinformation. 2019 Feb 28;15(2):104–15.
21. Yuan X, Chen Y, Zhang W, He J, Lei L, Tang M, et al. Identification of Pyrrolo[2,3- *d*]pyrimidine-Based Derivatives as Potent and Orally Effective Fms-like Tyrosine Receptor Kinase 3 (FLT3) Inhibitors for Treating Acute Myelogenous Leukemia. J Med Chem. 2019 Apr 25;62(8):4158–73.

International Journal of Multidisciplinary Research and Technology
ISSN 2582-7359, Peer Reviewed Journal, Impact Factor 6.325
www.ijmrtjournal.com

GOLD NANOPARTICLE COATED ANTIBIOTICS TO COMBAT ANTIMICROBIAL RESISTANCE AND TYPE 1 HYPERSENSITIVITY IN ASTHMA

[1]Saher M., [2]Shreya P., [3]Kruti P.
Department of Biotechnology, Jai Hind College, Mumbai 400020

Abstract:

Antibiotics are super drugs that have saved humans from invading microbes. However, indiscriminate use of antibiotics lead to emergence of antibiotic-resistant microbes. Prolonged and repeated use of antibiotics induce Type I Hypersensitivity in humans. According to the World Allergy Organization (WAO), a survey indicated that over 20% of the world population suffered from IgE mediated hypersensitivity. Research indicated lifetime and current asthma prevalence rate as 19.1% and 6.3% respectively. Reducing the dosage and administering an alternative plan may help in controlling AMR and HSI.

AuNP of 50 nm provides target specificity due to small size, aiding in efficient drug delivery and reducing intensity of side effects by a reduced dosage of drug. Gold conjugated antibiotics provide biocompatibility against Inflammation. AMR is caused due to excessive use of antibiotics affecting drug efficiency. Multidrug Resistance is a public health concern that functions to enhance drug delivery, lowering bacterial load and improving therapeutic efficiency. This project aims at targeting treatment options for Type I Hypersensitivity by checking the potency of antibiotics, Amoxicillin and Azithromycin coated with gold nanoparticles against *Staphylococcus aureus* and *Klebsiella pneumoniae* which are reportedly exhibiting *AMR.*

Keywords: *AuNP, HS I-Type 1 Hypersensitivity, Inflammation, Target therapy, Asthma, Antibiotic and Antimicrobial Resistance, Amoxicillin.*

Introduction:

Metal nanoparticles have gained significant popularity due to their uniqueness and wide application in the Medical Industry. AuNP is preferred over other metallic nanoparticles since they show an increased level of optical resonance. These nanoparticles exhibit a target specific response by binding to the inflamed area and reduce the severity of the reaction. AuNP contains a large surface area to volume ratio, thus enabling its surface to coat with various targeting agents, such as antibodies, peptides and sugar moieties. Interaction of these nanoparticles with light is proportional to their size and shape, causing a concerted oscillation of electron charge, known as surface plasmon. Other properties such as surface chemistry and state of aggregation influence the rate of reaction. Reactive Oxygen Species (ROS) are generated as a result of metallic ions present in metallic nanoparticles, which cause oxidative stress in bacterial cells. This activity is a phenomenon exhibited by AuNP, leading to cell lysis. Another mechanism is exhibited, wherein enzymatic degradation disrupts the metabolic mechanism, essential for survival.

Literature Review:

A plethora of antibiotic-resistant bacterial strains pose a major health hazard, causing urgent need for therapeutic measures which are significantly effective in eradication of the infection. In recent advancements, Nanotechnology has become a boon in the Medical Industry. Multiple testing has revealed the benefits of utilizing Gold Nanoparticles (AuNP) in empowering remedial measures against Inflammation. The Nanomedical Industry has particularly benefited in AuNP due to its highly target-specific action, used in drug-delivery systems without administration of a higher dosage. Dosage compensation studies reveal the increased use of Antibiotics have an antagonistic effect since they increase the severity of the numerous side effects. AuNP's can help combat the challenge of resistant bacterial strains, particularly focusing on their antimicrobial efficacy and the development of combination therapies.

Gold nanoparticles are characterized by their high surface area-to-volume ratio, biocompatibility, and multi-functionalization capacity, suitable for the hypothesis. Microbiologists have studied the effects of AuNP on Gram Positive and Gram Negative strains, indicating to reduce the toxicity imposed by the bacterial strains.

Functionalized gold nanoparticles can effectively target multi-drug-resistant strains such as *Staphylococcus aureus* and *Klebsiella pneumoniae*, providing better utilization of drugs.

Type I Hypersensitivity reactions are extremely common but unfortunately treatment options are extremely limited. The adverse reactions counteract the action of antibiotics, hence limiting therapeutic measures. Conjugation of antibiotics with AuNPs provides better stability and improves the antimicrobial efficiency.To overcome the challenges of drug-resistant bacterial strains, AuNP is the remedial tool. It can be used in Clinical therapies and improve the approach to antibiotic therapy.

Materials:

Synthesis Of Gold Nanoparticle:

The initial process for synthesizing gold nanoparticles involves usage of a high-purity gold foil (23.9k), the base component. A mixture of concentrated hydrochloric acid (HCl) and concentrated nitric acid (HNO_3) is prepared in 3:1, functioning as catabolic agents for the gold foil. They convert the gold in its bulk form to ionic, which can hence be reduced to form nanoparticles, using Top-Down Mechanism. Trisodium citrate ($Na_3C_6H_5O_7$) is exhausted for its properties of reduction and stabilization as it controls the size and dispersion during the synthesis process. Deionized water is especially used as it does not contain any ions or impurities that may hinder during the procedure and affect the overall product.

Glassware such as conical flask was used for storage, test tubes for scale-down process, thermometer for regulation of required temperature, cuvettes for Colorimetric and Spectral analysis post synthesis and measuring cylinder to obtain precise measurements. Other equipment such as a tripod stand and wire gauze were utilized for the double-boiler system, while an amber-colored bottle helps avoid reaction of the nanoparticle with light, by mimicking dark conditions. Instruments such as UV-Visible Spectrophotometer and Colorimeter help measure absorbance, formulating the optical properties of the AuNPs.

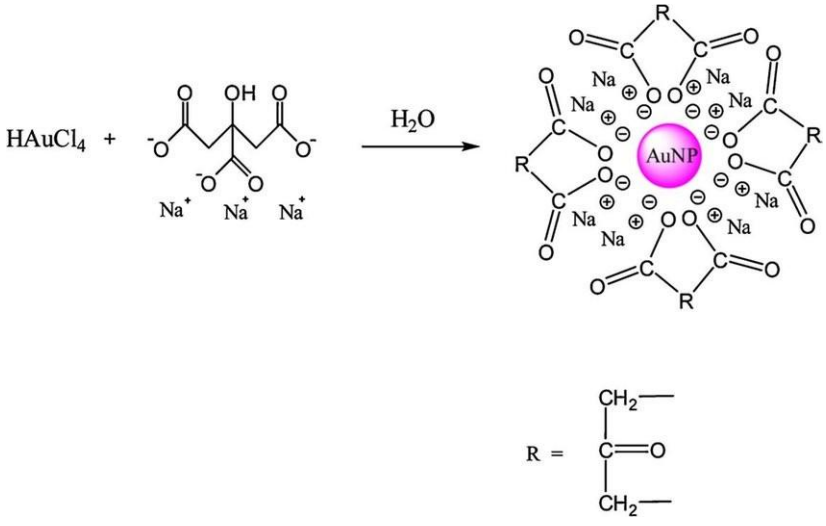

https://www.researchgate.net/profile/Zayar_Paing_Soe/publication/337669198/figure/fig12/AS:831355084623873@1575221906200/AuNP-synthesis-using-the-Turkevich-method-Zhao-Pengxiang-Na-Li-and-Didier-Astruc.jpg

Disc Diffusion Assay:

Disc Diffusion Assay involves assessing the antimicrobial efficiency of the synthesized AuNPs, wherein sterile saline suspension of a Gram Positive bacteria, *Staphylococcus aureus* and Gram Negative bacteria, *Klebsiella pneumoniae* were selected to draw a comparison. As a control, Amoxicillin antibiotic was utilized, against asthmatic pathogenic bacterial strains. The glassware used are sterile Nutrient Agar plates, sterile pipettes for transferring bacterial suspensions and test tubes for preparing dilutions. Nutrient agar served as the growth medium,

providing essential nutrients for bacterial lawn culture growth. Miscellaneous materials included sterile cotton swabs, which administer in matte growth formation. Sterile discs coated with AuNPs and Amoxicillin are tested against both bacterial strains, alcohol in a beaker for sterilization and forceps to handle the discs after coating. The plates were incubated at 37 degrees Celsius to promote optimal bacterial growth, after which zones of inhibition were measured to evaluate antimicrobial activity.

Cross-Strip Method:

The cross-strip method is another technique that involves comparing synergistic and antagonistic action of the sample. Antimicrobial efficacy of the antibiotic, Amoxicillin and the synthesized AuNP are compared simultaneously against *Staphylococcus aureus* and *Klebsiella pneumoniae*. The strips are 7x11 cm and sterilized prior to the experiment. For this method, sterile Nutrient Agar plates are used. Miscellaneous requirements include cotton swabs for inoculating agar plates with bacterial suspensions, Alcohol in a beaker and forceps. The strips are coated with either Amoxicillin or AuNP and placed in a 'cross' manner. Plates are incubated at 37 degrees Celsius for 24 hours and checked for zone of clearance.

Methodology:

Gold Nanoparticle synthesis: Using Aqua Regia Dissolution and Turkevich method

$HAuCl_4$ salt was synthesized using the Aqua Regia Dissolution Method. Aqua Regia solution was prepared using the standard volumes, 3 parts concentrated HCl mixed with 1 part concentrated HNO3. Gold foil was dissolved in Deionized water to obtain a homogenous mixture. Aqua Regia solution was added to the homogenous mixture of Deionized water. To evaporate Nitric acid, this solution was heated for 15-30 minutes. The colour change was observed from yellow to greenish yellow after heating. Trisodium citrate was added as a capping agent. It provides stability to the nanoparticle which increases longevity for further usage. The solution was allowed to cool down for 30 mins. The sample was then scanned through UV-Visible Spectrophotometer and Colorimeter to obtain maximum peak absorption. It can further be tested for obtaining morphological characteristics using Scanning Electron Microscope (SEM), Atomic Force Microscopy (AFM) and Dynamic Light Scattering (DLS).

Potency testing of Gold Nanoparticle against Asthmatic bacterial strains:

The AuNP synthesis was tested against two strains of Asthmatic bacteria

1. Staphylococcus aureus- Gram positive bacteria
2. Klebsiella pneumoniae- Gram negative bacteria

with the antibiotic Amoxicillin, a subclass of Penicillin antibiotics used to treat bacterial infections. The potency was checked using the Immunological Assay, "Disc Diffusion Method." In this method, Nutrient Agar was used as the preferred media and the bacterial culture was swabbed to obtain a lawn growth of both bacterial strains. Sterile discs were coated with AuNP and Amoxicillin. The plates were incubated for 24 hours at 37 degree Celsius. The results were observed after the incubation period.

Synergy testing of Gold Nanoparticle against Asthmatic bacterial strains:

The AuNP synthesis was tested against two strains of Asthmatic bacteria

Staphylococcus aureus- Gram positive bacteria

Klebsiella pneumoniae- Gram negative bacteria

with the antibiotic Amoxicillin, a subclass of Penicillin antibiotics used to treat bacterial infections. The potency was checked using the Immunological Assay, "Cross-strip method." In this method, Nutrient Agar was used as the preferred media and the bacterial culture was swabbed to obtain a lawn growth of both bacterial strains. Sterile strips were coated with AuNP and placed in the center, followed by Amoxicillin coated strips in a cross manner. The plates were incubated for 24 hours at 37 degree Celsius. The results were observed after the incubation period.

Result:

1. After heat was provided, the mixture turned from yellow to green.
2. Spectral analysis indicated peak absorbance between 520-550 nm. Colorimetric analysis showed maximum absorbance at 530 nm.
3. Post incubation, for Disc diffusion assay zones of clearance were visible.
4. Post incubation, for Cross-strip method zones of clearance were visible.

Discussion:

1. The colour change indicated the synthesis of Nanoparticles.The colour change indicated reduction of Au3+ions to elemental gold (Au0), thus highlighting its unique optical property. The Reduction reaction is favoured due to Surface Plasmon Resonance (SPR), a phenomenon causing oscillations to particles in light condition. It is an initial confirmatory test to check if a nanoparticle has been synthesised and further analysis can be done to formulate its size, shape and other characteristics.
2. The Lambda max for Spectral and Colorimetric analysis indicates that the size of nanoparticles lies between 40-60 nm. The 40-60 nm range of AuNP is particularly beneficial in Biological usage as it shows no toxicity if it enters in the body. The size distribution is an important parameter in Antibacterial assays and depending on this parameter, various properties are influenced.
3. The zone of clearance was observed after 24 hours of incubation. This indicates the potency of AuNP against both Gram positive and Gram negative bacteria.The zone of clearance indicates that the synthesized nanoparticle shows antimicrobial properties. The zone is an area wherein bacterial growth is inhibited since the diffused AuNP interferes with the bacterial lawn. Since antimicrobial activity was exhibited against both Gram positive and Gram negative bacterial strains, it widens its application and makes the nanoparticle highly versatile. There were 4 discs tested against both bacteria

1) Disc coated only with nanoparticles - for Staphylococcus aureus zone size 2.8cm, for Klebsiella pneumoniae zone size 3.2cm.
2) Positive control: Disc coated only with antibiotic – for Staphylococcus aureus zone size 3.4cm, for Klebsiella pneumoniae zone size 2cm
3) Synergistic action using 2 sets of data:
    - Disc coated with 1:5, antibiotic:AuNP -for Staphylococcus aureus zone size 2.8cm, for Klebsiella pneumoniae zone size 2.1cm.
    - Disc coated with 1:10, antibiotic:AuNP - for Staphylococcus aureus zone size 3cm, for Klebsiella pneumoniae zone size 2.3cm.
4) There were zones of clearance observed for all the 4 discs indicating that AuNP are effective against the Asthmatic bacterial strains.

Disc diffusion assay for AuNP and *Staphylococcus aureus*

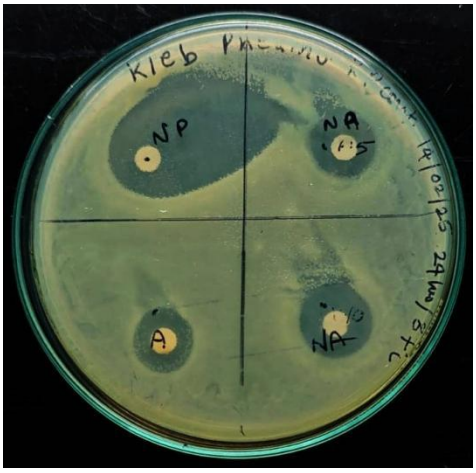

Disc diffusion assay for AuNP and *Klebsiella pneumoniae*

There were 2 strips tested against both bacteria

- Strip coated only with nanoparticle
- Strip coated only with antibiotic
- The zones of clearance showed a positive synergistic effect, thereby indicating that AuNP are effective against the Asthmatic bacterial strains. Studies pertaining Minimum Inhibitory Concentration (MIC) have shown lowered usage of drugs, thereby decreasing side effects and amplification of nanoparticle efficacy. Synergy implies that the combined effect of Antibiotic and nanoparticles is more effective in comparison to their individual effects, proving to enhance their antimicrobial activity. This results in administration of a lower dosage of antibiotic since it is compensated by target-specific AuNP. It aids in overcoming resistance mechanisms if opting for one-time therapies, causing hindrance in multiple resistance measures. A positive synergistic effect implies reduced toxic effects.

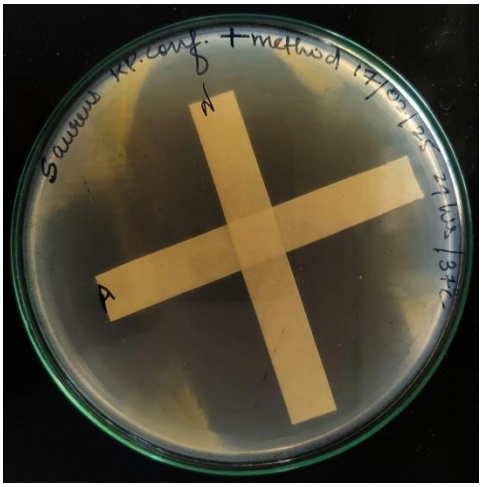

Cross-strip assay for AuNP and *Staphylococcus aureus*

Cross-strip assay for AuNP and *Klebsiella pneumoniae*

Conclusion:

The synthesis of Gold nanoparticles (AuNPs) was confirmed through colour change, implying the reduction of Au^{3+} ions to elemental gold (Au^0), due to Surface Plasmon Resonance (SPR). The Spectral and Colorimetric analysis showed that the size of the synthesized nanoparticles lies within the optimal range of 40-60 nm, appropriate for usage as a biomedical agent due to low toxicity. The zones of clearance against both Gram-positive and Gram-negative bacterial strains, indicate inhibition of pathogen survival.

The effectiveness of AuNPs was further enhanced through synergistic combinations with antibiotics, enabling for reduced dosage of antibiotics, minimizing potential side effects but also helps in overcoming bacterial resistance mechanisms. This proves the versatility and multi-usage techniques of AuNPs.

AuNP have proven beneficial to minimize side effects of chemotherapeutic drugs administered to cancer patients by acting as carriers to enhance the drug's efficacy. It can help in amplification of signaling for biosensory imaging due to better exhibition of surface plasmon resonance. Tumours can be detected using AuNP as contrast agents for optimal imaging, such as CT scans and MRI. These nanoparticles contain photothermal effects, hence thermal energy generated can be targeted to destroy cancer cells. Its imperative aspect is deployed to control release of therapeutic drugs due to a highly regulated drug-delivery system. Along with AuNP, Quantum dots can also be used as an excellent imaging tool for Research and Diagnostic purposes.

Acknowledgement:

We would like to express our sincere gratitude to the Department of Biotechnology of Jai Hind College for their invaluable support throughout our research.

References:

1. Aguilar-Garay, R., Lara-Ortiz, L. F., Campos-López, M., Gonzalez-Rodriguez, D. E., Gamboa-Lugo, M. M., Mendoza-Pérez, J. A., Anzueto-Ríos, Á., & Nicolás-Álvarez, D.
2. E. (2024). A comprehensive review of silver and gold nanoparticles as effective antibacterial agents. *Pharmaceuticals*, *17*(9), 1134. https://doi.org/10.3390/ph17091134
3. Borse, V., & Konwar, A. N. (2020). Synthesis and characterization of gold nanoparticles as a sensing tool for the lateral flow immunoassay development. *Sensors International*, *1*, 100051. https://doi.org/10.1016/j.sintl.2020.100051
4. Hammami, I., Alabdallah, N. M., Jomaa, A. A., & Kamoun, M. (2021). Gold nanoparticles: Synthesis properties and applications. *Journal of King Saud University - Science*, *33*(7), 101560. https://doi.org/10.1016/j.jksus.2021.101560
5. Low, A., & Bansal, V. (2010). A visual tutorial on the synthesis of gold nanoparticles.
6. *Biomedical imaging and intervention journal*, *6*(1), e9. https://doi.org/10.2349/biij.6.1.e9
7. Malarkodi, C., Rajeshkumar, S., Vanaja, M. et al. Eco-friendly synthesis and characterization of gold nanoparticles using Klebsiella pneumoniae. J Nanostruct Chem 3, 30 (2013). https://doi.org/10.1186/2193-8865-3-30
8. Oliveira, A. E. F., Pereira, A. C., Resende, M. A. C., & Ferreira, L. F. (2023). Gold Nanoparticles: A Didactic Step-by-Step of the Synthesis Using the Turkevich Method, Mechanisms, and Characterizations. *Analytica*, *4*(2), 250-263. https://doi.org/10.3390/analytica4020020
9. Pema Dechen, Peerapong Chumkaeo, Natcha Temnuch, Titiya Meechai, Laksamee Chaicharoen Molekul Chuaitammakit, Ninna Jansoon, & Ekasith Somsook. (2024). Simple Synthesis of Gold Nanoparticles (AuNPs) from Gold Leaf by Electrolysis. *Journal of Chemical Education*, *101*(9), 4018–4023. https://doi.org/10.1021/acs.jchemed.4c00601
10. Sengani, Manimegalai & Grumezescu, Alexandru & Rajeswari, Devi. (2017). Recent trends and methodologies in gold nanoparticle synthesis – A prospective review on drug delivery aspects. OpenNano. 2. 10.1016/j.onano.2017.07.001.
11. Sarma, P. P., Rai, A., & Baruah, P. K. (2024). Recent Advances in the Development of Antibiotics-Coated Gold Nanoparticles to Combat Antimicrobial Resistance. *Antibiotics (Basel, Switzerland)*, *13*(2), 124. https://doi.org/10.3390/antibiotics13020124
12. Xiaoning Li, Sandra M. Robinson, Akash Gupta, Krishnendu Saha, Ziwen Jiang, Daniel F.Moyano, Ali Sahar, Margaret A. Riley, and Vincent M. RotelloACS Nano 2014 *8* (10),10682-10686 DOI: 10.1021/nn5042625.

International Journal of Multidisciplinary Research and Technology
ISSN 2582-7359, Peer Reviewed Journal, Impact Factor 6.325
www.ijmrtjournal.com

BEYOND GREEN ENERGY: ADDRESSING ENVIRONMENTAL AND SOCIAL IMPACTS IN SOLAR DEVELOPMENT

[1]Siddhika Mohan, [2]Bharat Bushan Sharma, [3]Seema Mishra
SIES Indian Institute of Environment Management, Kukshet, MIDC
Juinagar, Navi Mumbai 400706, Maharashtra, India

Abstract

Energy consumption has increased rapidly in recent decades, as has environmental awareness within the energy industry. It is now widely recognized that traditional energy generation methods have a significant negative impact on the environment. To address this issue, the solar industry has emerged as a major player in renewable energy, experiencing widespread growth in recent years. However, the question remains: is this increased reliance on solar energy truly environmentally sustainable? Developing solar energy projects still has its own set of environmental and social concerns to be addressed. Environmental impacts like fugitive emissions, increased vehicular traffic, soil degradation due to excavation, impact on flora and fauna of the site etc. And the other social concerns like influence of migrant labourers on local communities, waste management, worker safety, continue to be cause for concern. Thus, a more holistic way to develop solar power is envisaged. The current paper proposes a solution to this problem by developing a methodology to rate the impacts of solar energy projects on environmental and social factors. This method of Sustainability Rating for Solar Energy (SRSE) can be used to rate the performance of a solar energy project construction site for its environmental, social and governance practices. This can help in developing better policies and promote best practices within the solar industry.

Keywords: Renewable Energy, Environmental Impact, Sustainable Development, Social Impact, Solar Energy, Methodology development.

Introduction

Renewable energy is an in trend in the current markets and has already contributed to over 10% of worlds electricity by 2022(Renewable 2022 Global Status Report 2022). Solar energy tops the list because of its ease of use, scalability, competitive pricing and low carbon technology(Ghaleb et al. 2023) (Sillman et al. 2023). India is set on a renewable energy target of 450 GW by 2030 of which approx. 300 GW is expected from solar(Shiradkar et al. 2022). However, this rampant development of solar power can also harm the environment if not developed in a responsible manner. Development of renewable power like any other construction project can cause harm to environmental and social factors.(Kaygusuz 2009) Hence, to truly focus on sustainable development we need to consider minimising these impacts as well.

This current study is an extension of studying in detail the environmental and social impacts of several solar energy projects. These impacts included the environmental impacts on the air, water, soil quality, noise and biodiversity and social impacts on the local communities, employment, waste management etc. The study also surveyed the solar energy professionals to understand their opinion on various matters. This led to the requirement of a simple and efficient system using which the development of solar can be done as per the principles of sustainable development.

The current paper develops a methodology of assessing the sustainability of solar energy development projects. This methodology can be used to score the solar projects as per their sustainability rating. This will help best practices to be developed in the solar industry and in a sustainable manner. This paper aims to propose and promote the sustainability in solar energy project development for wide scale applications.

Sustainability Rating for Solar Energy (SRSE) – the concept

There is much research that aims to solve solar energy and its impact on the environment as a challenge so that the solar industry can develop in a sustainable and holistic manner. This paper attempts to create a tool that can help gauge the impacts of solar projects in terms of its sustainability. This Sustainability Rating for Solar Energy (SRSE) is an attempt to make a simple rating methodology that can be put to direct use by the industries, policy making bodies, certification agencies etc. moreover the tool is very much adaptable to be used in different types of solar energy projects. The scoring methodology for this methodology is divided in 10 different categories. The rating

covers all areas of sustainable development including environment, social and governance aspects. This methodology caters specifically during the construction and development stage of solar energy. The rationale for considering these specific categories is as follows:

Environment: 5 out of 11 categories belong to the environment domain, these include Land use and Geology, water, waste, air and noise, Biodiversity.

1. Land use changes due to solar power has remained a major topic of concern since inception. Its concerns around changing land use of farming, poultry, gazing to be replaced with solar is an important aspect to consider. Along with it the geology of the soil is also important because the construction activities usually involve some levelling and topsoil removal impacting the soil quality.

2. Water consumption is major in solar projects as it is not only required for construction purposes but also in operations during cleaning.

3. Waste in solar project sites not only include solid waste of employees but also other waste of hazardous and non-hazardous nature like waste oils, plastic, metal scrap etc. this makes it very important to manage waste in efficient manner as it can not only have impact on the environmental factors like soil and water but also have impact on local communities. By ensuring that the waste is managed properly we ensure that the nearby land does not get affected, and there is no Odor nuisance to local communities.

4. Air pollution in solar sites can occur due to activities like land levelling, excavation, movement of trucks in and around the area, presence of diesel generators etc. this could have an adverse impact on the workers at site and nearby communities. Also, noise is generated in the project sites during movement of heavy-duty equipment's and vehicles, operation of generators, etc. hence it becomes an important factor to address during construction.

5. Biodiversity is the most evident impact of construction activities like levelling and excavation. Moreover, the solar panels will have structures dug into the ground permanently. All these can cause a permanent or temporary disturbance in biodiversity.

Social

1. Local communities' involvement plays a major role in ensuring sustainable development of any project. Local communities are also majorly impacted due to the development of the project, their gazing or farming lands may be of use here. They will be impacted by the traffic increase in the area, the influx of migrant labourers etc. so it is important to carefully consider the impact of any project on the local communities.

2. Employment given to the workers and site engineers are also stakeholders to the project and it is important to consider that there is adherence to good labour laws to ensure sustainable development.

3. It is required to ensure the safety of the site personnel and workers at the time of working. Safety practices like use of PPE and safety instructions and trainings are crucial to the proper construction and operation of the solar plant.

Governance

1. Governance as a subsection mainly concerns with the companies that are executing the work on site, if they have standard protocols and processes in place that makes the work efficient, and if they are providing as per the requirements of the customer/project proponent.

2. Supply chain management in any solar project plays a crucial role in ensuring sustainable development of solar power. It is also the category that contributes maximum to carbon emissions due to solar power. Thus ensuring sustainability in supply chain management can ensure reduction in carbon emission and development of business in regional areas.

3. Ethical disclosures of all the businesses associated with the development of solar power will go a long way to ensure the most efficient and effective output of the project.

The scores are allotted to each of the categories as mentioned below:

Category	Score
Land use and Geology	120
Water	100
Waste	130
Air and Noise	150
Biodiversity	100
Local communities	100
Employment	100
Safety	100
Governance	100
Supply Chain Management	100
Ethical Disclosures	100
Total	1200

The specific data points to be assessed in each of the categories is listed below;

Land use and Geology

No	Question	Maximum Points
1	Is the location of Construction being developed on waste land/reclaimed land	20
2	Was alternative site assessment done? (with evidence)	10
3	is the current land use of the area being changed? Is there a proper transition plan for this change?	10
4	Is there any resettlement and rehabilitation? if yes, what are the conditions of resettlement	20
5	Impacts on Soil identified	10
6	Mitigation measures identified	10
7	Mitigation measures implemented	10
8	Applicable land laws identified? Any conflict with the local, national and international laws?	10
9	Any special initiatives to reduce impact on land use/geology?	20

Water

No	Question	Maximum Score
1	Sources of water? How is water consumption being monitored?	20
2	Recycled water being used?	20
3	RWH system on site being used?	20
4	Identified potential impacts on water bodies in surrounding areas (10 KM radius)	10
5	Mitigation measures to reduce the impacts being implemented	10
6	Any other site level initiatives to reduce water consumption during construction	20

Waste

No	Question	Maximum Score
1	Inventory of possible waste generations categorised as hazardous and non-hazardous?	20
2	How is waste generation being monitored	20
3	Is there any recycled material used during construction?	25
4	Identify impacts of waste generated on site	10
5	Mitigation measures for reducing waste generation identified and implemented	20
6	Processes for proper disposal of waste along when implementation proof	20
7	Any buy back agreements of solar PV	15

Air and Noise

No	Question	Maximum Score
1	Impact on air and noise quality identified on site	10
2	Identified mitigation measures	10
3	Measures implemented to control fugitive emissions, SOx/Nox etc, Maintenance of all vehicles visiting site	20
5	Ambient air quality monitoring, DG stack monitoring	10
6	Measures on site, like Water sprinklers/tyre washers	10
7	Calculated Scope 1 emissions on site	20
8	Calculated Scope 2 emissions on site	20
9	Calculated emissions from employee commute	25
10	Calculated emissions from business travel	25

Biodiversity

No	Question	Maximum Score
1	Impacts on Biodiversity identified	10
2	Mitigation measures identified	10
3	List of mitigation measures implemented	10
4	Special initiatives to protect flora of the area	25
5	Number of trees transplanted	20
6	Special initiatives to protect fauna of the area	25

Local Communities

No	Question	Maximum Score
1	Process for grievance redressal mechanism	20
2	Implementation on site process and documentation related to Grievance redressal	15
3	No of grievances dealt with till date	15
4	Interaction with local communities with documentation	10
5	Impacts on local communities identified	10
6	Mitigation measures identified	10
7	Mitigation measures implemented	10
8	Other social good initiatives	10

Employment

No	Question	Maximum Score
1	Job creation for local communities	20
2	Human rights assessment by external/internal party on site	20
3	Wages for workers and on-site employees- check against minimum wage laws	10
4	Diversity and inclusion initiatives	10
5	Stay facilities for workers (contract or permanent) and employees -	20
6	Other employee and worker welfare initiatives on site	20

Safety

No	Question	Maximum Score
1	Process related to safety identified on site	10
2	On site implementation of all safety protocols - process display boards etc	20
3	Toolbox talks provided to onsite workers on various safety related topics	10
4	training sessions provided to employees and workers on safety- with documentation	10
5	PPE used by all employees and workers	10
6	Safety certifications acquired by site	20
7	safety measures of products used - the onsite equipment's used are designed as per good safety protocols	20

Governance

No	Question	Maximum Score
1	On site risk management - Processes, register and other documentation	20
2	Disaster management plan	20
3	Business continuity plan	20

4	Green certified products used	20
5	Customer satisfaction process- rating, feedback and improvements done	20

Supply Chain Management

No	Question	Maximum Score
1	Processes on supply chain management and greening setup	10
2	Distance of supplier from site - additional points for processes that reduce the distance	20
3	Mode of transport of goods	10
4	carbon emissions due to transportation	10
5	carbon emissions for purchased good and services and capital good	10
6	Initiatives to reduce carbon	20
7	% share of local/international companies on all of procurement	10
8	Green certification of products bought	10

Ethics and Disclosures

No	Question	Maximum Score
1	Annual report of the company containing balance sheet, P&L statement etc	25
2	Anti-corruption and Anti bribery policy of the company	25
3	Anti-competitive clause in company policy	25
4	Ethical behaviours	25

There is also guidance prepared against each data point for the assessor to check, it is not disclosed in this paper as it would increase the length and can have subjectivity in interpretation. If there is any need for details of the of the guidance, the corresponding author can be reached out.

Benefits and future directions

This methodology can be used in

1) Developing a certification in the field of solar energy which ensures the sustainable development of solar energy.
2) It will help in understanding and propagating the best practices in the solar industry among the developers.
3) It will urge the developers to innovate and develop solutions that can reduce the impacts of solar energy.
4) It can help develop policies in solar along these lines.
5) It will support in reducing the environmental and social impacts of solar energy.

Limitations

Although, this methodology comprehensively covers the different aspects of sustainable development of solar energy. There are also few limitations to it, which when addressed can lead to better future directions.

1. The current methodology is qualitative assessment leading to subjectivity in the implementation of the methodology.

2. The assessment can only be done by a third party to ensure the sustainability of the project.
3. Is open ended basis the various initiatives to be taken in some of the areas, where the needs might differ as per the geographical region.
4. Additional areas may need to be introduced based on the type of solar being developed eg floating solar.
5. Incurring additional cost for implementing this methodology could dissuade the companies from adopting this methodology.

Conclusion

The current paper addresses the question on how solar energy development can be made sustainable. With the rampant development of solar energy in India, it has become imperative that solar energy can cause environmental impacts like fugitive emissions, impact on soil quality, water quality etc. It can cause of social impacts like issues to local communities, employment and stay facilities, waste management etc. The current methodology ensures that al these concerns are addressed to arrive at a better solution. The methodology developed is spread across 11 major categories in environment, social and governance. There is total 76 questions addressing the various categories and issues.

This methodology can be used to development a certification and promote the best practices in solar industry. There are certain limitations to this methodology like its qualitative nature, subjectivity and generic approach. However, due to the rampant development of solar it is imperative that the industry needs some guidelines to develop solar in a sustainable manner. In summary the development of solar is crucial to transition to a low carbon economy. However, this development needs to be carried out in a sustainable manner. It is our collective responsibility to make this transition a success, for the well-being of both our planet and future generations.

References

1. Ghaleb B, Abbasi SA, Asif M 2023. Application of solar PV in the building sector: Prospects and barriers in the GCC region. Elsevier BV. Energy Reports 9: 3932– 3942.
2. Kaygusuz K 2009. Environmental impacts of the solar energy systems. Energy Sources, Part A: Recovery, Utilization and Environmental Effects 31: 1376– 1386.
3. Renewable 2022 Global Status Report 2022.
4. Shiradkar N, Arya R, Chaubal A, Deshmukh K, Ghosh P, Kottantharayil A, et. al. 2022. Recent developments in solar manufacturing in India. Elsevier BV. Solar Compass 1: 100009.
5. Sillman J, Hynynen K, Dyukov I, Ahonen T, Jalas M 2023. Emission reduction targets and electrification of the Finnish energy system with low-carbon Power- to-X technologies: Potentials, barriers, and innovations – A Delphi survey. Elsevier Inc. Technological Forecasting and Social Change 193: 1–11.

International Journal of Multidisciplinary Research and Technology
ISSN 2582-7359, Peer Reviewed Journal, Impact Factor 6.325
www.ijmrtjournal.com

NANOMATERIALS AND NANOTECHNOLOGY : SURFACE CHEMISTRY DEPOSITION OF COPPER NANOPARTICLES

[1]Om Prakash Yadav, [2]Vijay D. Gangan

[1]Department of Physics, Patkar Varde College of art Science and Commerce
Goregaon (West), Mumbai - 400062.
[2]Department of Chemistry, Reena Mehta College of Arts, Commerce, Science and Management studies, Bhayander (West), Thane - 401101.

Abstract : Deposition of nanoparticles are proportional to the intensity of plasma. Deposition of Nanoparticles under influence of vacuum pressure, argon gas and materials with DC power supply. The materials (copper) deposited after bombarding the argon gas with flow rate 10-60 sccm by mass flow controller and power supply from 540 V DC source to sputter source which is attached from vacuum chamber. There are different parameters which help to make stable and intense plasma inside vacuum pressure with argon gas and this deposition of copper Nanomaterials was done by me in 2011 from Excel Instruments and polycrystalline from eco-friendly diamond by Seki machine CVD process, power supply. Plasma triggering source can be different design like circular, rectangular and square *etc*. include the Silver Nano platform for using silver nanoparticles as an antibacterial agent, nanoparticle based transparent sun screens and the pure form of metal-based nanoparticles, which are also called metal nanoparticles (e.g., silver, copper, gold, titanium, platinum, magn, iron *etc*). Sputter source is used for growth of copper, aluminium, iron, gold and silver under vacuum pressure in the presence of DC source, argon gas and sample holder inside vacuum chamber.

Key words : Nanoparticles, plasma, copper, TiO_2, aluminium, titanium, nichrome, gold, SiO_2 *etc.*

Introduction

The plasma physics enormously contribute to nanotechnology for obtaining Nanoparticles[1] of different materials like Copper, Alumina, titanium, titanium dioxide (TiO_2), gold, silver *etc.* the different materials are used as target can be obtained deposition of materials. Deposition of materials to be used for coating. The coating of materials are obtained from different sputter source. It is used for chip coating and for low power voltage which are used in electronic devices and it is also for growth of Polly and single crystalline[2-3].

Materials and Methods

Methods of plasma Deposition : Check sputter source is properly connected from cooling line, create base vacuum pressure upto 2-3 milli Bar inside vacuum system and now inject 10-30 sccm argon gas in system and maintain pressure and power one by one and maintain pressure same as above then the plasma will glow inside system and it is started to deposition on sample holder which is mounted inside vacuum system.

Results and Discussion

Experimental : Plasma deposition is obtained with the help of a sputter system which is attached with a water cooled sputter source, pumping for vacuum, 1kv DC power supply, digital display for vacuum pressure.the following parameters are used for deposition or coating of nanoparticle for different materials.

1. Copper target of 2 inch diameter
2. DC voltage 342 volt
3. Current in 82 mA
4. Gas pressure in system 262 m. Torr
5. Argon gas injected in system 0-30 SCCM.
6. Plasma stay time : 20 min

Plasma glowing in the below image and coating on glass.

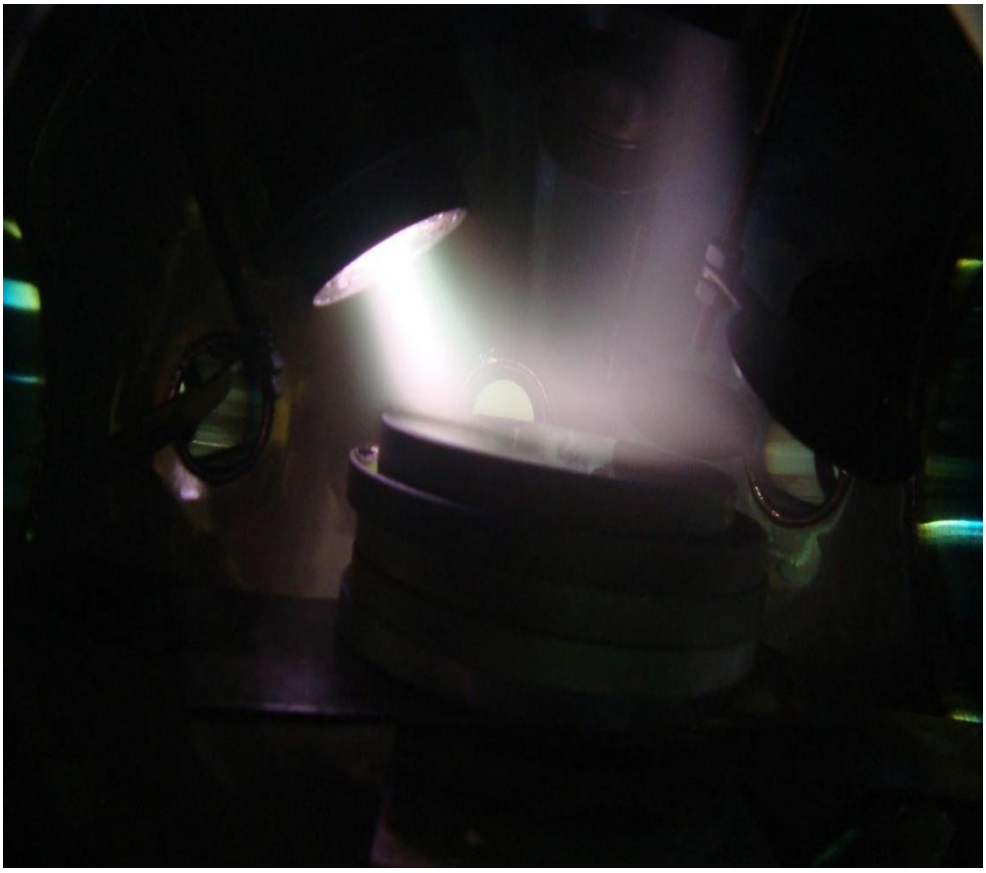

Low and high intensity plasma

Applications

They are widely used as coating materials in biomedical sciences as antimicrobial[4] and antifouling agents. Copper NPs are being used as insulating agents on medical implants to block pathogen growth. Effectivity of copper nanoparticles is found in varied applications such as Antifungal, Antiviral, Antibiotics, Anticancer, Photocatalytic, in biomedical, agriculture fields *etc*.

Conclusion

1. Plasma physics makes easier for Nanoparticle deposition on mobile chip as conductor for minor voltage and used for coating on watches, Glass windows, coating for partial transparent glass and for cancer treatment.
2. Carbon based single crystalline seki CVD diamond is use in the process of thin atomic layer deposition at depositing thin layers of material.
3. CVD Diamond is also used for cutting glasses. And also used for making bores in the ground.
4. It is used in in high power in electronics and radiation detection.
5. In defence system for high thermal conductivity n the range of 600 to 1200^0C.

References

1. Heyer S., Janssen W., Turner S., Lu Y. G., Yeap W. S., Verbeeck J., Haenen K., Kruger A. (2014), *ACS Nano*, 8, pp. 5757 - 5764 and the references cited theirin.
2. Heiligtag, Florian J.; Niederberger, Markus (2013). The fascinating world of nanoparticle research. *Materials Today*. **16** (7–8), pp. 262 - 271.
3. Gong, Yan; Luo, Da; Choe, Myeonggi; Kim, Yongchul; Ram, Babu; Zafari, Mohammad; Seong, Won Kyung; Bakharev, Pavel; Wang, Meihui; Park, In Kee; Lee, Seulyi; Shin, Tae Joo; Lee, Zonghoon; Lee, Geunsik; Ruoff, Rodney S. (April 24, 2024). "Growth of diamond in liquid metal at 1 atm pressure". *Nature*. **629** (8011), pp. 348–354 and the references cited theirin.
4. Ramyadevi, J.; Jeyasubramanian, K.; Marikani, A.; Rajakumar, G.; Rahuman, A. A. (2012). "Synthesis and antimicrobial activity of copper nanoparticles". *Mater. Lett*. **71**: 114–116. doi:10.1016/j.matlet.2011.12.055

International Journal of Multidisciplinary Research and Technology
ISSN 2582-7359, Peer Reviewed Journal, Impact Factor 6.325
www.ijmrtjournal.com

EVALUATING THE AUTHENTICITY OF *MESUA FERREA* L. STAMENS AND ITS ADULTERANTS USING CHEMICAL FINGERPRINTING TECHNIQUE.

[1]Liviya Gaikwad, [2]Aparna Saraf
Department of Botany, The Institute of Science, Dr. Homi Bhabha State University
15, Madame Cama Road, Fort, Mumbai – 400032 India

Abstract

This investigation examines the substitution of adulterants for authentic *Mesua ferrea* L. stamens, a vital component in traditional herbal medicine whose quality is critical for therapeutic efficacy. Driven by economic and supply challenges, the increasing use of substitute materials raises concerns regarding safety and bioactivity. Samples of *Mesua ferrea* L. stamens and their purported adulterants were compared through preliminary phytochemical screening and HPTLC analysis. The phytochemical profiles revealed distinct differences between the authentic and substituted materials. Two mobile phases—Toluene: Chloroform: Ethanol (4:4:1, v/v/v) and Toluene: Ethyl acetate: Formic acid (5:4:1, v/v/v)—were employed for HPTLC to optimize the separation of key constituents. The resulting chromatographic fingerprints clearly distinguished the authentic stamens from their adulterants, confirming that the substituted materials do not replicate the unique chemical composition of *Mesua ferrea* L. These findings highlight the necessity for rigorous scientific validation of traditional substitution practices, reinforcing the need for strict quality control and regulatory measures in herbal medicine preparations.

Keywords: *Mesua ferrea* L., adulteration, preliminary phytochemical screening and HPTLC.

1. Introduction

Herbal medicines have long served as the foundation of traditional healthcare systems and continue to gain global acceptance due to their natural origin and therapeutic potential (1). However, the rising demand for these products has been accompanied by increasing instances of adulteration and substitution, posing significant risks to both efficacy and patient safety (2). Economic pressures and supply limitations often incentivize the use of inferior substitutes in place of authentic herbal ingredients, thereby compromising the quality of traditional formulations (3).

Mesua ferrea Linn., commonly known as Nagkesar, is one such medicinal plant whose stamens are integral to various therapeutic preparations. Renowned for their unique bioactive compounds, the stamens of *Mesua ferrea* are valued for their role in delivering specific pharmacological benefits (4). Yet, the authenticity of these stamens is frequently undermined by the intentional or accidental incorporation of adulterants, which may differ markedly in chemical composition and biological activity.

Ensuring the integrity of herbal raw materials is essential, and this necessitates the use of robust analytical methods. Preliminary phytochemical screening provides a baseline understanding of the chemical constituents present in plant extracts, while High-Performance Thin-Layer Chromatography (HPTLC) offers a detailed fingerprint of these complex mixtures. The application of two distinct mobile phases—Toluene: Chloroform: Ethanol (4:4:1, v/v/v) and Toluene: Ethyl acetate: Formic acid (5:4:1, v/v/v)—in HPTLC enhances the separation and resolution of key phytoconstituents, thereby enabling a clear differentiation between authentic *Mesua ferrea* stamens and their substitutes.

This study aims to compare the phytochemical profiles and HPTLC fingerprints of genuine *Mesua ferrea* stamens with those of their adulterants. By integrating preliminary phytochemical screening with dual mobile phase HPTLC analysis, we seek to establish reliable markers for authenticity and develop a robust quality control framework. The outcomes of this research are anticipated to contribute to the scientific validation of traditional substitution practices and support the implementation of stringent regulatory measures to safeguard the integrity of herbal medicinal products.

2. Materials And Methods

2.1 Collection and authentication of plant materials

Flowers of *Mesua ferrea* Linn. were collected in February from Veermata Jijabai Bhosale Udyan in Mumbai. The immature fruits of *Cinnamomum tamala* T. Nees & Eberm., the fruits of *Dillenia pentagyna* Roxb., and the buds of *Myristica fragrans* Houtt. were obtained in June. The first was collected from a botanical garden in Dahanu (Palghar, Maharashtra), while the latter two were sourced from Dapoli (Jalgaon, Maharashtra). Similarly, unripe fruits of *Cinnamomum wightii* Meisn. and floral buds of *Ochrocarpus longifolius* Benth & Hook f. were collected during May and June from a local botanical garden in Mira Road, Mumbai. Buds of *Calophyllum inophyllum* L. were collected from BPT garden, Mumbai. The sample of *Mesua ferrea* Linn. used in the study was verified and authenticated at the Blatter Herbarium, St. Xavier's College, Fort, Mumbai. The voucher specimen number given was NDG-2259. The other plants were identified by Dr. C.S. Latoo, an eminent botanist, taxonomist, and former herbarium in-charge at The Institute of Science, Mumbai.

2.2 Preparation of powder

The flowers of *Mesua ferrea* Linn., unripe fruits of *Cinnamomum tamala* T. Nees & Eberm., and *Cinnamomum wightii* Meisn., flower buds of *Ochrocarpus longifolius* Benth and Hook f., *Myristica fragrans* Houtt. and *Calophyllum inophyllum* L., fruits of *Dillenia pentagyna* Roxb. were shade dried for a week. Subsequently, stamens from the flowers of *Mesua ferrea* Linn. were separated and ground into a fine powder using a mixer blender. Similarly, the shade-dried unripe fruits of *Cinnamomum tamala* T. Nees & Eberm. and *Cinnamomum wightii* Meisn., as well as the flower buds of *Ochrocarpus longifolius* Benth and Hook f., *Myristica fragrans* Houtt. and *Calophyllum inophyllum* L., fruits of *Dillenia pentagyna* Roxb. were mechanically ground into powder.

2.3 Preparation of extracts

Two grams of powdered stamens of *Mesua ferrea* Linn., unripe fruits of *Cinnamomum tamala* T. Nees & Eberm., and *Cinnamomum wightii* Meisn., flower buds of *Ochrocarpus longifolius* Benth and Hook f., and *Myristica fragrans* Houtt., fruits of *Dillenia pentagyna* Roxb., buds of *Calophyllum inophyllum* L. were extracted in methanol using Soxhlet extraction. The extracts were then filtered and evaporated to obtain the concentrated residues for qualitative analysis of secondary metabolites.

2.4 Phytochemical Screening

Preliminary Phytochemical Screening for presence of various secondary metabolites such as tanins, saponins, alkaloids, flavonoids, glycosides, quinones, phenols, terpenoids, cardiac glycosides, coumarins, steroids, phlobatanins, anthrocyanins and anthroquinones were carrired out using standard tests (5).

2.5 HPTLC

The HPTLC analysis was carried out using TLC Silica gel 60 F254 plates. The standards and soxhleted methanolic extracts were applied onto TLC Silica gel 60 F254 plates using a CAMAG Linomat 5 applicator to ensure precise and uniform application. The applicator was set to deliver samples as 6 mm wide bands, maintaining a consistent distance of 10 mm from the bottom edge of the plate to facilitate proper development. The tracks were spaced at 8 mm intervals to prevent overlap and ensure distinct resolution of bands.

Each track was designated for a specific sample or standard: track 1 for Mesuaferrone A, track 2 for Quercetin, track 3 for Chrysin, track 4 for Rutin, track 5 for a blank, and subsequent tracks for the herbal samples, including *Mesua ferrea* Linn., *Ochrocarpus longifolius* Benth and Hook f., *Cinnamomum wightii* Meisn., *Cinnamomum tamala* T. Nees & Eberm., *Myristica fragrans* Houtt., *Dillenia pentagyna* Roxb. and *Calophyllum inophyllum* Linn. The automated application with the Linomat applicator minimized variability, ensuring reproducible band intensity and enhancing the accuracy of the HPTLC analysis.

Two different mobile phases were used for the analysis. The first mobile phase comprised of Toluene: Chloroform: Ethanol in the ratio 4:4:1 (v/v/v), while the second mobile phase was Toluene: Ethyl acetate: Formic acid in the ratio 5:4:1 (v/v/v). The plates were pre-saturated with the respective mobile phase for 20 minutes before development, and the development distance was set at 70 mm.

For derivatization, anisaldehyde sulphuric acid reagent (ASR) was used. The reagent was prepared by mixing 170 mL of methanol with 20 mL of acetic acid and 10 mL of sulphuric acid in an ice-cooled bath. After thorough mixing and cooling to room temperature, 1 mL of anisaldehyde was added. The developed plates were observed under white light, 254 nm, and 366 nm wavelengths, both before and after derivatization, to identify and confirm the presence of the markers- Mesuaferrone A, Chrysin, Quercetin, and Rutin in the extracted samples.

The documentation of the HPTLC analysis was conducted using the VisionCATS software, which is integrated with the CAMAG HPTLC system. The VisionCATS software automatically captured high-resolution images of the developed plates, both before and after derivatization, ensuring precise visualization of the chromatographic results.

Results

The preliminary phytochemical screening of *Mesua ferrea* L. stamens and its potential adulterants (Table 1), which include the buds of *Ochrocarpus longifolius* Benth and Hook f., unripe fruits of *Cinnamomum wightii* Meisn. and *Cinnamomum tamala* T. Nees & Eberm., buds of *Myristica fragrans* Houtt., fruits of *Dillenia pentagyna* Roxb., and buds of *Calophyllum inophyllum* L. revealed the following:

- **Tannins:** Detected exclusively in *Mesua ferrea* L. and absent in all adulterants.
- **Flavonoids:** Present in *Mesua ferrea* L., *Ochrocarpus longifolius* Benth and Hook f., *Cinnamomum wightii* Meisn., and *Calophyllum inophyllum* L.; absent in *Cinnamomum tamala*, *Myristica fragrans*, and *Dillenia pentagyna*.
- **Quinones and Terpenoids:** Consistently present across all samples.
- **Phenols:** Found in *Mesua ferrea* L., *Ochrocarpus longifolius*, *Cinnamomum wightii* Meisn., and *Calophyllum inophyllum* L.; not detected in the other adulterants.
- **Anthocyanins and Anthraquinones:** Identified solely in *Mesua ferrea* L.
- **Steroids:** Present in all samples tested.
- **Alkaloids, Saponins, and Glycosides:** Not detected in any of the samples.

These findings establish a distinct phytochemical profile for *Mesua ferrea* L. that differentiates it from its potential adulterants.

The HPTLC analysis, highlighted the chemical profiles of *Mesua ferrea* Linn. stamens and their adulterants using Toluene: Chloroform: Ethanol (4:4:1) as the mobile phase. Tables 2 and 3 and figures 1 to 12 in the study present detailed HPTLC fingerprints and corresponding densitograms for the phase Toluene: Chloroform: Ethanol (4:4:1), clearly illustrating the separation of compounds and supporting the identification of species-specific markers. The reference Rf values established for key phytochemicals were 0.26 for Mesuaferrone A, 0.23 for Quercetin, and 0.50 for Chrysin, while Rutin was not detected. In the chromatographic profiles of *Mesua ferrea* stamens, a prominent peak at Rf 0.26 confirmed the presence of Mesuaferrone A, and a distinct band at Rf 0.50 corresponded to Chrysin. Additionally, Quercetin (Rf = 0.23) was observed in certain adulterants, such as *Cinnamomum wightii* Meisn. and *Myristica fragrans* Houtt., under the same conditions. When the analysis was performed using a second mobile phase, Toluene: Ethyl Acetate: Formic Acid (5:4:1), the reference Rf values shifted to 0.55 for Mesuaferrone A, 0.49 for Quercetin, and 0.64 for Chrysin. The study includes detailed HPTLC fingerprints and corresponding densitograms for mobile phase -Toluene: Ethyl Acetate: Formic Acid (5:4:1), which are presented in the tables 4 and 5 and figures 13 to 24. Under these conditions, a peak at Rf 0.55 was clearly observed in the stamens of *Mesua ferrea* Linn., while none of the adulterants—such as *Ochrocarpus longifolius* Benth and Hook f., *Cinnamomum tamala*, *Myristica fragrans* Houtt., *Dillenia pentagyna* Roxb., or *Calophyllum inophyllum* L.—exhibited a corresponding peak. However, overlapping Rf values (0.02, 0.07, 0.22, and 0.71) were noted between *Mesua ferrea* and its adulterants, indicating that this mobile phase provided less specificity in differentiating the samples.

Discussion

In the context of quality control in herbal medicine, ensuring the authenticity of plant materials is critical for therapeutic efficacy and patient safety (6) . The combined preliminary phytochemical analysis and HPTLC

fingerprinting performed in this study offer valuable insights into the chemical differences between authentic *Mesua ferrea* L. stamens and their adulterants.

Previous studies have reported on the preliminary phytochemical analyses of the leaves and flowers of *Mesua ferrea* L (4,7) . However, this study is the first to examine the stamens, where tannins, anthocyanins, and anthraquinones are reported for the first time. The exclusive presence of these compounds in the stamens makes them reliable markers for authenticity, effectively distinguishing genuine *Mesua ferrea* L. stamens from adulterants.

For HPTLC, different solvent systems were worked out, and these two mobile phases i.e. Toluene: Chloroform: Ethanol (4:4:1) and Toluene: Ethyl Acetate: Formic Acid, (5:4:1) provided effective separation of bands. Notably, Mesuaferrone A was first detected by HPTLC in the stamens of *Mesua ferrea* L. The first mobile phase (Toluene: Chloroform: Ethanol, 4:4:1) provided superior specificity for distinguishing *Mesua ferrea* stamens from its adulterants. The distinct detection of Mesuaferrone A at an Rf value of 0.26 and Chrysin at an Rf value of 0.50 serves as a robust fingerprint for authentic *Mesua ferrea* L. material, whereas the occurrence of Quercetin in the adulterants underscores the need for reliable markers in sample authentication. Although the second mobile phase (Toluene: Ethyl Acetate: Formic Acid, 5:4:1) confirmed the presence of Mesuaferrone A in *Mesua ferrea* at an Rf value of 0.55, the overlapping Rf values observed for other compounds between the authentic sample and its adulterants reduce its discriminatory power. This overlap indicates that the first mobile phase provided better resolution for identification, particularly when distinguishing between closely related chemical profiles.

These findings suggest that for accurate detection of adulteration in *Mesua ferrea*, the first mobile phase is preferable. The unique band for Mesuaferrone A reinforces its utility as a species-specific marker, while also highlighting the need for further chromatographic optimization—especially to resolve compounds like Rutin, which were inadequately separated under the current conditions. Thus, this underscores the potential of HPTLC as an effective quality control tool within the Indian system of medicine, ensuring both the authenticity and integrity of herbal preparations.

Table 1: Preliminary phytochemical analysis of Mesua ferrea Linn. and its adulterants.

Phytochemicals	Results						
	Stamens of *Mesua ferrea* Linn.	**Buds of *Ochrocarpus longifolius* Benth and Hook f.**	**Unripe fruits of *Cinnamomum wightii* Meisn.**	**Unripe fruits of *Cinnamomum tamala* T. Nees & Eberm.**	**Buds of *Myristica fragrans* Houtt.**	**Fruits of *Dillenia pentagyna* Roxb.**	**Buds of *Calophyllum inophyllum* L.**
Tanins	+	-	-	-	-	-	-
Saponins	-	-	-	-	-	-	-
Alkaloids	-	-	-	-	-	-	-
Flavonoids	+	+	+	-	-	-	+
Glycosides	-	-	-	-	-	-	-
Quinones	+	+	+	+	+	+	+
Phenols	+	+	+	-	-	-	+
Terpenoids	+	+	+	+	+	+	+
Cardiac glycosides	+	+	+	-	-	-	-
Coumarins	+	+	+	-	-	-	+
Steroids	+	+	+	+	+	+	+
Phlobatanins	-	-	-	-	-	-	-
Anthrocyanins	+	-	-	-	-	-	-
Anthroquinones	+	-	-	-	-	-	-

Key: '+': positive, '-': negative

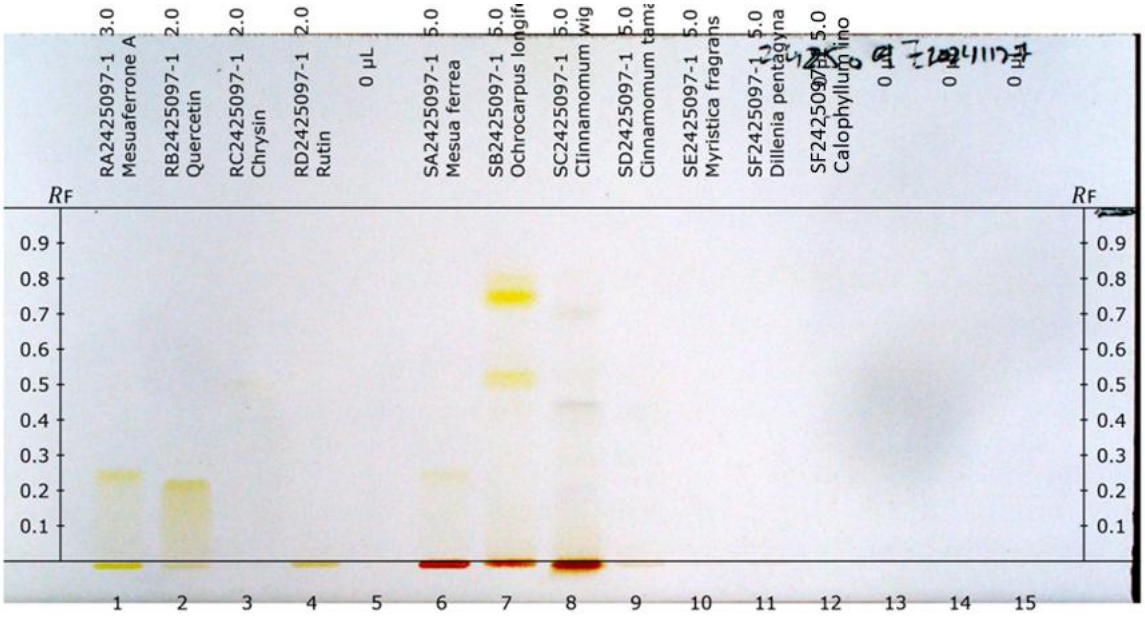

Figure 1: HPTLC fingerprints of Mesua ferrea Linn. and its adulterants in white light before derivatization using Toluene: Chloroform: Ethanol (4:4:1) as mobile phase.

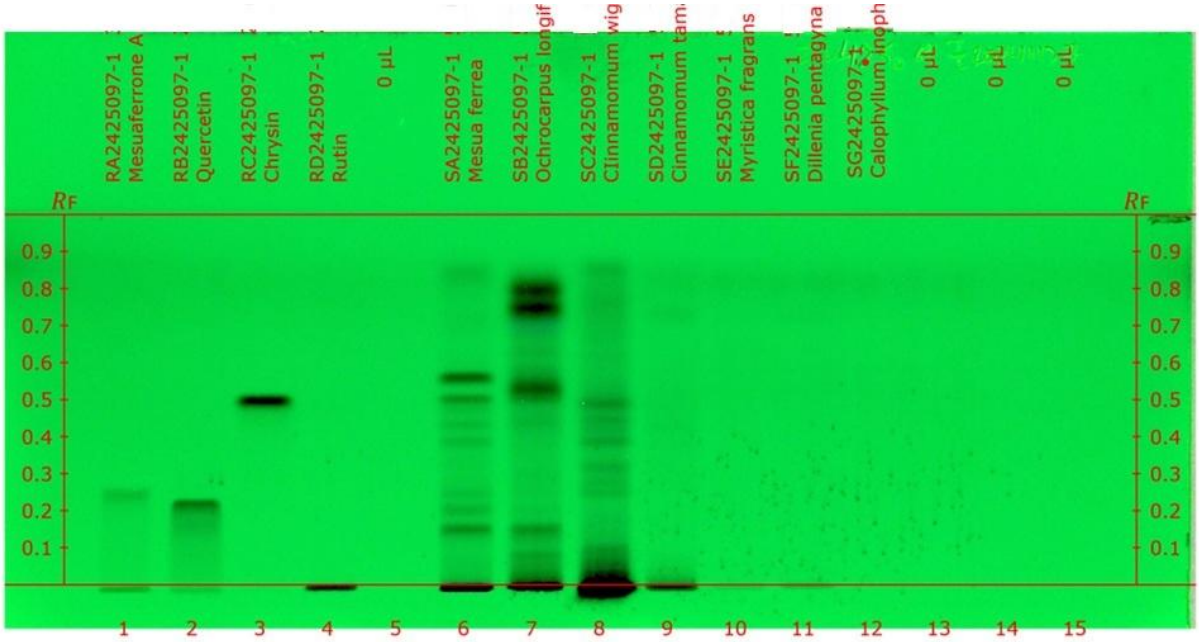

Figure 2: HPTLC fingerprints of Mesua ferrea Linn. and its adulterants at 254nm before derivatization using Toluene: Chloroform: Ethanol (4:4:1) as mobile phase.

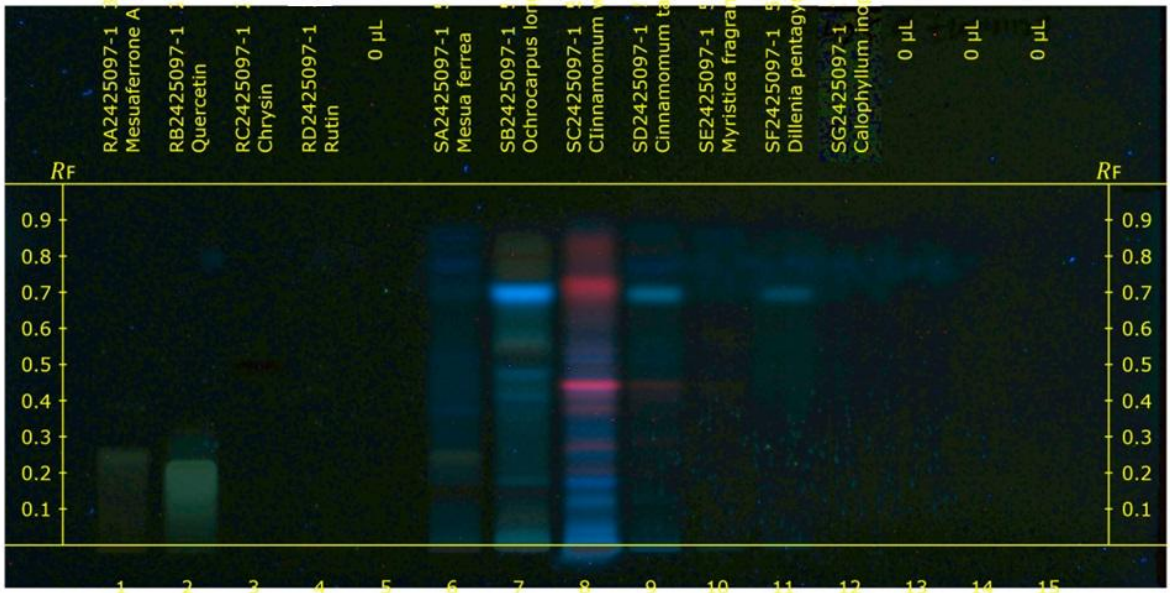

Figure 3: HPTLC fingerprints of Mesua ferrea Linn. and its adulterants at 366nm before derivatization using Toluene: Chloroform: Ethanol (4:4:1) as mobile phase.

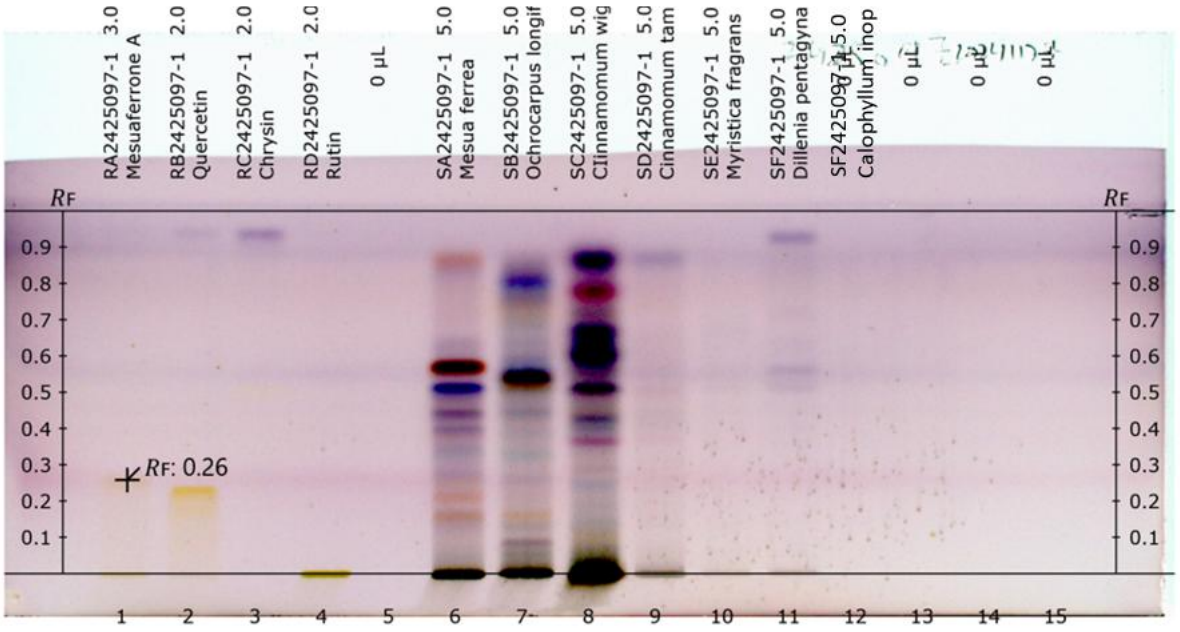

Figure 4: HPTLC fingerprints of Mesua ferrea Linn. and its adulterants in white light after derivatization using Toluene: Chloroform: Ethanol (4:4:1) as mobile phase.

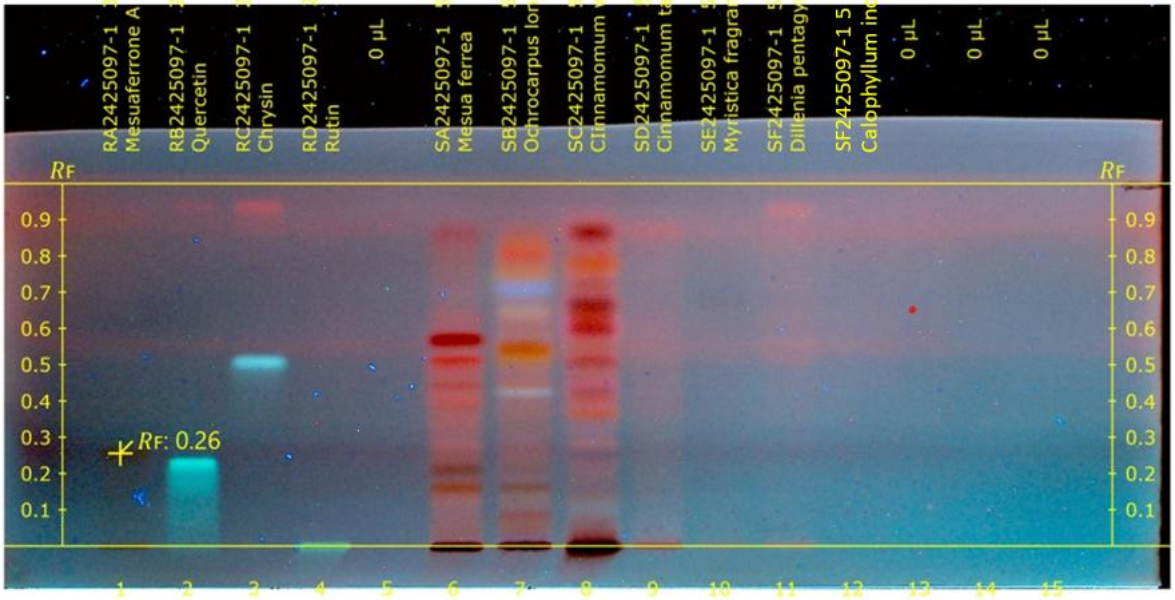

Figure 5: HPTLC fingerprints of Mesua ferrea Linn. and its adulterants at 366nm after derivatization using Toluene: Chloroform: Ethanol (4:4:1) as mobile phase.

Table 2: Rf values of reference standards using Toluene: Chloroform: Ethanol (4:4:1) as mobile phase.

Standards	Mesuaferrone A	Quercetin	Chrysin	Rutin
Rf values	0.26	0.23	0.50	ND

ND-Not detected

Table 3: Rf values of Mesua ferrea Linn. and its adulterants using Toluene: Chloroform: Ethanol (4:4:1) as mobile phase.

Peak	Stamens of *Mesua ferrea* Linn.	Buds of *Ochrocarpus longifolius* Benth and Hook f.	Unripe fruits of *Cinnamomum wightii* Meisn.	Unripe fruits of *Cinnamomum tamala* T. Nees & Eberm.	Buds of *Myristica fragrans* Houtt.	Fruits of *Dillenia pentagyna* Roxb.	Buds of *Calophyllum inophyllum* L.
1	0.14	0.07	0.02	0.03	0.03	0.01	0.19
2	0.20	0.11	0.23	0.13	0.23	0.03	0.30
3	**0.26**	0.24	0.27	0.24	0.31	0.07	0.34
4	0.39	0.43	0.35	0.35	0.33	0.11	0.43
5	0.43	0.52	0.41	0.54	0.52	0.15	0.57
6	**0.50**	0.79	0.49	0.84	-	0.23	0.73
7	0.56	-	0.59	-	-	0.42	0.84
8	0.85	-	0.65	-	-	0.53	-
9	-	-	0.76	-	-	0.69	-
10	-	-	0.84	-	-	0.90	-

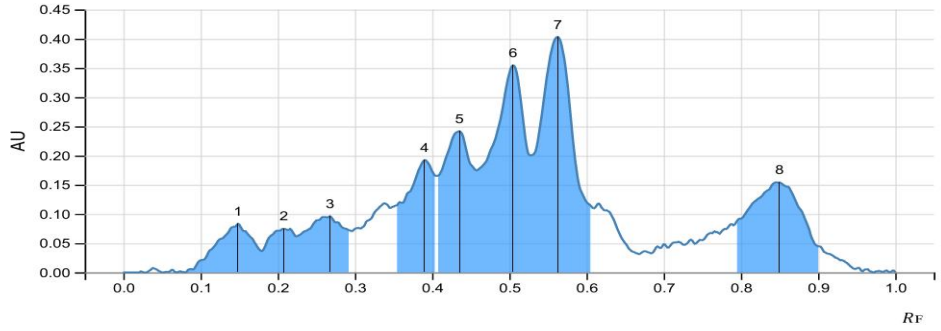

Figure 6: Densitogram of stamens of Mesua ferrea L. using Toluene: Chloroform: Ethanol (4:4:1) as mobile phase.

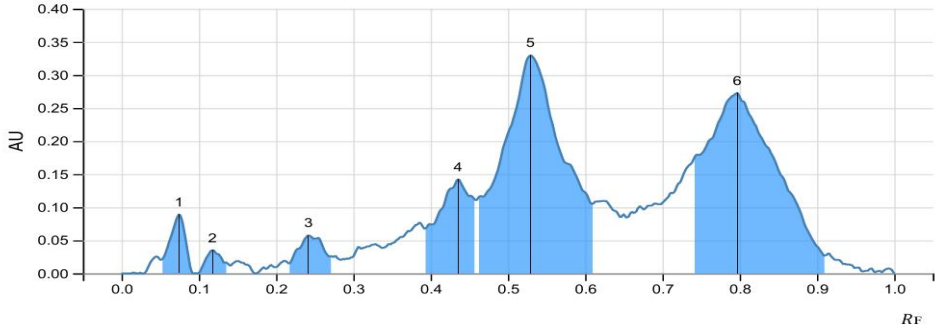

Figure 7: Densitogram of buds of Ochrocarpus longifolius Benth and Hook f. using Toluene: Chloroform: Ethanol (4:4:1) as mobile phase.

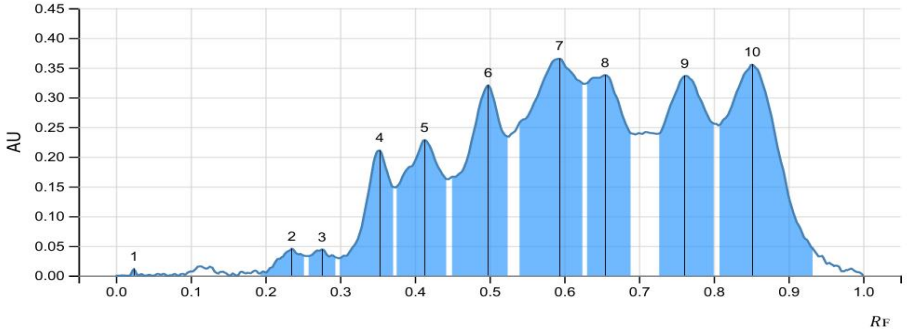

Figure 8: Densitogram of unripe fruits of Cinnamomum wightii Meisn. using Toluene: Chloroform: Ethanol (4:4:1) as mobile phase.

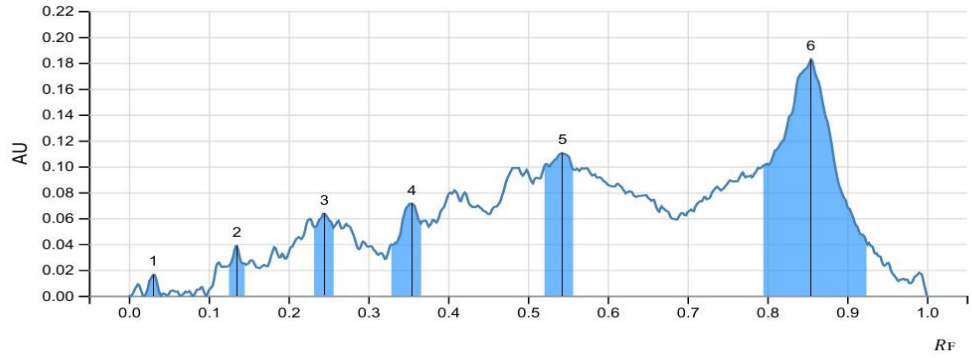

Figure 9: Densitogram of unripe fruits of Cinnamomum tamala T. Nees & Eberm. using Toluene: Chloroform: Ethanol (4:4:1) as mobile phase.

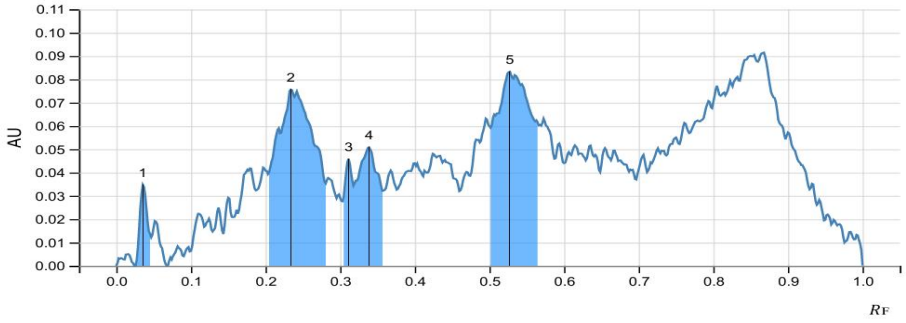

Figure 10: Densitogram of Buds of Myristica fragrans Houtt. using Toluene: Chloroform: Ethanol (4:4:1) as mobile phase.

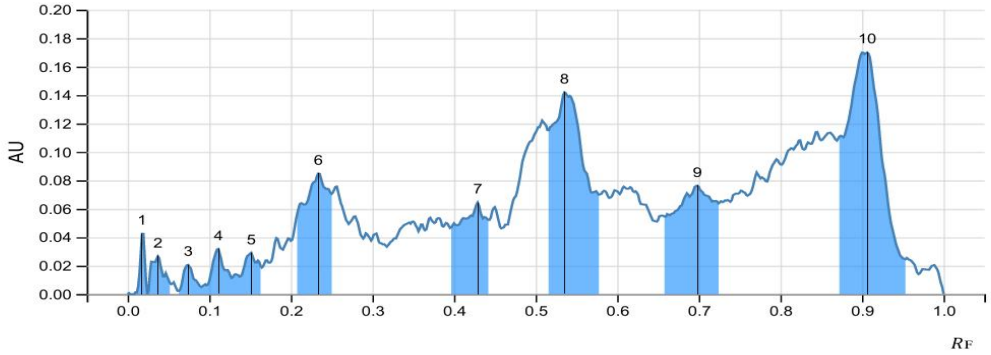

Figure 11: Densitogram of Fruits of Dillenia pentagyna Roxb. using Toluene: Chloroform: Ethanol (4:4:1) as mobile phase.

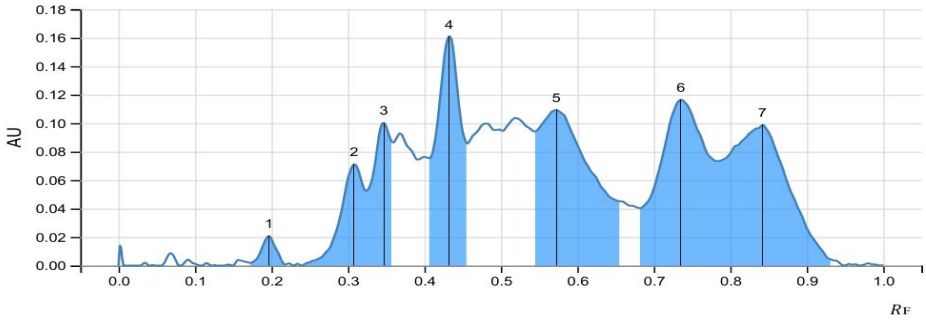

Figure 12: Densitogram of buds of Calophyllum inophyllum L. using Toluene: Chloroform: Ethanol (4:4:1) as mobile phase.

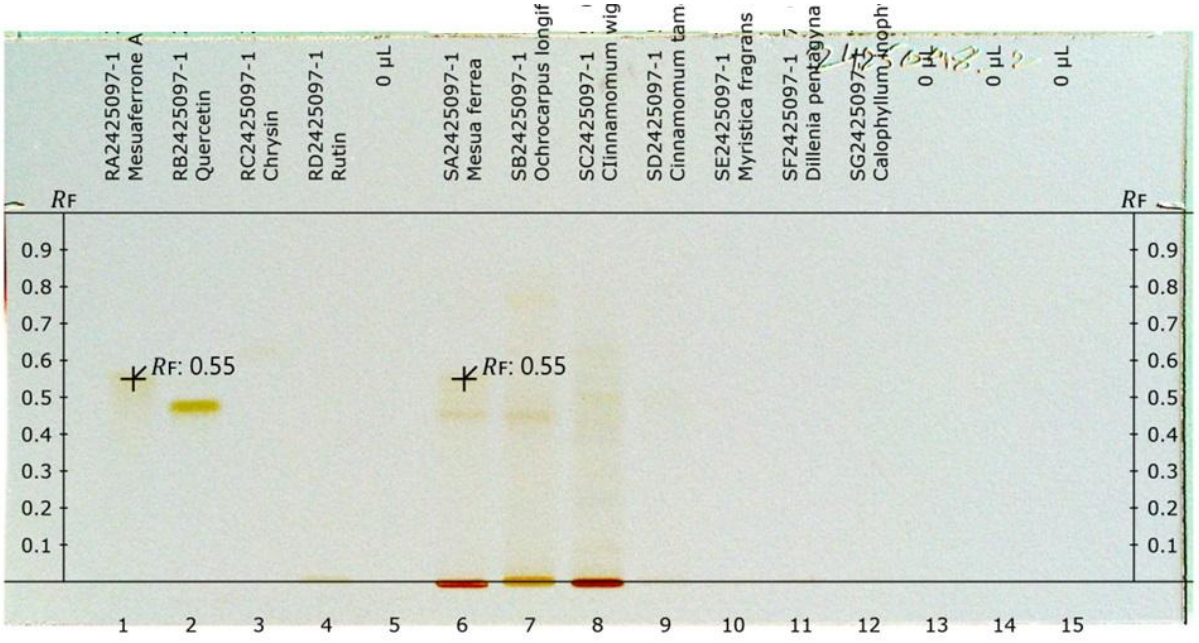

Figure 13: HPTLC fingerprints of Mesua ferrea Linn. and its adulterants in white light before derivatization using Toluene: Ethyl Acetate: Formic Acid (5:4:1) as mobile phase.

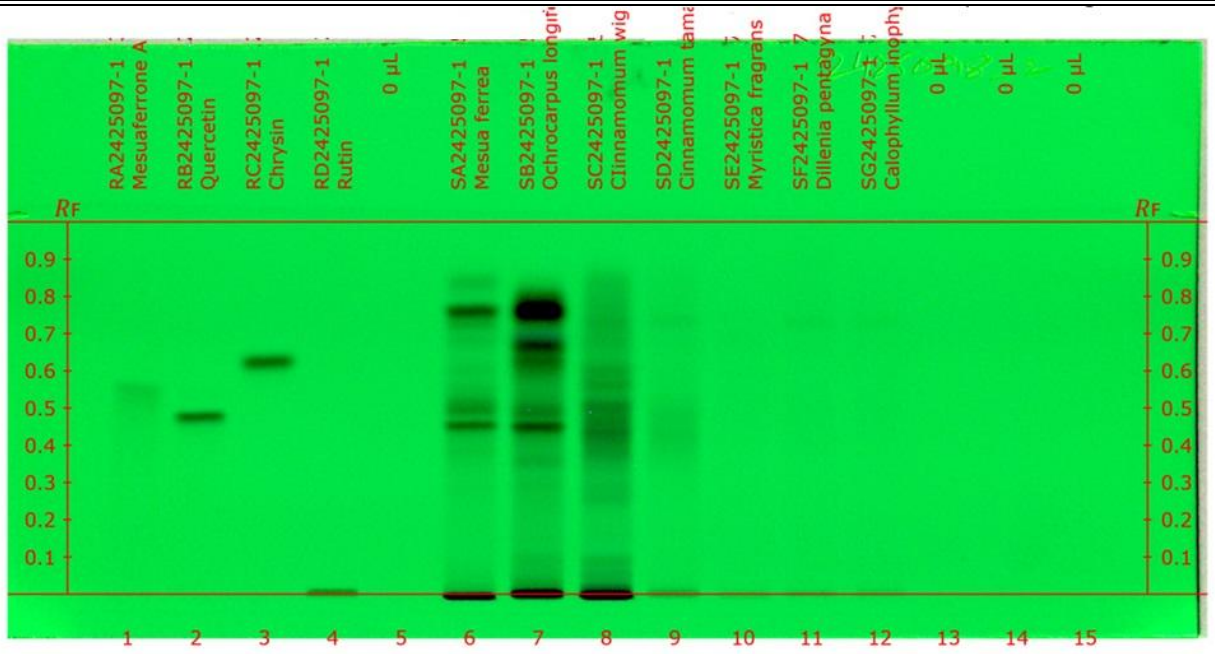

Figure 14: HPTLC fingerprints of Mesua ferrea Linn. and its adulterants at 254nm before derivatization using Toluene: Ethyl Acetate: Formic Acid (5:4:1) as mobile phase.

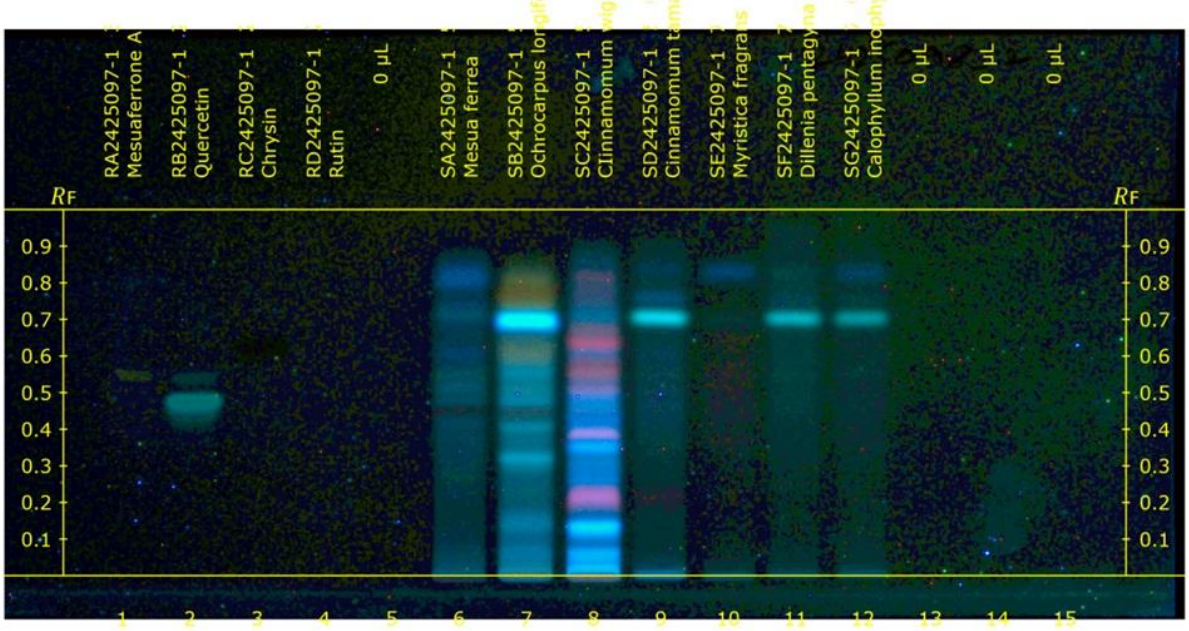

Figure 15: HPTLC fingerprints of Mesua ferrea Linn. and its adulterants at 366nm before derivatization using Toluene: Ethyl Acetate: Formic Acid (5:4:1) as mobile phase.

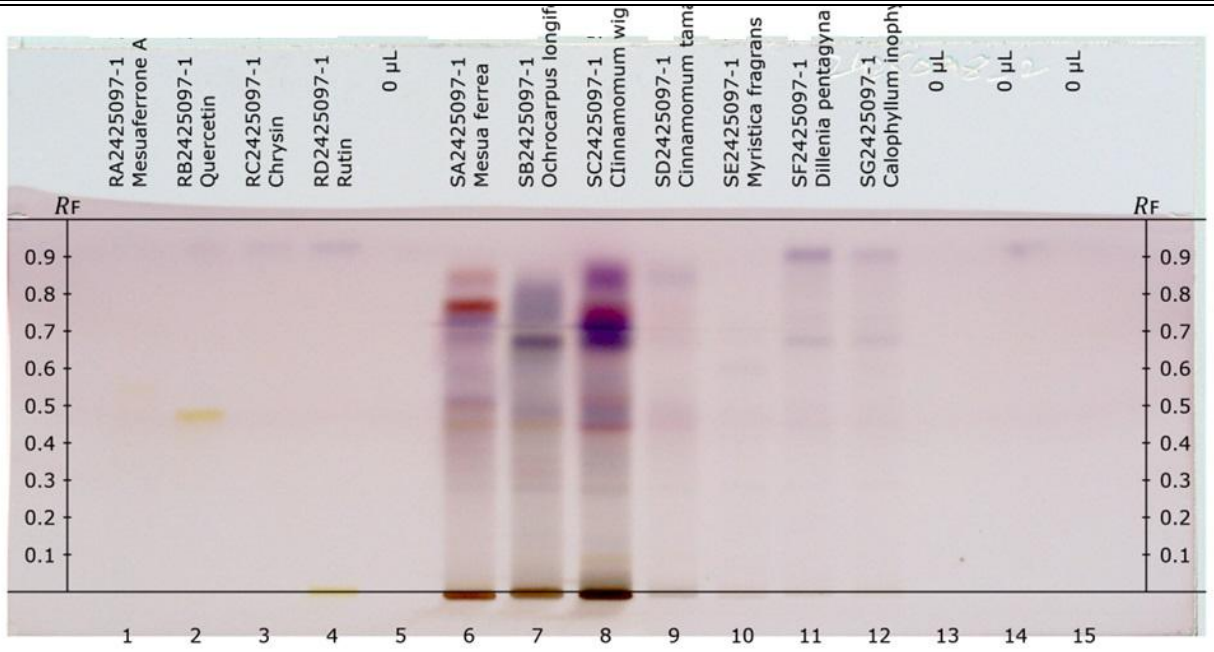

Figure 16: HPTLC fingerprints of Mesua ferrea Linn. and its adulterants in white light after derivatization using Toluene: Ethyl Acetate: Formic Acid (5:4:1) as mobile phase.

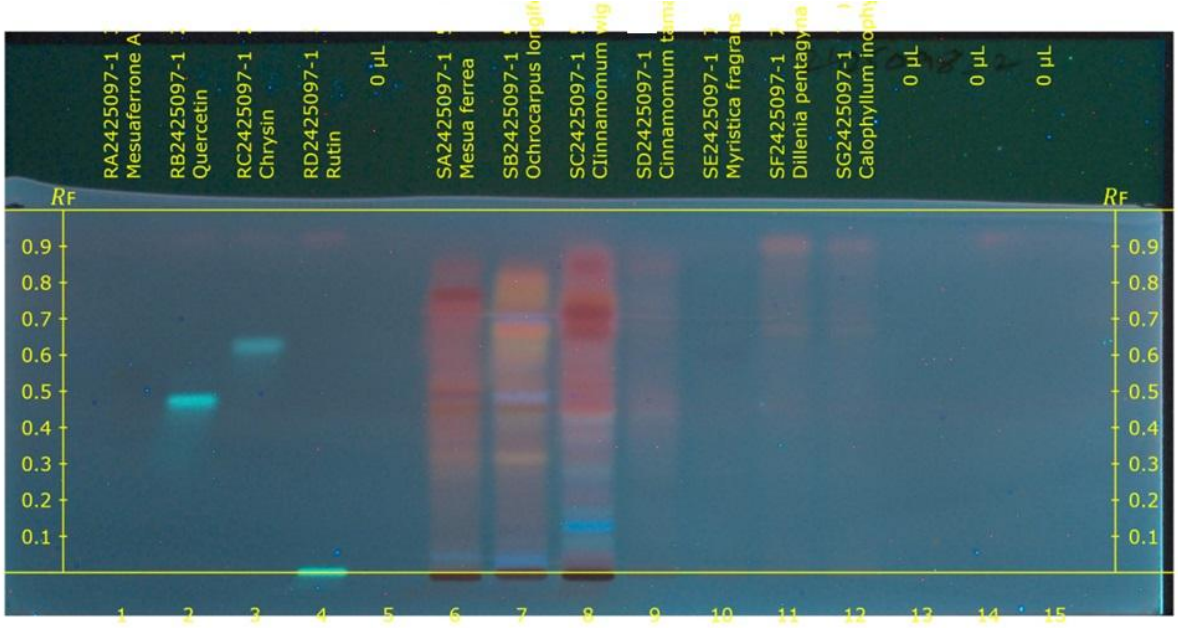

Figure 17: HPTLC fingerprints of Mesua ferrea Linn. and its adulterants at 366nm after derivatization using Toluene: Ethyl Acetate: Formic Acid (5:4:1) as mobile phase.

Table 4: Rf values of reference standards Toluene: Ethyl Acetate: Formic Acid (5:4:1) as mobile phase.

Standards	Mesuaferrone A	Quercetin	Chrysin	Rutin
Rf values	0.55	0.49	0.64	ND

ND-Not detected

Table 5: Rf values of Mesua ferrea Linn. and its adulterants using Toluene: Ethyl Acetate: Formic Acid (5:4:1) as mobile phase.

Peak	Stamens of *Mesua ferrea* Linn.	Buds of *Ochrocarpus longifolius* Benth and Hook f.	Unripe fruits of *Cinnamomum wightii* Meisn.	Unripe fruits of *Cinnamomum tamala* T. Nees & Eberm.	Buds of *Myristica fragrans* Houtt.	Fruits of *Dillenia pentagyna* Roxb.	Buds of *Calophyllum inophyllum* L.
1	0.02	0.02	0.03	0.01	0.01	0.02	0.02
2	0.07	0.07	0.06	0.01	0.08	0.07	0.10
3	0.12	0.15	0.14	0.15	0.10	0.09	0.14
4	0.22	0.24	0.22	0.23	0.11	0.15	0.25
5	**0.49**	0.32	0.26	0.38	0.20	0.17	0.43
6	**0.55**	0.37	0.31	0.50	0.22	0.25	0.56
7	0.61	0.41	0.36	0.56	0.24	0.30	0.71
8	0.71	0.48	0.39	0.71	0.27	0.40	0.97
9	-	0.56	0.43	0.76	0.29	0.43	0.98
10	-	0.70	0.50	0.84	0.36	0.71	-
11	-	0.83	0.56	0.91	0.38	0.76	-
12	-	-	0.64	0.94	0.51	0.89	-
13	-	-	0.71	-	0.56	-	-
14	-	-	0.92	-	0.58	-	-
15	-	-	0.95	-	0.60	-	-
16	-	-	-	-	0.64	-	-
17	-	-	-	-	0.84	-	-

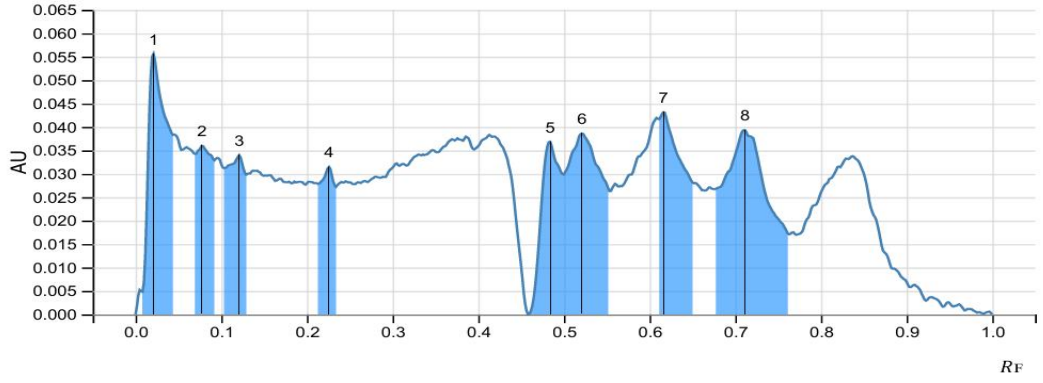

Figure 18: Densitogram of stamens of Mesua ferrea L. using Toluene: Ethyl Acetate: Formic Acid (5:4:1) as mobile phase.

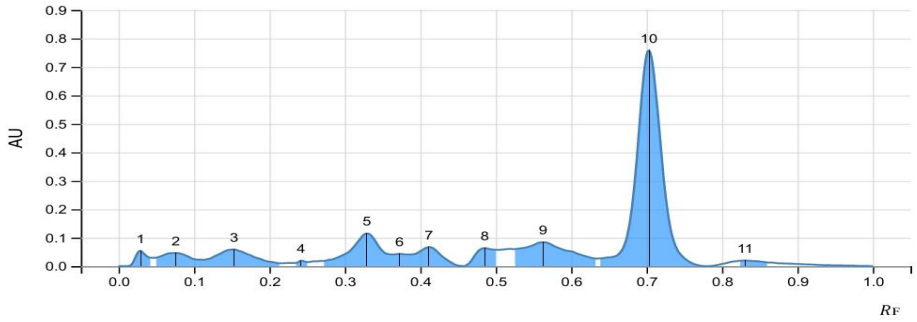

Figure 19: Densitogram of buds of Ochrocarpus longifolius Benth and Hook f. using Toluene: Ethyl Acetate: Formic Acid (5:4:1) as mobile phase.

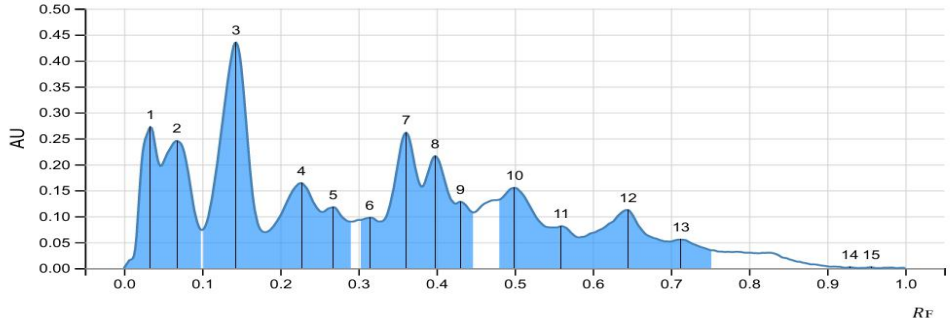

Figure 20: Densitogram of unripe fruits of Cinnamomum wightii Meisn. using Toluene: Ethyl Acetate: Formic Acid (5:4:1) as mobile phase.

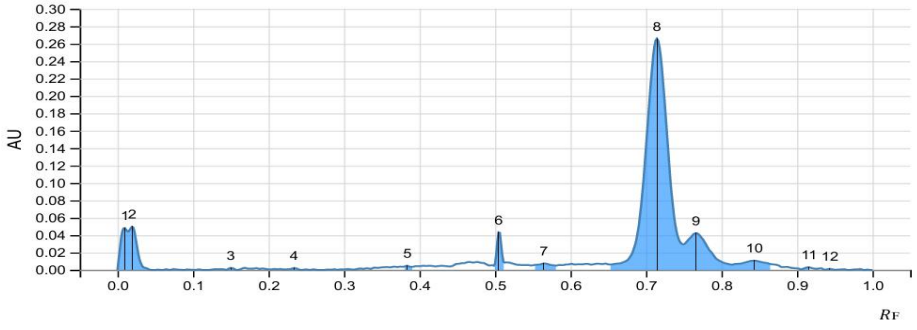

Figure 21: Densitogram of unripe fruits of Cinnamomum tamala T. Nees & Eberm. using Toluene: Ethyl Acetate: Formic Acid (5:4:1) as mobile phase.

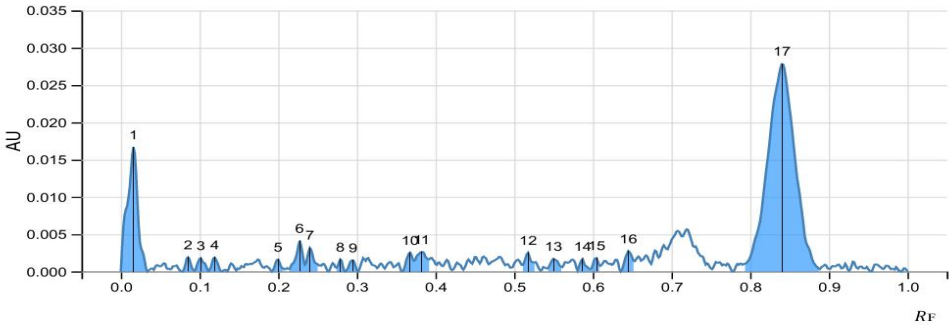

Figure 22: Densitogram of Buds of Myristica fragrans Houtt. using Toluene: Ethyl Acetate: Formic Acid (5:4:1) as mobile phase.

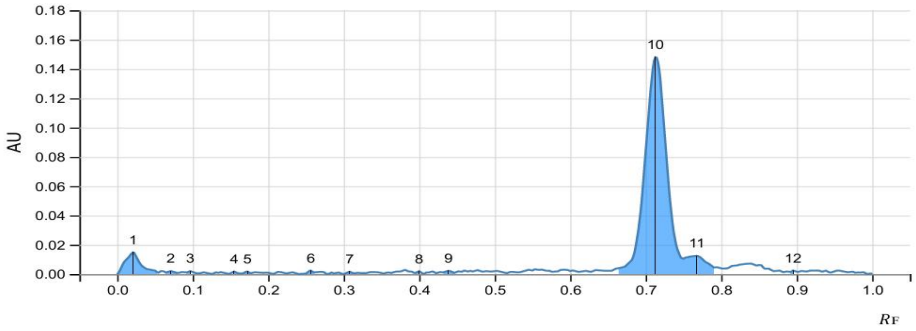

Figure 23: Densitogram of Fruits of Dillenia pentagyna Roxb. using Toluene: Ethyl Acetate: Formic Acid (5:4:1) as mobile phase.

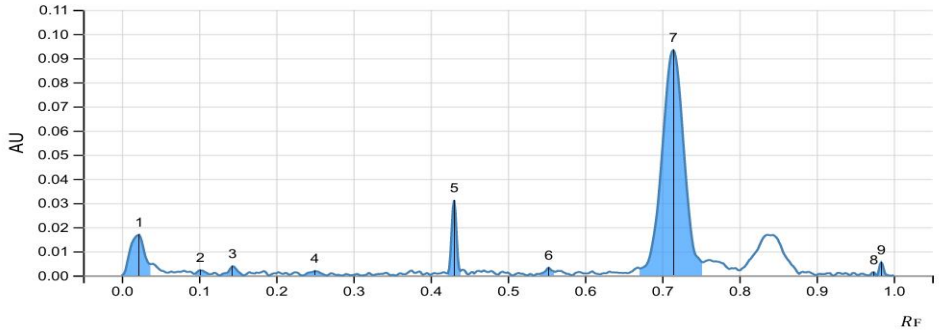

Figure 24: Densitogram of buds of Calophyllum inophyllum L. using Toluene: Ethyl Acetate: Formic Acid (5:4:1) as mobile phase.

Conclusion

This study presents a comprehensive phytochemical and HPTLC analysis of *Mesua ferrea* L. stamens, establishing a distinct chemical fingerprint that differentiates authentic *Mesua ferrea* L. from its adulterants. The exclusive presence of tannins, anthocyanins, and anthraquinones—as well as marker compound such as Mesuaferrone A — underpins the unique bioactivity and therapeutic potential of *Mesua ferrea*, which includes anti-inflammatory, antioxidant, antimicrobial, antidiabetic, analgesic, and wound-healing properties. The significantly different chemical profiles of the adulterants result in divergent bioactivities, rendering them incapable of replicating the medicinal efficacy of *Mesua ferrea*. This work fills a critical gap in the literature by developing a comprehensive phytochemical profile for *Mesua ferrea* L. stamens, thereby enhancing its authenticity in traditional medicine and setting a precedent for standardized methods in herbal product verification. Thus, these findings bridge traditional knowledge with modern analytical techniques, supporting the safety, efficacy, and reliability of herbal medicines.

Refernces

1. Mukherjee PK. Quality control and evaluation of herbal drugs: Evaluating natural products and traditional medicine. Elsevier; 2019.
2. Parveen B, Parveen A, Parveen R, Ahmad S, Ahmad M, Iqbal M. Challenges and opportunities for traditional herbal medicine today, with special reference to its status in India. Ann Phytomed. 2020;9(2):97–112.
3. Ernst E. Adulteration of Chinese herbal medicines with synthetic drugs: a systematic review. J Intern Med. 2002;252(2):107–13.
4. Asif M, Jafari SF, Iqbal Z, Revadigar V, Oon CE, Majid ASA, et al. Ethnobotanical and Phytopharmacological attributes of Mesua ferrea: a mini review. J Appl Pharm Sci. 2017;7:242–51.
5. Harborne AJ. Phytochemical methods a guide to modern techniques of plant analysis. springer science & business media; 1998.
6. Liang YZ, Xie P, Chan K. Quality control of herbal medicines. Journal of chromatography B. 2004;812(1–2):53–70.
7. Sahu AN, Hemalatha S, Sairam K. Quality control studies of Mesua ferrea Linn. flowers. 2013;

International Journal of Multidisciplinary Research and Technology

ISSN 2582-7359 | Peer Reviewed Journal | Impact Factor 6.325

www.ijmrtjournal.com